Finding the climate optimal cruise altitude for a selection of aircraft types and mission combinations

by

Rick Martin Rosenkrantz

to obtain the degree of Master of Science in Aerospace Engineering
at the Delft University of Technology
to be defended publicly on Thursday December 12th, 2019 at 10:00 AM

Student number:	4224612	
Thesis committee:	Prof. dr. V. Grewe,	DLR, TU Delft, chair and supervisor
	Ir. J.A. Melkert,	TU Delft, supervisor
	Dr. I.C. Dedoussi,	TU Delft
	Dr. F. Yin,	TU Delft, external member

An electronic version of this thesis is available at `http://repository.tudelft.nl/`.

TU Delft

Preface

I would like to take this opportunity to thank my supervisors for their support on this project. First of all Prof. Grewe for giving me the opportunity write my Thesis at the Aircraft Noise and Climate effect department and for all the constructive feedback you have given me throughout the project. I look back to some memorable web conferences as well as personal meetings which were serious at times but also quite enjoyable. Thank you for those moments. I would also like to thank Joris Melkert for his time and enthusiasm in the research topic and good ideas on how to approach things. I really enjoyed the visiting hours we had. Above all I would like to thank my family and fiancé Carlein for their unconditional support and patience.

Rick Martin Rosenkrantz
Delft, November 2019

Contents

List of Figures

List of Tables

Abstract

The climate impact of aviation is assessed as function of the emission altitude for two individual aircraft types with a large difference in operational cruise altitude range: the Boeing 787-800 (B787-800) and Boeing 777-300ER (B777-300ER). As a basis for the study a dataset of 2,738 historical trajectories distributed over two separate days is assembled. The fuel consumption and produced emissions of these original trajectories are calculated by using the aircraft performance model Piano-X and are corrected for the effect of wind by incorporating atmospheric data from the European Centre for Medium-range Weather Forecasts (ECMWF). The constructed emission inventories served as input for the climate response model AirClim which calculated the climate response over time in terms of radiative forcing and global temperature rise. To analyze the effect of changes in cruise altitude, the fuel consumption and corresponding emissions were recalculated for scenarios with a relocated altitude profile ranging from an upward shift of 2000 ft to a downward shift of 18000 ft with respect to the original flown altitude found in the trajectory data.

By evaluating the climate impact of the original flown trajectories of the two aircraft types it was found that the total climate impact of the B777-300ER is about 15% larger compared to the B787-800 as quantified per flown kilometer. This difference is mainly due to the larger quantity of emissions, increasing the forcings of CO_2 and O_3. Furthermore it was found that the contribution of the individual forcing components to this total climate impact is significantly different for both aircraft types. Due to the larger emission quantity per flown kilometer, the climate impact of the forcing components of O_3, CH_4 and CO_2 are larger for the B777-300ER. The forcings of water vapor and contrail cirrus on the other hand are larger for the B787-800 mainly due to the higher emission altitude.

By shifting cruise altitudes down, the total climate impact is reduced for both aircraft types where the minimal climate impact is found for the lowest analyzed cruise altitude. A relocation of the cruise altitude down by 6000 ft was found to result in a reduction in climate impact of 24% for the B787-800 and 18% for the B777-300ER. As a consequence, the fuel consumption and associated fuel costs were found to increase by respectively 13% and 14%. By reducing the cruise altitude further down by 18000 ft resulted in a reduction in climate impact of 49% and 59% for the B787-800 and B777-300ER respectively. The resulting increase in fuel consumption increased to respectively 57% and 38%. Relocating the cruise altitude up by 2000 ft resulted in an increase in climate impact for both aircraft types of respectively 13% and 14%.

1 Introduction

Climate change has gained increasing attention of policy makers and the public. The reason for this is that the effects of climate change are becoming more and more apparent mainly in the form of extreme weather. Furthermore, the knowledge regarding the effects and causes of the changing climate is improving which increases the awareness and understanding of the necessity of the required change. This change is required since the causes for climate change are primarily anthropogenic greenhouse gas (GHG) emissions [41] part of which are emitted by aircraft. Additionally, aircraft produced contrail cirrus clouds contribute to anthropogenic climate change as well [46].

1.1. Aircraft emissions

According to one of the most recent assessments in 2009, aviation contributed for 3.5% to the global anthropogenic forcing due to greenhouse gases in 2005 [49]. These gases include CO_2, ozone and methane. The forcing of CO_2 is a direct result of burning kerosine whereas ozone and methane forcings are influenced by the emission of nitrogen oxides by aircraft. Other aircraft emissions responsible for affecting climate are water vapor which under the right circumstances can result in the formation of linear contrails and cirrus clouds which have a warming effect as well. By including the best estimates for cirrus clouds, air traffic emissions contribute for 4.9% to anthropogenic warming with a 90% likelihood range of 2-14 % [49]. This is significant in comparison to the entire transport sector which according to Fuglestvedt et al. [17] was responsible for 11% of the total climate forcing in the year 2000. This includes both road and rail transport, shipping and aviation. It should be noted however that this contribution reflects the shorter history of the transport sector compared with other sectors such as industry [17].

Climate forcings are a function of the concentration of greenhouse gases in the atmosphere which are a result of all historical emissions from time of origin of the sector until the present. Considering that significant emissions from aviation only go back to 1940 whereas the industrial revolution began in the 18th century, it can be argued whether this quantification metric gives an appropriate bases to compare the different emission sources. Therefore it is stated by Fuglestvedt et al. (2008) [17] that a forward looking perspective is more relevant to compare different sectors and be able to evaluate emission reduction policies. By using a forward looking perspective the contribution of current emissions to the future climate impact is evaluated. An example of a forward looking perspective is global surface temperature increase. Both climate metrics will be discussed further in Section 2.3.

The most important factor influencing the future climate impact is the current emission of green house gases and other climate forcing agents. According to the fifth assessment report (AR5) of the IPCC [41] aircraft GHG emissions contributed to approximately 10.6% of the total GHG emissions produced by the transport sector in 2010 which is equivalent to 750 Mt (Megatonnes or million tonnes) CO_2. More recently these numbers increased to 12% [27] and 859 Mt for the year 2017 according to the Air Transport Action Group (ATAG)[1].
The transport sector on the other hand is responsible for 23% of the total anthropogenic GHG emissions [41]. This leads to the observation that aviation contributes to approximately 2.4% to global GHG emissions on a global scale. This number should not be confused with the aforementioned 3.5% contribution of aviation to forcing from GHG emissions. The difference is due to the climate forcing is not only dependent on the quantity of the emission but on the emission location as wel, as will be elaborated upon in Section 2.4.

1.2. Aircraft emission growth

The contribution of aviation to future climate change is expected to grow since the emissions of the transport sector and especially air transport is one of the fastest growing industrial sectors [19]. The CO_2 emissions from aviation grew by 25% from 1990 to 2000 whereas global CO_2 emissions from all sectors combined grew by 13% [17]. The growth of air traffic emissions originates from the continuous growth of air transport observed in the past decades measured in revenue passenger kilometers (RPK). This growth in RPK is accompanied by a growth in fuel consumption which is directly related to CO_2 emissions.
This is illustrated by Figure 1.1 which shows the RPK growth and corresponding fuel consumption from 1940 until 2005. RPK numbers are taken from ICAO traffic statistics[2] and fuel consumption is taken from Sausen and Schumann [63] updated by data from the international energy agency (IEA)[38].

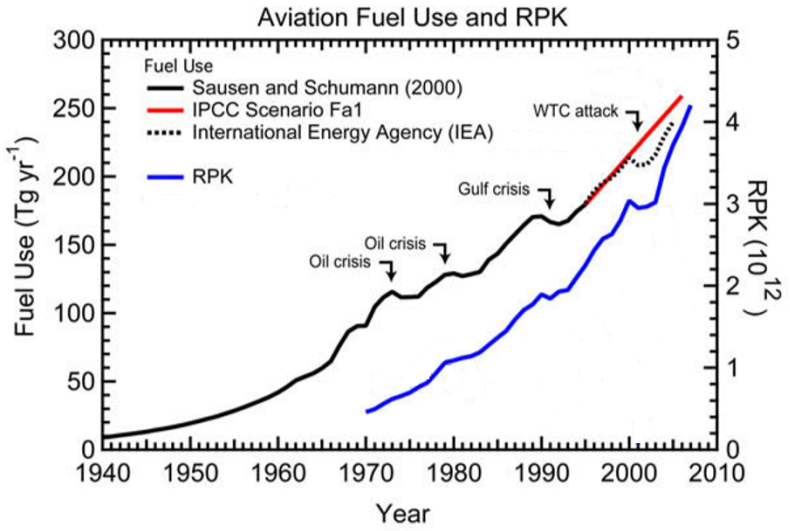

Figure 1.1: Temporal evolution of fuel use and revenue passenger kilometres of aviation taken and adapted from Lee et al.[48]

[1] https://www.atag.org/facts-figures.html
[2] https://www.icao.int/publications/Pages/annual-reports.aspx

From Figure 1.1 it is observed that the growth in RPK is faster than the increase in fuel use. More recent numbers which show this trend is continuing are found in RPK numbers published by ICAO[3]. In the period from 2008 to 2017 the RPK grew from 4.608 billion to 7.699 billion which translates to an average annual growth rate of 5.9%. Emissions of CO_2 on the other hand grew from 700 Tg (1 Teragram equals 1 million tons) in 2004[63] to 859 Tg in 2017[4] which translates to an annual growth rate of approximately 1.6%. This emission growth is directly proportional to the growth in fuel use and is very close to the IPCC Fa1 predicted traffic growth scenario corresponding to an annual increase in fuel consumption of 1.7% [57].

The reason for a faster growth of RPK compared to emissions is partly due to the advancements made in aircraft technology where aircraft have become more fuel efficient over the years [45]. Another factor involved is the worldwide observed increase in average passenger load factor which has increased from 75% to 82% in 2018 according to ICAO statistics[37].

More recently, according to the latest annual report by ICAO [37] the global RPK grew by 8% over 2017 and doubled since 2004 which translates to an average growth rate of 5.5%. This growth is likely to persist or even increase since ICAO forecasts an annual RPK growth of 4.5% up until the year 2042 [34]. Based on this traffic forecast ICAO predicts that as a result global CO_2 emissions from aviation would increase an additional 150% above 2006 levels by 2036 and at this rate, emissions would quadruple by 2050 [36]. This indicates that the rate of improvement in technology is not sufficient to compensate for the demand growth and will lead to more emissions in the future.

1.3. Climate impact aviation

Besides the growth of the aviation sector and its resulting effect on emissions, the contribution of the emissions towards climate impact from aircraft has "the potential to grow overproportional compared to other transport sectors" as stated by Grewe and Stenke [22].

This is because the climate impact of aviation relative to fuel consumption is larger than for other sectors [17]. This has multiple causes, where most dominant is that the largest portion of the emissions are emitted at cruise altitude where the atmospheric residence time of non-CO_2 emissions such as NO_x and its chemical product ozone is longer which allows concentrations to accumulate resulting in a larger climate impact [22], [19]. Additionally the formation of condensation trails or contrails and cirrus clouds by aircraft increases the climate impact since they reduce the outgoing thermal radiation from the earths atmosphere [52]. The formation of contrails highly depends on ambient atmospheric conditions such as humidity and temperature which vary with altitude [13]. Especially the upper troposphere and tropopause region where most aircraft fly allows for the formation of contrails since this region is cold and moist enough [13]. These altitude effects of the non-CO_2 emission component are therefore only present for air transport.

This explains the disproportional contribution of aviation emissions to climate impact discussed in Section 1.1. As mentioned only a 2.4% contribution to the global anthropogenic GHG emissions results in a 3.5% contribution to the climate forcing. Furthermore, by incorporating contrails and contrail cirrus this number increases to almost 5%. This effectively results in that although air traffic is responsible for only 10.6% of the transport emissions, their contribution to climate forcing represents almost half that of the entire transport sector (approximately 5% compared to 11 %).

[3] https://www.icao.int/publications/Pages/annual-reports.aspx
[4] https://www.atag.org/facts-figures.html

1.4. Objectives to reduce emissions from aviation

Although a contribution of 5% to climate change is still small compared to other sectors, one should bear in mind that the respective contribution of air traffic emissions will grow faster than for other sectors and as a result the contribution of air traffic to anthropogenic climate change is expected to increase [12]. This statement is supported by the IPCCs third working group report [41] which states that transport emissions could increase at a faster rate than emissions from the other energy sectors if "no aggressive and sustained mitigation policies will be implemented".

Objectives to reduce the adverse effects from aviation have been set by the air transport action group (ATAG) and are adopted by the International Air Transport Association (IATA) and The International Civil Aviation Organization (ICAO). These objectives include improving the fuel efficiency by an average of 1.5% per year from 2009 to 2020 and stabilizing emissions from 2020 onward with carbon neutral growth[30]. Furthermore, a goal is set to reduce the net emissions of aviation by 50% by 2050 compared to 2005 levels [30].

A few initiatives have been introduced to meet these objectives of which the EU emission trading system is one. Since 2012 all airlines operating in Europe are required to monitor and report their emissions. They receive tradeable allowances which is supposed to work as an incentive to reduce emissions and make a profit of the sold allowance. This initiative however was limited to flights within the European economic area. This was done to support the development of a new global measure initiated by ICAO which entails an offsetting scheme to compensate for emission growth from 2020 levels. In 2016 ICAO member states agreed on this resolution named CORSIA which is a global market based measure to address CO_2 emissions from international aviation from 2021 [6].

The carbon offsetting and reduction scheme for international aviation (CORSIA)[5] aims to stabilise CO_2 emissions at 2020 levels by requiring airlines to offset the growth of their emissions after 2020. This offsetting can be done by purchasing emission units generated by projects that reduce emissions in other sectors. CORSIA is the first climate agreement to address an entire sector. This initiative however is still under development and it will have to prove its effectiveness. Furthermore, this measure will allow emissions to go unaddressed until 2020 after which further growth will be compensated. Besides that, the scheme is voluntary until 2027 and therefore it can be argued whether this will be a successful measure.

Although these resolutions may result in an overall stabilisation of the global CO_2 emissions it still does not reduce the actual CO_2 emissions produced by aircraft. These are merely incentives for airlines to compensate CO_2 emissions and reduce them elsewhere. Furthermore, this resolution does not address the non-CO_2 climate forcing components produced by aircraft such as NO_x emissions and produced contrails. For these forcing components to be reduced, other mitigation strategies will have to be implemented which actively reduce the overall climate impact of aviation.

[5] https://carbonmarketwatch.org/wp/wp-content/uploads/2016/10/Post-Assembly-Policy-Brief-Web-1.pdf

1.5. Emission mitigation strategies

In light of the emission goals adopted by ICAO and IATA and considering the increasing growth of the emissions from aviation it can be stated that other mitigation strategies are necessary.

There are several means to achieve these objectives of which the most effective and realistic will be discussed. The mitigation strategies can be categorized into three different areas of improvements, namely technological improvements, operational improvements and alternative fuels. Each of these improvement areas will be discussed briefly in the next sections.

1.5.1. Technological development

One of the means to achieve these objectives lies in the area of technological development of aircraft. This can be in the area of aerodynamics, engine performance and structural design. A study was conducted by the international council on clean transportation (ICCT) [45] which investigated the fuel efficiency improvement of new generations of commercial jet aircraft. For this study a database was used which consisted of the number and type of new aircraft into service and a performance model which determined their average fuel efficiency. As a result Figure 1.2 shows the temporal development of aircraft fuel efficiency over the years. From the figure it is observed that new aircraft have become 45% more fuel efficient from 1968 to 2014 measured in fuel/passenger-km. This corresponds to annual improvement of approximately 1.3%. Between the present and 2014 several new aircraft came into service such as the Airbus A320neo and the Boeing 737MAX which as stated in the study will further increase the fuel efficiency and will continue the observed trend.

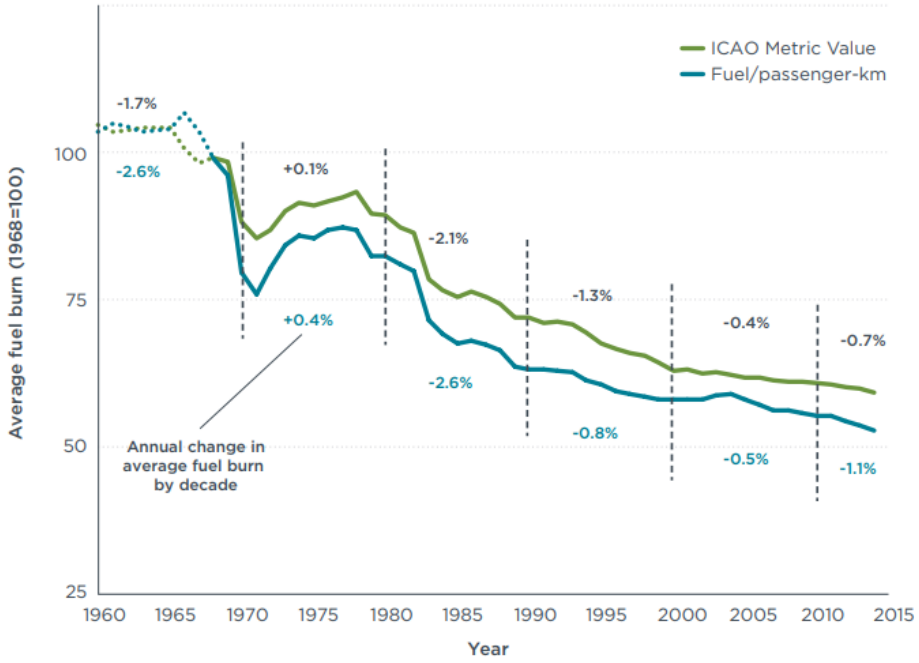

Figure 1.2: Average fuel consumption for new commercial jet aircraft coming into service (1968 = 100) taken from [45]

The emissions of the entire aircraft fleet however depend on the fleet wide fuel performance which depends on the fleet mix. This fleet mix will be composed of several generations of aircraft where the older generations will have a lower fuel efficiency. Each year a set of older aircraft will be replaced by new ones which results in a small increase in overall fuel efficiency. This phasing out of generations of aircraft however is a gradual process in which it takes years to replace all current operating aircraft to aircraft of the newest generation. According to IATA[6] the average aircraft retirement age over the last 36 years was 26.5 years which indicates that more than 50% of aircraft are still in operation after the age of 25 years. Furthermore, the average age of aircraft in operation is approximately 12 years old and has been stable for a while. Combining these numbers it can be stated that all current aircraft have another 14 to 15 years before all aircraft are replaced by aircraft with standards from now or higher. This indicates that the implementation time of technological development in aircraft is significant.

It should be noted however that in the recent past the average retirement age has decreased from 30 years in the period from 2005-2009 to 27 in 2010-2015. A probable cause for this trend are the recent incentives for airlines to cut their emissions by renewing their fleet. Another cause for airliners to renew their fleet is to reduce their operating costs. By using more fuel efficient aircraft operating costs can be decreased significantly since fuel costs contribute to more than 20% of the overall costs of an airline[7]. For this reason the oil price is also one of the drivers for aircraft retirement.

What should be considered as well is that there is a limit to the technological improvements which are feasible within for example engine technology such as the pressure ratio, the bypass ratio and the turbine inlet temperature. In the past years bypass ratios have increased to reduce the fuel consumption. This however did come with negative side effects. A larger bypass ratio results in a larger engine cowling and nacelle which result in more drag and weight which will increase the fuel efficiency. For this reason there is a limit to the maximum bypass ratio which can be attained. Furthermore, increasing the turbine inlet temperature and pressure ratio over the years both resulted in higher thermodynamic efficiencies which led to higher propulsive efficiency and lower fuel use. On the other hand, a larger pressure and temperature causes the formation of NO_x to increase [21].

1.5.2. Alternative fuels

An alternative to reduce the climate impact of aviation is by making use of alternative fuels such as bio fuels. The principle of using bio fuels instead of kerosine is that by producing bio-fuels, CO_2 is taken up from the air which will compensate for the emitted CO_2 when burned in flight. IATA claims that a 80% CO_2 reduction from the adoption of alternative fuels is possible. The same was concluded by a study from Snijders and Melkert [68] which compared the climate impact of hydrothreated renewable jet fuel (HRJ) to conventional jet fuel. With the assumption that 80% of the CO_2 emitted was absorbed by the biomass used for producing HRJ this resulted in a significantly lower climate impact. These sources of propulsion however have not yet reached a matured state of development. Therefore, other means will have to be investigated to contribute to reaching the short term environmental goals. Mitigation strategies which have the shortest implementation time are in the area of operational improvements which will be discussed next.

[6] https://www.iata.org/whatwedo/workgroups/Documents/MCC-2016-BKK/D2-1000-1030-aircraft-retirement-sgiaviation.pdf

[7] `http://web.mit.edu/airlinedata/www/Expenses&Related.html`

1.5.3. Operational improvements

Besides alternative fuels and technological improvements there is the possibility for improvements related to the operational aspect of air transport. In this area improvements can be made by increasing the passenger load factor, adjusting the flight speed and or flight altitude. Aircraft performance and fuel consumption are closely related to airspeed and altitude and therefore improvements within this region can provide significant increases in efficiency and consequently reduce aircraft emissions. Another advantage over technological improvements is that the time to implement these improvements is shorter resulting in earlier emission reductions [51]. Research was done by Jensen et al. (2015) [43] to determine the effect of altitude and speed optimisation based on actual flight data and it was found that by analysing 217,000 US domestic flights an adjusted altitude profile could result in a 1.96% decrease in fuel consumption. For the optimisation of speed this resulted in a fuel saving of 1.93%. Since speed and altitude optimisation are two completely different strategies these will be discussed separately in further detail.

Velocity optimisation

There exists a potential to reduce aviations climate impact of CO_2 by flying more economically. As a result less fuel is consumed which reduces the emissions of CO_2 and NO_x. To fly as economically as possible, the objective is to maximise the range for a given amount of fuel. An approximate analytic expression for the range of a jet aircraft is the Brequet range equation shown in Equation 1.1 [61]. This expression is approximate since it assumes quasi-level and quasi-steady flight. In Equation 1.1 R is the total range which is dependent on the airspeed V, the ratio of C_L over C_D, the specific fuel consumption c_T and the ratio of the weight at the start of the cruise W_1 over the weight at the end of the cruise W_2. From this expression it is observed that airspeed is a determining factor to reach the objective since the product of speed and C_L/C_D is sought to be maximized to maximize the range. Additionally the ratio of C_L/C_D also depends on the airspeed as well.

$$R = \int_{W_2}^{W_1} \frac{V}{c_T} \frac{C_L}{C_D} \frac{dW}{W} \tag{1.1}$$

Depending on the aircraft weight and cruise altitude there exists a speed which minimizes the fuel used for a given distance covered. This speed is defined as the maximum range cruise speed (MRC) and is found by maximising the product of V and C_L/C_D. This translates to maximising C_L/C_{D^2} since airspeed squared is inversely proportional to C_L. Therefore by flying the speed corresponding to this criterion, the airliner will burn a minimal trip fuel and minimize the cost of fuel. As a result, emissions will be minimized as well. Flying at a higher speed than MRC will effectively reduce the value for C_L and thereby reduce C_L/C_D to a larger extent than the relative gain in speed.

There is a factor however which in practice often drives cruise speeds above this MRC speed which is the cost index (CI). The cost index represents the balance between the cost of fuel and the time dependent costs of a flight. Although flying faster will cost extra fuel due to the larger fuel consumption, the flight time will be reduced resulting in a reduction of maintenance costs and labour costs. Furthermore, it increases the availability of the aircraft which allows it to be used for other operations. Therefore, since the objective of an airline is to reduce the total costs, aircraft in general fly at the speed which is dictated by the cost index [51]. This economically most profitable speed is defined as the ECON speed and includes trade-offs between the flight time and fuel burn which is dependent on the price of fuel, the aircraft type and even the route dependent [60]. Furthermore, ECON speed takes the effect of wind into account by flying faster in case of a head wind to minimize the penalty associated with the headwind.

Another theoretical speed selection for the cruise phase of the flight is long-range cruise (LRC) speed. LRC has been defined as the speed above MRC that will result in a 1% decrease in terms of distance flown per kilogram fuel burned [60]. The advantage is that 1% of range is traded for 3 to 5% higher cruise velocity [60] which is visualized in Figure 1.3.

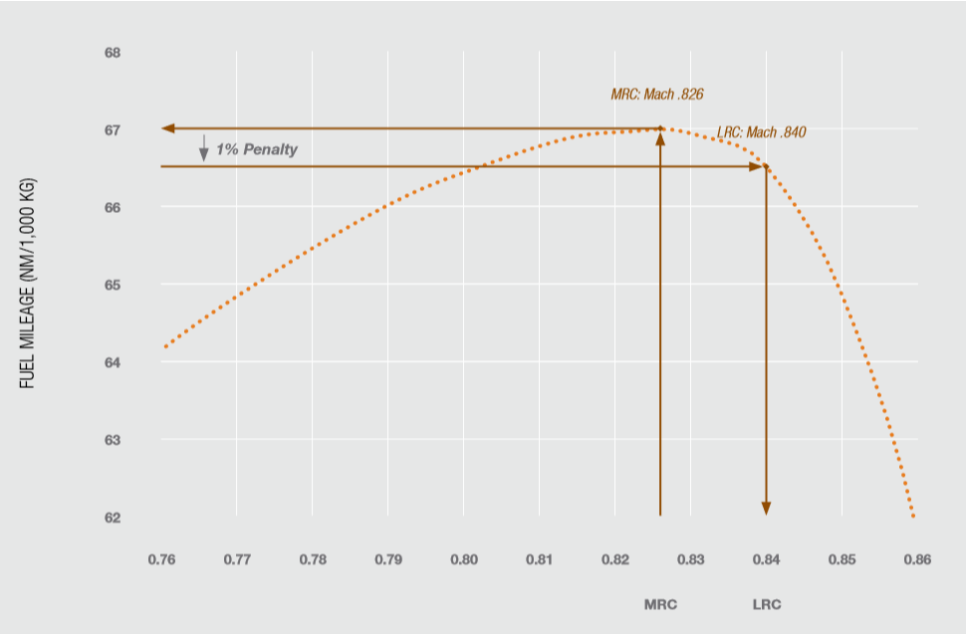

Figure 1.3: Long-range cruise speed in comparison to Maximum-range cruise speed taken from [60]

The speed corresponding to ECON speed typically lies between the speed for minimising the fuel consumption, (MRC) speed and the LRC speed [60].

The selection of the cruise speed is in addition to the mentioned trade-off between time dependent and fuel related costs also dependent on other parameters which can not be influenced. These include for example the presence of other traffic on a route segment which will yield a limitation to the allowed speed by air traffic control. Furthermore, an aircraft can be forced to fly faster to make up for a previous delay. In this case the aircraft will need to arrive close to its required arrival time to ensure passengers can get to a connecting flight and with that avoid any claims. All in all it can be concluded that minimizing fuel consumption and thereby minimizing part of the climate impact is only part of the objective of airliners. The operating speed is mainly a result of the objective of an airliner to minimize the total operating costs and being compliant to constraints imposed by air traffic control.

Altitude optimisation

Aircraft cruise altitudes mainly result from fuel and flight time efficiency with constraints imposed by aircraft performance and air traffic management [13]. In general the objective of an airliner is to fly at an altitude which minimizes the fuel consumption without compromising the flight time to a large extent. The fuel consumption can be decreased by reducing the aircraft drag. The drag is both a function of the atmospheric properties such as air density and the angle of attack at which the aircraft needs to fly to generate sufficient lift. At higher cruise altitudes the air is thinner which results in less atmospheric drag and therefore a reduced fuel consumption. However, for an aircraft to be able to cruise at this altitude and generate less drag the angle of attack should remain small to ensure it is in the so called low drag bucket. This effectively means that heavy aircraft do not cruise as high as light aircraft because they can not produce enough lift without compromising the optimum angle of attack corresponding to the lift coefficient maximizing C_L/C_{D^2}.

It is stated by Poll [58] that there exists an ideal flight level at which the fuel consumption is minimal depending on the instantaneous weight of the aircraft. This ideal flight level increases as the flight progresses since fuel is burned making the aircraft lighter. For an aircraft flying at a constant Mach number the ideal altitude will be maintained when climbing exactly the rate required to keep the lift coefficient constant [58]. This lift coefficient is the one maximizing C_L/C_{D^2} as discussed in the previous section. Furthermore, Poll [58] states that the final cruise altitude is approximately the same for all aircraft and is around 39,000 ft (37,000 to 41,000 ft) whereas the initial optimum cruise altitude is primarily driven by the distance to be flown where the longer the flight, the lower the initial cruise altitude. In practice, aircraft generally perform regular step climbs to higher altitudes since they have to be cleared by air traffic control before climbing to a different altitude.
Other constraints imposed by air traffic management originate from the minimum separation criteria which stipulates aircraft must be separated at least 1000 ft in vertical direction. With aircraft flying both directions this means that aircraft flying in eastward direction either have to fly at 38,000 ft or have to climb to 40,000 ft because aircraft are flying in opposite direction at 39,000 ft.

In the process of determining the optimum cruise altitude, the overall climate impact is not considered. This is because a decrease in fuel consumption will not evidently result in a reduced climate impact due to the large effect of the non-CO_2 forcing components. For this reason a flight altitude optimal for fuel efficiency does not ensure the altitude is climate optimal as well. This is because the climate forcing is dependent on both the quantity of the emission and the emission location [19],[13]. There exists a potential to reduce the overall aircraft climate impact further by reducing aircraft climate effects other than that of CO_2. As the climate impact of non-CO_2 forcings is strongly dependent on ambient conditions, changing the emission location can result in a large climate impact reduction. In particular, the coverage by persistent contrails might be reduced, as their formation is dependent on ambient atmospheric conditions, which vary with altitude. Additionally, aircraft NO_x emissions and the subsequent production of ozone are affected as well for a change in flight altitudes. In this study the mitigation option of relocating cruise altitudes is explored to analyze the sensitivity of the climate impact to emission altitudes. This will be done by globally relocating cruise altitudes for a set of flight trajectories for two different aircraft types. Two different aircraft types are chosen with a different nominal cruise altitude because it is expected that due to the differences in cruise altitude between aircraft types, their respective climate optimal cruise altitude and potential climate impact reduction will be different as well. The research objective of this study is presented in the next section.

1.5.4. Research objective

The external goal of this research is stated as follows:

The external goal of the research or the research objective is to contribute to the mitigation of aircraft induced climate change by proposing better operational alternatives in terms of optimal cruise altitudes with a reduced climate impact.

To be able to reach this objective the following research questions will be addressed within this study:

- Which aircraft types have the largest potential for climate impact reduction and therefore should be included in the analysis.
- What is the standard altitude profile of a typical mission performed by each specific aircraft type flying as of now? And what are the factors driving this altitude?
- How much emissions do these aircraft types produce by maintaining their actual altitude profile?
- At what location in the atmosphere considering latitude longitude and altitude do these emissions take place?
- What is the climate impact in terms of radiative forcing and temperature increase from the total amount of emissions corresponding each of these aircraft types.
- Can the climate impact be reduced if cruise altitudes are adjusted and which forcing components contribute the largest share to this reduction?
- Which cruise altitude results in the lowest amount of radiative forcing and temperature increase and therefore the smallest climate impact for each aircraft type?

2

Literature review

2.1. Aircraft combustion process and emissions

Aircraft produce emissions by burning kerosine where the most common used fuel type is Jet A -1. Jet fuel is a complex mixture of hydrocarbons that varies depending on the petroleum source and distillation process [54]. The mixture contains molecules having 6 to 16 carbon atoms and therefore it is impossible to define the exact composition of jet fuel. However the nominal chemical formula used in approximating the reaction products is $C_{12}H_{24}$ [21]. In the combustion chamber the fuel is mixed with air after which it is burned resulting in the combustion products CO_2 and H_2O. Other species in the exhaust plume are nitrogen, N_2 and oxygen, O_2 which are already present in the air and sulfur oxides, SO_x. Sulfur oxides are formed by the oxidation of sulfur present in the fuel. These combustion products are the result of complete combustion of the fuel. An actual engine however produces other products as well such as carbon monoxide (CO) which is formed by incomplete combustion. Incomplete combustion can also result in other unburned hydrocarbons (UHC). Furthermore, the air used for the combustion consists for the greater part of nitrogen which under high temperature and pressure conditions present in the combustion chamber can react with oxygen to form nitrogen oxides. In this reaction primarily NO is formed where nitrogen dioxide is formed after the combustion when there is sufficient oxygen present. A schematic of the combustion process is presented in Figure 2.1.

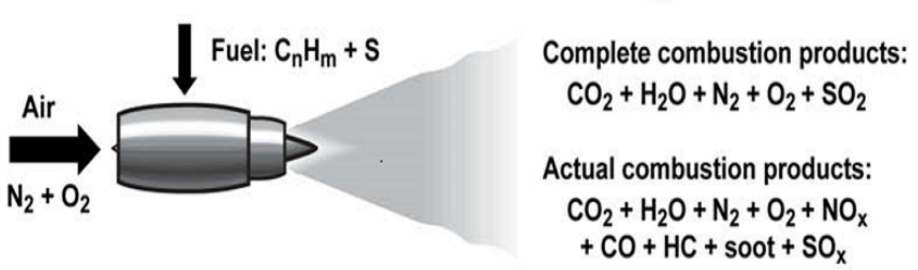

Figure 2.1: Aircraft emissions as a result of burning kerosine taken from [48]. In this figure unburned hydrocarbons are referred to as HC.

The quantity of the produced emission gases is determined by several factors including the fuel consumption, combustion efficiency and the fraction of hydrogen and carbon in the fuel. [15]. Most dominant is the fuel consumption where the more fuel is burnt the more emissions

are produced. For the ideal combustion products CO_2 and H_2O fuel consumption is the only factor involved. For the emissions of NO_x, SO_x, CO and UHC however, the combustion circumstances are of influence as well. Most important is the combustion temperature which is directly related to the thrust setting. Emissions of NO_x are increased for higher thrust settings when the temperature in the combustor is increased [21]. At these high trust settings nitrogen oxides are produced in the high temperature regions of the combustor through the oxidation of molecular nitrogen[15]. This is because at higher temperatures and pressure oxygen and nitrogen are more reactive resulting in more NO_x. Emissions of CO and UHC are commonly the result of incomplete combustion which can occur at lower thrust settings when the temperature and pressure in the engine are low [21].

Produced emissions are usually quantified by making use of an emission index which is defined by the amount of produced emissions per species in grams as a result of the combustion of 1 kg of fuel. Average values for emission indices for the combustion of kerosine are presented in Table 2.1 which is taken from Lee et al. (2010) [49]. Emission indices for NO_x, CO, soot and UHC are taken from 2002 fleet averages computed within AERO2K [11]. Furthermore the emission rate (in million tonnes per year) is based on data from the international energy agency (IEA) [38]. In the next section the discussed emissions from aircraft will be categorized and elaborated upon.

Species	**Emission index, (g/kg)**	**Emission rate, (Mt/yr) for 2004**
Kerosine	-	224 (180-224)
CO_2	3160	700
H_2O	1240	275
NO_x	14 (12-17)	3
Soot	0.025 (0.01-0.05)	0.006
SO_2	0.8 (0.6-1.0)	0.18
CO	3 (2-3)	0.67
UHC	0.4 (0.1-0.6)	0.09

Table 2.1: Emission species with their respective emission indices and annual emission rate taken from [49]

2.2. Climate impact of individual emission species

In this section all emission species will be discussed which are formed directly or indirectly by aircraft. Additionally the effect of contrails will be discussed. Thereafter their estimated impact on the climate will be evaluated based on most recent studies.

2.2.1. Carbon containing species

As observed from Table 2.1 the emitted gas of the largest quantity is CO_2 which is a widely recognized greenhouse gas. For complete combustion 3,160 grams of CO_2 form per kilogram of kerosine. Similar to other greenhouse gases CO_2 absorbs and emits part of the infra red radiation emitted by the earths surface and thereby keeps part of the energy in the earths system causing a warming effect. CO_2 is considered a long term greenhouse gas because it has an average atmospheric lifetime of more than 100 years [21]. Not one single lifetime for CO_2 can be defined because of the different uptake rates by different removal processes [40]. Examples of uptake processes are oceanic uptake and uptake by vegetation. This average lifetime is long compared to other greenhouse gases such as ozone which has an average lifetime in the order of weeks [49]. This effectively means that CO_2 emissions produced now will still have a warming effect in the future.

Other carbon containing species are CO and other unburned hydrocarbons (UHC) which are the result of incomplete combustion. Their emission indices are greater at lower power conditions [49]. Although to a lesser extent than emissions of NO_x, increases in carbon monoxide and non-methane hydrocarbons can perturb the ozone balance in the upper troposphere and lower stratosphere [15]. This is by affecting the ozone production and loss mechanisms. Non-methane hydrocarbons react with OH and O_2 and thereby enhance HO_2 formation and with that the formation of ozone [49]. This process will be discussed in more detail in the next section.

2.2.2. Nitrogen containing species

Aircraft emissions of NO_x are not radiatively active themselves, but they do have an effect on the budgets of the radiatively active gases CH_4 and O_3 [12]. In the upper troposphere and lower stratosphere emissions of NO_x lead to the production of O_3. Furthermore NO_x emissions have the effect of reducing the lifetime of methane. The effect of increased ozone concentrations have warming effect whereas the reduced levels of methane concentrations have cooling effect since they are both green house gases [49]. Furthermore emissions of NO_x have the effect of reducing stratospheric ozone [19]. All of these effects will be discussed in more detail in the following sections.

Ozone formation

Ozone is being formed as a result of the photochemical oxidation of carbon monoxide and higher hydrocarbons under the influence of solar radiation and in the presence of nitrogen oxides [19]. The processes involved are visualized in Figure 2.2 where it can be seen that NO_x is a key molecule in the reaction process acting as a katalyst. Furthermore, carbon compounds are required to react with OH to produce HO_2 which is necessary to form NO_2 [49]. The main reactions resulting in the production of ozone are shown in Equation 2.1 to 2.5 [12].

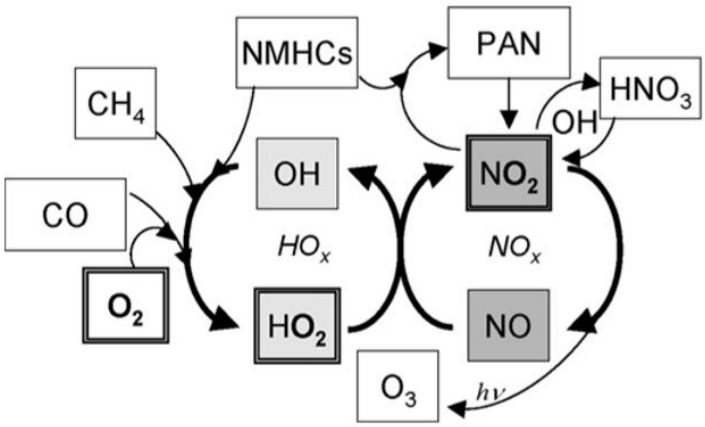

Figure 2.2: Main tropospheric O_3-related chemistry taken from [49]

$$CO + OH \rightarrow CO_2 + H \tag{2.1}$$

$$H + O_2 + M \rightarrow HO_2 + M \tag{2.2}$$

$$NO + HO_2 \rightarrow NO_2 + OH \tag{2.3}$$

$$NO_2 + h\nu \rightarrow NO + O \tag{2.4}$$

$$O + O_2 + M \rightarrow O_3 + M \tag{2.5}$$

In reaction 2.1 and 2.2 the oxidation of carbon monoxide through OH leads to the formation of HO_2. Reaction 2.3 shows the reaction of HO_2 with NO to form NO_2. In reaction 2.4 NO_2 is photolyzed resulting in atomic oxygen which reacts with oxygen to form ozone in reaction 2.5 where M represents any third body [49]. Besides carbon monoxide, the oxidation of CH_4 or other non-methane hydrocarbons ($NMHCs$) can lead to ozone formation as well. In this case reactions 2.1 to 2.2 are replaced by reactions 2.6 to 2.9 [12].

$$CH_4 + OH \rightarrow CH_3 + H_2O \tag{2.6}$$

$$CH_3 + O_2 + M \rightarrow CH_3O_2 + M \tag{2.7}$$

$$CH_3O_2 + NO \rightarrow CH_3O + NO_2 \tag{2.8}$$

$$CH_3O + O_2 \rightarrow CH_2O + HO_2 \tag{2.9}$$

As can be seen from the reactions and Figure 2.2 the main influence of NO_x on the formation of ozone is that is changes the HO_2 to OH ratio in the atmosphere. The influence of NO_x however is dependent on the background NO_x concentration where at present background mixing ratios of NO_x in the upper troposphere and lower stratosphere, additional NO_x produced by aircraft lead to enhancement of reactions 2.3 and 2.4 [49][12]. In this case the HO_2 to OH ratio is changed in favor of OH which increases the net O_3 production through reactions 2.4 and 2.5. At high background NO_x concentrations however, additional NO_x can result in a net loss of OH and HO_2 (together HO_x) followed by a decrease in O_3 production [12]. These high NO_x concentrations can be found in the lowermost stratosphere at northern high latitudes. Additional NO_x can reduce HO_x concentrations through reactions 2.10 and 2.11 [12]. As a result of this shortage of HO_x reactions 2.1 to 2.3 are diminished resulting in a lower ozone production. The non-linear dependency of the OH concentration and ozone production rate on the background NO_x mixing ratio is shown in Figure 2.3 [4] where it can be observed that ozone production increase at NO_x mixing ratios up to about 0.1-0.2 ppbv.

$$OH + NO_2 + M \rightarrow HNO_3 + M \tag{2.10}$$

$$HO_2 + NO_2 + M \rightarrow HNO_4 + M \tag{2.11}$$

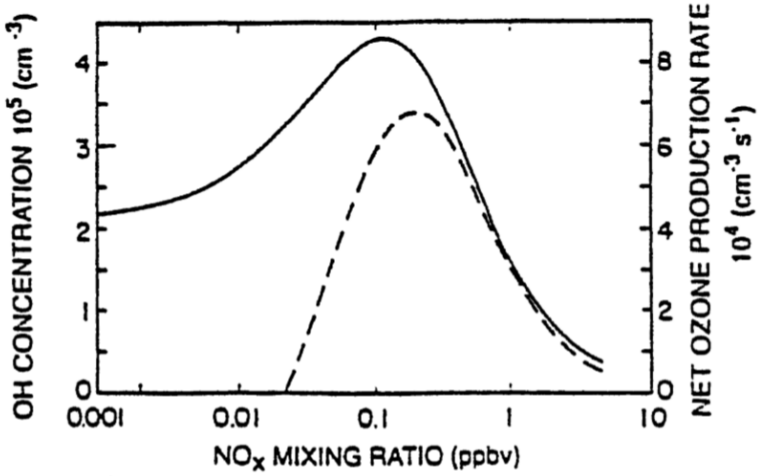

Figure 2.3: Model calculated net ozone production (dashed line) and OH-concentration as function of the ambient NO_x mixing ratio in parts per billion volume (ppbv). Figure taken from Brasseur et al. (1998) [4].

By influencing the HO_2 to OH ratio in the atmosphere, NO_x emissions not only have an influence on the ozone production rates but on the ozone destruction rates as well. In the mid and lower troposphere with low NO_x background conditions, O_3 loss is enhanced by the reaction of ozone with HO_2 or OH through reactions 2.12 and 2.13. On the other hand, in the lower stratosphere in northern high latitudes where the background NO_x concentration is high, ozone loss is reduced because of reduced OH and HO_2 mixing ratios [12].

$$O_3 + HO_2 \rightarrow OH + 2O_2 \tag{2.12}$$

$$O_3 + OH \rightarrow HO_2 + O_2 \tag{2.13}$$

In summary, the change in NO_x concentrations non-linearly affects the simulated ozone production and destruction rates depending on the location in the atmosphere [24]. The increases in production rates is mainly due to the increased concentrations of NO_2 as a result of reaction 2.3 which photolyzes according to reaction 2.4 and subsequently results in the production of ozone. Furthermore an increase in ozone concentrations results in higher destruction rates in the mid and lower troposphere. All influences combined an approximate linear relation between NO_x emissions and O_3 perturbations has been found for magnitudes similar to present aircraft NO_x emissions [25]. Furthermore because of low background NO_x concentrations, a high NO/NO_2 ratio and low HO_x concentration, ozone production is most efficient in the upper troposphere and lower stratosphere in mid-latitudes [57].

The NO_x emissions from aircraft only represent only 3% of the total emissions of NO_x from man-made and natural sources in the 1990's [65]. However the contribution of aviation to the NO_x concentration in the upper troposphere is much larger, namely 30-40% for traffic in 1990 according to Grewe et al. (2002) [24]. This is because aircraft emit the NO_x emissions directly in the upper troposphere and lower stratosphere where the exhaust gases have a longer lifetime than at the earth surface. This is due to less vertical mixing and the absence of washout processes [19]. These processes are more active at lower altitudes resulting in less forcing. A longer residence time allows the concentrations of NO_x and ozone to accumulate to larger and more persistent perturbations [19].

Furthermore Hansen et al. (1997) [28] found that the typical cruise altitude of aircraft is more sensitive to changes in ozone concentration than other altitudes. An equal perturbation of the ozone concentration in different layers of the atmosphere resulted in a larger temperature response between 8 and 13 km altitude. Schumann et al. (1997) [65] stated that this sensitivity is partly due to the low background concentrations. Furthermore this is the effect of the low temperature at these altitudes [71]. The latter is because the radiative forcing from ozone is proportional to the temperature difference at which infrared radiation is emitted and absorbed by ozone [12]. Therefore because they are emitted at high altitudes, aircraft NO_x emissions are disproportionately important to the total O_3 radiative forcing [19].

Tropospheric methane reduction

Besides the effect of NO_x emissions on the ozone concentration, they generally also increase the concentrations of OH radicals in the troposphere [18]. This was already observed in reaction 2.3 [12]. Higher levels of tropospheric OH reduce the lifetimes of gases removed by reaction with OH of which methane is one. This is because OH enhances the oxidation of hydrocarbons. This reaction is shown in Equation 2.14 [12]. Furthermore a second effect is that destruction of the previously formed ozone also results in the formation of more OH by Equation 2.12 [12]. Therefore the presence of NO_x and ozone both have a reducing effect on the ambient concentrations of methane. Since methane is a strong greenhouse gas a reduction results in negative effect on the climate forcing.

$$CH_4 + OH \rightarrow CH_3 + H_2O \tag{2.14}$$

Another effect of the reduction of methane is that less ozone is formed. As discussed above and shown by reactions 2.6 to 2.9, methane is an important precursor of tropospheric ozone. Therefore the induced methane reduction results in a small but long-term reduction in ozone which is referred to as primary mode ozone (PMO) [16].

Stratospheric ozone depletion

As mentioned, NO_x leads to ozone production in the troposphere and lower stratosphere due to the oxidation of hydrocarbons. Higher up in the stratosphere however these hydrocarbons become less abundant. Thereby reducing the ozone production. Furthermore ozone will deplete under the influence of NO_x due to catalyctic ozone depletion cycles [44]. The corresponding reactions are shown in Equations 2.15 and 2.16 [47].

$$NO + O_3 \rightarrow NO_2 + O_2 \tag{2.15}$$

$$NO_2 + O \rightarrow NO + O_2 \tag{2.16}$$

From these reactions it can be seen that the NO molecule is recycled and can destroy many ozone molecules. It should be noted however that subsonic aircraft emit NO_x in the stratosphere only directly in the mid and high latitudes where the circulation is directed downwards [49]. Consequently, ozone depletion can only occur due to emissions of NO_x in the tropical regions where the emissions can circulate upwards. However in this region there still are NO_x washout processes present which limit the impact of stratospheric ozone depletion by subsonic aviation. Therefore this effect is small [19] [24].

2.2.3. Water vapor and contrails

Similar to CO_2, water vapor is a greenhouse gas and therefore water vapor emissions have a warming effect. Although large quantities of water vapor are emitted as observed from Table 2.1, the climate impact of water vapor from subsonic aircraft is small compared with other emissions. The reason for this is that the amount of additional water vapor from aircraft is small compared to the background levels in the tropopause region [12]. When emitted in the stratosphere however, where the background water vapor concentration is low, aircraft water vapor emissions have a larger effect. The dependency of the emission location to the climate impact will be further elaborated upon in Section 2.4

Contrail formation

Besides being a greenhouse gas, water vapor emissions in the upper troposphere and lower stratosphere are the precursor of the formation of condensation trails (contrails) in the wake of an aircraft. Contrails can be short or long lived depending on the atmospheric conditions [46]. Long lived contrails are contrails which remain for at least 10 minutes [46]. Contrails can be subdivided into two different groups depending on their shape. If the contrails remain a linear shape they are referred to as persistent contrails whereas if they do not remain line-shaped they are referred to as contrail cirrus [46]. The two types combined are called aircraft-induced clouds [46] however sometimes also referred to as contrail cirrus [5]. To avoid confusion, in the rest of this work the effect of both contrail types, line shaped and contrail cirrus will be addressed as contrail cirrus. Contrails have an effect on the climate because they reduce the incoming short wave radiation by reflecting sunlight while also reducing the outgoing long wave radiation [9] [49]. On average the reduction in long wave forcing dominates the negative short wave forcing resulting in an overall warming effect [53]. The climate effect of contrails is mainly dependent on the size of the contrail, measured in coverage and the optical dept [53] where largest climate impact by contrails is from thick and wide contrails [66].

Contrails consist of very small ice particles and form behind an aircraft engine if, among other conditions, the ambient air is cold enough [52]. To form contrails the ambient air typically must be colder than -40 degrees centigrade however the precise value depends on other ambient conditions including air pressure and humidity [64]. Furthermore the properties of the engine exhaust gases such as the amount of heat and water vapor released are of relevance as well. All of these parameters are included in the so called Schmidt-Appleman criterion [2] which determines if a contrail will form. More into detail, Appleman et al. [2] states that contrails originate from the emitted water vapor leading to condensation on nuclei which can be preexisting or formed in the exhaust with subsequent freezing.

For contrails to be formed, the air needs to be saturated with respect to water at some point during the mixing of the exhaust gases with the ambient air. This is when the water vapor concentration exceeds saturation water concentration. This saturation concentration however increases with temperature due to the simultaneous heat release. Therefore the temperature at which contrails can form must be low to have a low saturation concentration [2]. Additionally, for the contrails to persist, the ambient air needs to be saturated with respect to ice, otherwise the contrails will evaporate after formation[12] [64]. The contrails then persist until its relative humidity drops below ice saturation.

Besides the dependency on the atmospheric conditions, the characteristics of the engine exhaust gases play an important role in the formation of contrails as well. The theoretical model of Schmidt and Appleman [2] states that the only relevant engine exhaust parameter is the ratio of water and heat released into the exhaust plume. Furthermore Schumann et al. (1996) [64] found that the threshold temperature at which contrails form increases with overall propulsive efficiency. This is because engines with higher overall propulsion efficiency distribute a smaller fraction of the combustion heat into the exhaust plume and thereby cause plume conditions which during the mixing reach a higher relative humidity for the same ambient temperature. This effectively results in the formation of contrails at higher ambient temperatures found at lower altitudes.
In addition to the contrail formation criteria, the optical contrail properties are found to be influenced by altitude as well. The optical properties of contrails have an influence on the respective radiative forcing where mainly the optical dept is of importance where optically thicker contrails are expected to cause a larger radiative forcing than thinner ones [53].

When a contrail is formed in a region where the air is supersaturated with respect to ice, the contrails can spread and grow by uptake of ambient water vapor [52]. These ice super saturated regions (ISSRs) cover a large horizontal area (width and length in the order of 100 km) [20] This spreading of the linear contrail results in cirrus clouds which are called contrail cirrus and can not be distinguished from natural cirrus. Contrails and contrail cirrus can vanish by means of evaporation. This takes place when the ice particles sediment into dryer layers or the air warms [52]. The average lifetime of persistent contrails is in the order of hours and are therefore considered short-lived forcings [55].

2.2.4. Sulphur containing species

Although the sulphur content of kerosine is small, there are emissions of sulphur containing gases present in the exhaust plume. This is because fuel sulphur is oxidized to SO_2 in the combustor. These emissions of sulphate particles result in a negative radiative forcing or cooling [49].

2.2.5. Aerosols

Anthropogenic aerosols can be microscopic airborne particles or droplets can reflect solar radiation which leads to a cooling effect on the climate. Soot particles on the other hand tend to warm the climate system because they can absorb solar radiation [40]. Soot particles are composed of organic compounds and of elemental or black carbon [49]. Furthermore aerosol particles can have an effect on the formation of clouds by changing their properties and lifetimes [40]. Therefore, although they have a short lifetime in the order of days to weeks because they are removed by precipitation, they can have a significant effect which overall is estimated to be cooling. This effect however is complex and not yet well known.

2.3. Quantification of aviations climate impact

The climate impact of aviation is by convention quantified using the metric of radiative forcing (RF) [48]. Radiative forcing or climate forcing is a quantification metric which is defined by the difference of energy absorbed by the earths atmosphere and the energy radiated back. It can be seen as nett flux of energy into the system. According to the IPCC [39] such a perturbation can originate from changes in the concentrations of radiatively active species such as for example CO_2, ozone and methane, changes in the solar irradiance incident upon the planet, or other changes that affect the radiative energy absorbed by the surface such as changes in surface reflection properties. This imbalance in the radiation budget has the potential to lead to changes in climate parameters and result in a new equilibrium temperature of the climate system. The radiative forcing is quantified at the tropopause or at the top of the atmosphere in units of watts per square meter (mWm^{-2}) of the Earth's surface. It is measured by the nett radiative flux change calculated to occur in the response to a perturbation [28]. The reason for using this metric is that experiments have found an approximately linear relationship between a change in global mean radiative forcing and a global mean surface temperature change [49]. This linear relationship can be characterised by Equation 2.17.

$$\Delta T_s \approx \lambda \cdot RF \tag{2.17}$$

In this equation T_s is the surface temperature for which the system has found an equilibrium where the input solar radiation equals the output radiation from Earth. Furthermore, λ is the climate sensitivity parameter ($K/(mWm^{-2})$ which is dependent on the forcing component as shown in Table 2.2 [59]. As a result the same radiative forcing from ozone and produces a different temperature response. Furthermore it should be noted that the global mean surface temperature change is calculated by assuming that the RF remains constant over the years [48].

Species	CO_2	O_3	CH_4	H_2O	Contrails
λ	0.73	1.00	0.86	0.83	0.43

Table 2.2: Climate sensitivity parameter λ in ($K/(mWm^{-2})$ determined by Ponater et al. (2006) [59]

2.3.1. Climate impact of individual forcing components

According to research from Lee et al. (2009) [48] the total radiative forcing from aviation in the year 2005 accounts to 55 (mWm^{-2}) excluding the influence of contrail induced cirrus. By including the effect of contrail cirrus the best estimate for the total radiative forcing as a result of aviation is 78 (mWm^{-2}) The contribution of the individual emission species and contrails is presented in Table 2.3.

Species	CO_2	O_3	CH_4	H_2O	contrails*	SO_4	Soot	Total
RF (mWm^{-2})	28.0	26.3	-12.5	2.8	11.8	-4.8	3.5	55.0

Table 2.3: Contribution to total radiative forcing per emission species according to Lee et al. (2009). *in this table only the climate impact of linear contrails is shown.

In this assessment the RF for CO_2 was calculated explicitly whereas the non-CO_2 RFs are scaled with fuel usage from reference values calculated with other climate models. However they do account for non-linear effects in the case of for example contrails where more traffic does not necessarily result in more contrails.

The reason for not including the effect of contrail induced cirrus or aircraft induced cirrus (AIC) is that the uncertainties are relatively high [48]. This does not mean that the estimated radiative forcings from contrail induced cirrus are expected to be low, on the contrary the mean climate effect is estimated to be 33 (mWm^{-2}) which is greater than the effect of the emission of CO_2. This forcing is in close agreement with the contrail cirrus forcing (including line shaped contrails) of 37.5 (mWm^{-2}) presented by Burkhardt and Kärcher (2011) [5]. What can be concluded from these radiative forcing numbers is that the contribution of CO_2 is only one third of the radiative forcings of all forcing agents combined (including contrail cirrus). This explains why aviation contributes disproportionately to the global climate forcing compared to the total transport sector as was mentioned in Chapter 1.

As discussed in the introduction the climate metric of RF is a function of the concentrations of greenhouse gases in the atmosphere. In the case of aviation these emission concentrations have build up from somewhere midway the 20th century until now. According to Lee et al. (2010) the RF from aviation is an increasing evolving mix of components where CO_2 emissions accumulate in the atmosphere and its RF increases whereas RF from ozone, methane aerosols and contrails are in a quasi steady-state [49]. The reason for this is that the lifetime of these emissions is significantly smaller compared to the lifetime of CO_2. As a result the RF from these short lived species reflects only the most recent emissions [49].

The downside of using RF as a climate metric is that it is an instantaneous metric which is based on the current emission concentrations in the atmosphere. Therefore it does not account for the timescales of climate response in terms of ΔT which is related to heat uptake by oceans [49]. Global mean surface temperature change or ΔT on the other hand is a more forward looking metric for assessing future climate impact [17]. This is because it stands close to the real impact on the climate. Furthermore ΔT does incorporate the history of RF and timescales of the systems response. If emissions from aviation would for example start to decrease, the radiative forcing from CO_2 would decrease slowly because it has a long lifetime. On the other hand radiative forcings from short lived species will decay much faster and with that the temperature increase will stabilize as well. Global mean surface temperature change is usually calculated for a certain time in the future where emissions and radiative forcings are calculated based on an assumed traffic growth scenario. Research from Frömming et al. (2012) [16] determined the global temperature increase and corresponding values for radiative forcing for the year 2100 based on TRADEOFF 2000 traffic and assuming a traffic growth according to the Fa1 scenario extended to 2100 [57]. This growth scenario constitutes of a average traffic growth rate of 3.1% per year and average growth rate of fuel burn of 1.7%. The results are presented in Table 2.4

Species	CO_2	O_3	CH_4	H_2O	Contrails	Total
RF (mWm^{-2})	101.3	57.5	-34.4	6.9	27.0	158.2
Δ T (mK)	54.3	42.5	-19.1	4.1	8.4	90.3

Table 2.4: Global annual mean net radiative forcing and global annual mean surface temperature response in the year 2100 for an increase of air traffic according to the $FA1_{2100}$ scenario [16]

From the Table 2.4 it is observed that CO_2 remains the largest contributor to climate forcing both in terms of radiative forcing and global mean surface temperature increase. Nevertheless the contribution of contrails to the overall radiative forcing is still considered significant enough to be addressed. It should be noted however that in the work from Frömming only the effect of linear contrails is considered. The climate impact of contrail cirrus is found to be about nine times larger than that of linear contrails according to Burkhardt and Kärcher (2011) [5].

2.4. Aviation climate impact dependency on emission altitude

The climate impact dependency on the emission location is different for each forcing component where in general a long atmospheric lifetime results in a low effect of the emission location. This is because when the atmospheric lifetime is long, for example in the order of 100 years for CO_2, the emissions eventually will be homogeneously distributed through the atmosphere making the emission location irrelevant. For this reason, especially the climate impact of the short-lived forcing components is influenced by the emission location. These include ozone, water vapor, contrails and to a lesser extent methane. This is because methane itself has a relatively long lifetime however the NO_x emissions influencing the methane lifetime have a much shorter lifetime in the order of hours to days. The dependency of the individual forcing components to the emission location will be elaborated on in the next section.

2.4.1. Effect of cruise altitude on the forcings of water vapor and contrails

The lifetime of water vapor perturbations in the atmosphere is very dependent on the emission altitude where simulations with the climate chemistry model E39/CA calculated perturbation lifetimes of 1 hour at ground level up to 24 months in the upper stratosphere [22]. As the climate effect of water vapor emissions qualitatively follow the pattern of the lifetime, emissions higher in the atmosphere result in a larger positive radiative foricing [22].

As explained, the formation of contrails is highly dependent on the atmospheric properties including the air temperature, pressure and humidity which are all dependent on the cruise altitude. Regions where the air is moist and cold enough to allow for the formation of contrails mainly occur in the tropopause region [13]. The altitude at which the tropopause starts however varies with latitude where it starts higher in the tropical region than at mid latitudes. This makes the location at which contrails can form not only dependent on altitude but also on latitude. Additionally there is a strong seasonal cycle of potential contrail coverage which reinforces contrail formation during winter [13].

In this context potential contrail coverage is defined as the maximum contrail coverage that could be obtained for a given atmospheric state if aircraft were flying everywhere. This coverage is significantly higher then the actual coverage. Furthermore the formation criteria is based on the thermodynamic theory of contrail formation according to the Schmidt-Appleman criterion [2].

To visualize the potential contrail coverage as function of altitude and latitude Figure 2.4 is shown (Fichter 2005). Here the tropopause is indicated by the solid black line and dotted lines are indicate the altitude band at which aircraft typically fly at. This is between 250 and 200 hPa corresponding to an altitude of approximately 34,000 and 39,000 ft.

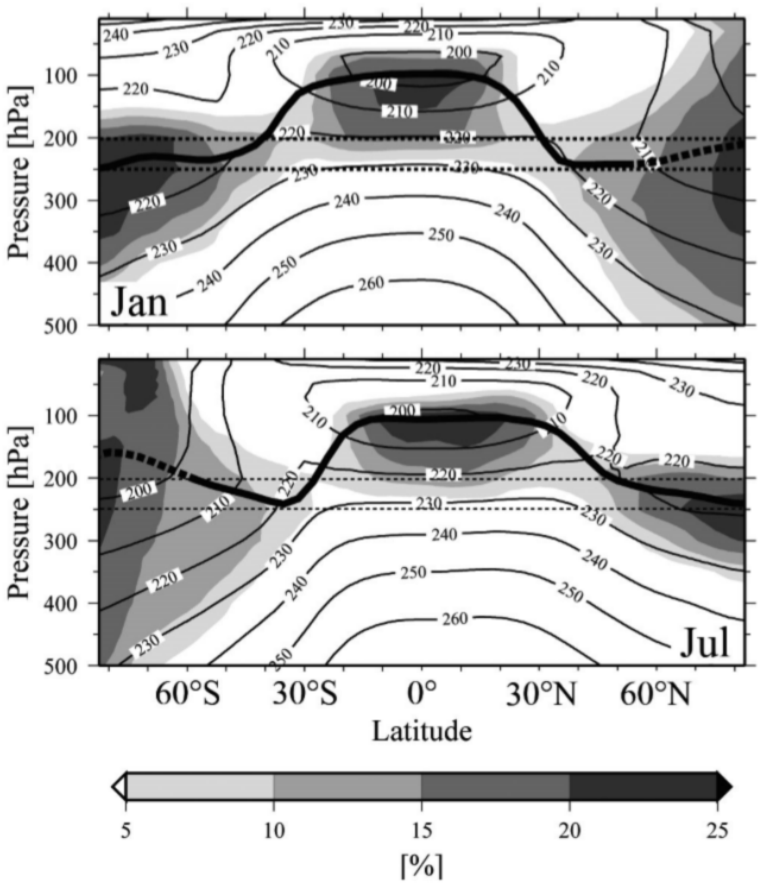

Figure 2.4: Mean potential contrail coverage with persistent contrails taken from [13]

From Figure 2.4 it is observed that the potential contrail formation is very dependent on altitude as well as latitude. For this reason Fichter [13] analyzed the impact of cruise altitude changes on the formation of contrails and the associated radiative forcing. This was done for the TRADEOFF emission scenario of which the details are shown in Appendix C. In this research standard flight altitudes which were based on actual flight data were lowered with respectively 2,000, 4,000 and 6,000 ft. As a result the global contrail coverage was reduced linearly with altitude with a maximum decrease of 45% for an altitude decrease of 6,000 ft. Consequently, the global annual mean radiative forcing is reduced by 45% as well. Increasing the flight altitude by 2,000 ft resulted in an increase in contrail coverage of 6%.

Interestingly, it was observed that by reducing flight altitudes not all regions showed a lower contrail coverage. For example in the northern mid-latitudes where most long haul- intercontinental flights are located an increase in contrail formation was observed with decreasing flight altitude. This is because long distance flights generally fly at higher altitudes in the lowermost stratosphere where ambient conditions are not suitable for contrail formation since it is too cold and dry [13]. This can be confirmed by looking at Figure 2.4 where for higher latitudes than approximately 50 degrees it is observed that the region above the mean tropopause facilitates a lower potential contrail coverage compared to flying at the tropopause itself. Therefore by shifting these flights downward into the upper troposphere where ambient conditions are suitable will therefore increase the contrail coverage. Apart from this, all other regions including the tropics, subtropics and low-level air traffic in the mid-latitudes showed to have a lower contrail coverage. This indicates that the benefit of shifting flights down is very dependent on the initial cruise altitude and the tropopause height which is a function of latitude. Displacing

flights upward by 2,000 ft on the other hand results in a lower contrail coverage in the northern mid-latitudes where most high altitude flights are located.

Besides the effect of geographical location influencing the tropopause altitude, there is also a seasonal effect present affecting the formation of contrails. It was found that during summer all regions show a reduced contrail formation by shifting cruise altitudes 6,000 ft down whereas during winter the high altitude traffic shows an increase in contrail formation.

2.4.2. Effect of cruise altitude on emissions of NO_x and resulting ozone and methane forcings

Research from Frömming et al. (2012) analyzed the effect of relocated cruise altitudes on the forcings of ozone and methane. Since the budgets of ozone and methane are influenced by the emissions of NO_x first the effect of flight altitude changes on the NO_x mixing ratios was analyzed. It was found that for a 2000 ft higher cruise altitude, the NO_x mixing ratios at 200 hPa increase by nearly 30 pptv whereas at lower flight altitudes corresponding to 300 hPa only a small (not listed) reduction in mixing ratios is found. When cruise altitudes are reduced by 6000 ft a large decrease in NO_x mixing ratios was found at the original flight level (around 250 hPa) whereas only a small increase was found at the lower altitudes although in total more NO_x is emitted due to the increased fuel consumption. Frömming states that the reason for this behaviour is the decreasing NO_x residence time with decreasing altitude. Due to the longer NO_x residence time at high altitudes, NO_x emissions can accumulate and NO_x mixing ratios can increase.

As a result of the lower NO_x mixing ratios at standard flight levels for the scenario with a cruise altitude relocated down, the O_3 production is decreased. At the lower flight levels however to where the cruise altitudes are relocated, the O_3 production is increased due to the higher NO_x mixing ratios. The overall effect on the nett ozone production however is negative since the lifetime of O_3 increases with altitude. Therefore the decrease in O_3 production at standard cruise altitudes is larger then the increase in O_3 production at lower cruise altitudes. This overall lower O_3 production results in a decrease of O_3 mixing ratios which reduces the O_3 forcing. For cruise altitudes relocated 2000 ft up, nett ozone production is increased since again the change in NO_x mixing ratios at higher altitudes is dominant over the change in NO_x mixing at lower altitudes. As a result the ozone forcing is increased.

The results found by Frömming are in agreement with the results found by Grewe et al. (2002) [24]. Here it was found that for flight levels located 1 km lower, NO_x concentrations at higher flight levels decreased up to 30% compared to when flying at standard flight altitudes. At the lower flight levels however the concentration of NO_x did increase although only 10%. The smaller increase at these lower altitudes compared to the large decrease at the higher altitudes was attributed to the increased mixing and a shorter lifetime at lower altitudes. The result of the changes in NO_x concentrations is that when flying at the original cruise altitudes the total induced ozone is 12.5 Tg whereas when flying lower this decreases to 11 Tg thereby reducing the climate impact.

The effect of the changed NO_x mixing ratios as function of a reduction in cruise altitude on the forcing of methane is analyzed by Frömming as well. Relocating cruise altitudes 6000 ft down was found to increase the total global mean OH concentration which results in a reduction of methane lifetime. As a result of this reduced lifetime the methane forcing is reduced. For higher flight altitudes the changed NO_x mixing ratios pattern was found to decrease the global OH concentration which increased the methane lifetime and the forcing.

2.4.3. Overall climate effect of changing cruise altitudes

Apart from the effect of the emissions of NO_x, Frömming et al. (2012)[16] analyzed the combined effect of relocating cruise altitudes on the climate impact of the emisions of H_2O and CO_2 as well. Similar to the research from Fichter et al. (2005) [13], Stordal et al. (2006) [69] and Grewe et al. (2002) [24] it was found that radiative forcings of short lived species (contrails and ozone) are reduced when flying lower whereas long term forcings of CO_2 are increased. By flying 6,000 ft lower it was found that the fuel consumption and with that the emission of CO_2 increased by more than 5% which is substantial. However in the long term this results in a total annual radiative forcing reduction of 26% for the year 2100. From this research it was concluded that incorporating knowledge about the altitude sensitivity of aviation impact offers substantial mitigation potential.

By analysing the effect of one single typical continental flight, Snijders and Melkert [68] found that the lowest climate impact after 150 years resulted for a cruise altitude of 6 km altitude. In this research all emission species were included including CO_2, ozone, contrails and cirrus. At higher cruise altitudes it was found that the lower fuel consumption resulting in less forcing by CO_2 was counteracted by the increase in climate forcings from contrails and cirrus clouds. Therefore the highest climate impact was found for an altitude of 10 km. By analysing the radiative forcings for a common cruise altitude of 11 km it was found that the largest forcing resulted from the combined contribution of contrail and cirrus clouds which is conform the findings in Sausen et al. (2005) [62].

All discussed studies show a potential for reducing climate effects by lowering the aircraft cruise altitudes. However the studies are based on scenarios that imply a general shift in altitude and therefore only investigates a generalized approach. A relocation method which makes a distinction in aircraft types would therefore have the potential to reduce the climate impact even further. This method will be discussed in the next section.

3

Methodology

3.1. General methodology

This analysis will compare the climate impact of actual flown trajectories with trajectories with a shift in cruise altitudes. The used method is schematically shown in Figure 3.1 and requires three types of input data: flight trajectory data, aircraft performance data and atmospheric weather data. These will be combined to calculate the fuel consumption for each flight and determine the corresponding emissions. These emissions will serve as input for a climate chemistry model which will evaluate the total climate impact of the data set used as input. This climate impact will be compared to the climate impact of a set of trajectories with a shifted altitude profile. Comparing the climate impact for different altitude scenarios will allow to determine the climate optimal altitude resulting in the lowest climate impact.

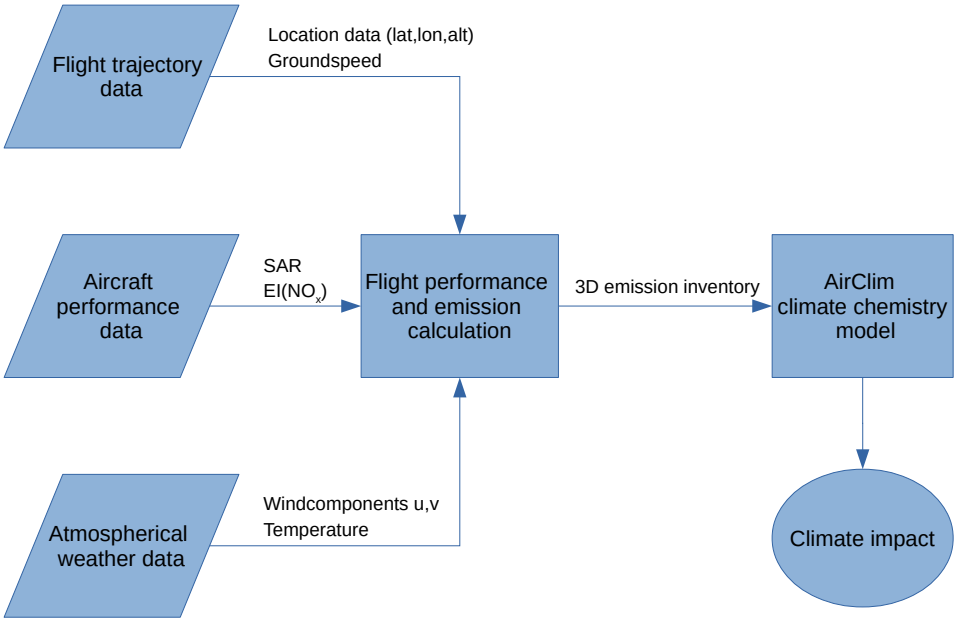

Figure 3.1: Overview of the general methodology followed in this study

3.2. Selection of aircraft types

Based on the findings of other studies discussed in Section 2.4 it can be stated that there is a potential for reducing the climate impact of aviation by changing aircraft cruise altitudes. The general outcome of the discussed studies however is based on scenarios that imply a shift in cruise altitude which is equal for all analyzed aircraft types and therefore is based on a generalized approach. The objective of this research is therefore to assess whether the climate optimal cruise altitude and the potential reduction in total climate impact are dependent on aircraft type. It is expected that due to the differences in cruise altitude between aircraft types their respective climate optimal cruise altitude and potential climate impact reduction will be different as well. This is because the further away an aircraft is shifted from its original trajectory the higher the fuel penalty is expected to be since the original altitude is assumed to be fuel optimal. This assumption will be justified in Section 4.7.4. To analyse the climate impact reduction as function of a shift in altitude and aircraft type, two different aircraft types will be selected for the analysis based on the criteria outlined in the next section. By following this approach it is expected that an even greater reduction in climate impact will be possible compared to the generalized approach.

3.2.1. Aircraft type selection criteria

Aircraft types for which the climate impact is analyzed in this study are selected based on the following five criteria:

- The aircraft types should generally perform long haul flights to maximise the potential for climate impact reduction.
- The market share of the aircraft types should be significant. The the larger the market share of the aircraft type, the larger the potential for climate impact reduction.
- The aircraft types should have a large difference in nominal cruise altitude. It is expected that a large initial difference in cruise altitude will result in large difference in climate optimal altitude.
- The average age of the aircraft fleet should be minimal. The older the aircraft type, the closer it is to its retirement age and the sooner it will be out-phased which lowers the potential for climate impact reduction.
- The chosen aircraft types should be represented in the Piano-X performance module.

The next sections will discuss the evaluation criteria in more detail and will narrow down the possible aircraft types for the to be performed analysis.

3.2.2. Cruise distance

The criterion for long cruise distance is based on two factors. First of all, long haul flights are considered to have a larger potential for climate impact reduction compared to short haul flights [8]. This is because of all flight phases, the cruise phase contributes most to the climate impact of each flight due to the larger quantity of the emissions and the more sensitive emission altitude. This second factor was found by research from Dahlmann et al. (2016) [8] which showed that short haul flights with a flight distance below 1,000 km have a lower climate impact per kilometre compared to long haul flights due to their lower cruise altitudes. Flying at a low cruise altitude results in a lower climate impact of the short term forcings including ozone, water vapor and contrail cirrus [8]. Additionally, the cruise phase offers the highest flexibility for

changes in altitude compared to take-off and approach which are more restricted by air traffic management constraints [8].

Secondly, aircraft types which typically perform short haul flights may not refuel at every destination and can carry the fuel required for trip number two already on board at trip one. This principle is called fuel tankering and can be economically more profitable due to location dependent fuel prices. Furthermore this reduces the turn around time since passengers can immediately board the aircraft after landing. Because of this reason it is more difficult to accurately estimate the fuel taken on board on a short haul flights compared to a long haul flights. For long haul flights fuel tankering is generally not possible since restrictions on maximum take-off weight and maximum landing weight make it infeasible to carry the extra fuel to the first destination. Based on these two reasons the analysis will focus on aircraft types which generally perform long haul flights.

Data from the MIT data project [1] showed that on average wide body aircraft types fly 8 hours per flight whereas narrow body aircraft fly less than 3 hours. For this reason, based on the requirement of long cruise distance it was chosen to focus on wide-body aircraft.

3.2.3. Market share

An overview of the market share of wide body aircraft types was constructed by the aviation research department of the DVB Bank [10] of which the ten most frequently occurring aircraft types are presented in Figure 3.2.

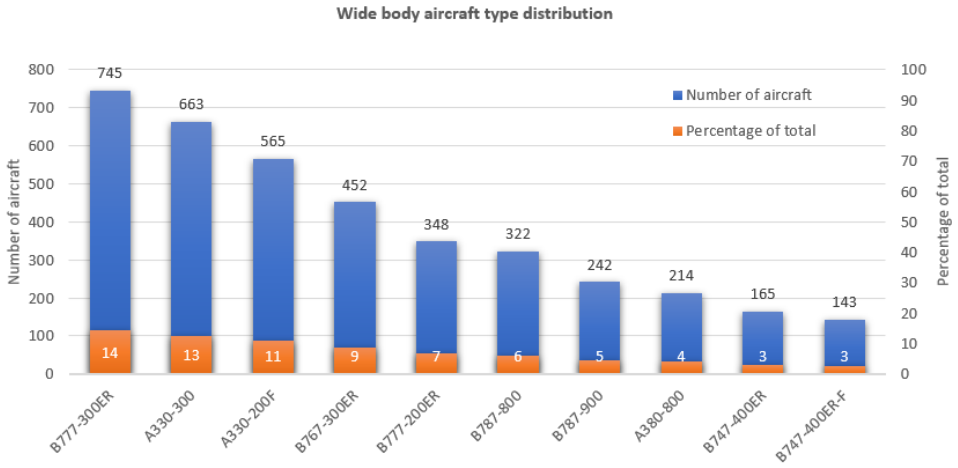

Figure 3.2: Top 10 wide body aircraft types of which there are the most in service where the total number is shown on top of the blue bar and the percentage of the total is shown inside the bar. Numbers are data found in [10] representative for September 2017

It this work it is assumed that aircraft types of which there are more in service fly more kilometres per year and therefore produce more emissions compared to aircraft types occurring less frequently. For this reason it is expected that by optimising the altitude profile of one of these ten aircraft types will result in the largest climate impact reduction.

[1] http://web.mit.edu/airlinedata/www/Res_IndusResources.html

3.2.4. Cruise altitude analysis based on Opensky network data

Aircraft generally fly at a cruise altitude between 30,000 and 40,000 ft (approximately 9 and 12 kilometres) with a peak between 33,000 and 38,000 ft [13]. However large differences between individual aircraft types were found by analysing aircraft trajectory data. To get a better insight in the nominal cruise altitude range of individual aircraft types an analysis was performed by using data from the Opensky network [2]. Similar to Flightradar24, Opensky provides real-world air traffic data based on collected ADS-B (Automatic Dependent Surveillance-Broadcast) and Mode S data. This data consists of the aircraft geographical location, altitude, groundspeed and aircraft identifier. The difference between Flightradar24 is that collected raw data by Opensky is archived in a large historical database which is primarily used for research. Flightradar24 on the other hand supplies data on a trajectory by trajectory basis which can be downloaded when a commercial subscription is acquired.

The advantage of the Opensky database is that it is freely accessible for research and that there is no limit on the amount of data that can be retrieved. This is not the case for Flightradar24 which is a commercial institution where there is a limit on the available data depending upon the acquired subscription level. Flightradar24 however does provide a better coverage due to its larger amount of receivers (20,000 compared to 2,275 for Opensky). This better coverage translates in a higher resolution of data instances per flight and results in smaller data loss periods per trajectory.

For the purpose of this preliminary analysis of the differences in cruise altitude between certain aircraft types it was chosen to use Opensky data instead of Flightradar24 data. This is because a large quantity of data was required (minimal 500 trajectories per aircraft type) over a short period of time (one day). Furthermore a very high resolution of data is not required since this preliminary analysis is performed merely to get a better insight in the flown altitude levels of the different aircraft types.

To assess the differences in flown cruise altitude per aircraft type, trajectory data was retrieved from the Opensky database by filtering on one specific aircraft type and limiting the time span to one week. This was done for six different aircraft types, the Boeing 787-800, Boeing 777-300ER, Boeing 767-300ER, Boeing 747-400, Airbus A330-300 and Airbus A380-800. Covered cruise distance were accumulated for each altitude band of 1000 ft. The results of this analysis are shown in Appendix A.

From Figure A1 it is observed that the Boeing 787-800 cruises at the highest cruise altitude of all analyzed aircraft types between 39,000 to 41,000 ft with a small peak at 43,000 ft. Aircraft flying significantly lower are the Boeing 767-300ER, Boeing 777-300ER and Boeing 747-400 which all show a peak at 35,000 ft as shown in Figures A2, A3 and A5. The Airbus A330-300 and Airbus A380-800 fly in between the two extremes, in the range from 35,000 ft to 40,000 ft as shown in Figures A4 and A6 respectively.

Based on these findings the Boeing 787-800 and Boeing 777-300ER are selected for the analysis. The Boeing 787-800 is selected because it flies at the upper region of the cruise altitude range which is unique. Furthermore the aircraft is in service since 2011 and therefore is expected to continue flying for the coming decades. The Boeing 777-300ER is selected because it flies significantly lower than the Boeing 787-800. Furthermore it is the youngest aircraft comparing it to the Boeing 747-400 and the Boeing 767-300ER and therefore is considered to have a larger potential for climate impact reduction.

[2] `https://opensky-network.org/`

3.3. Flight trajectory data

Flight trajectory data is acquired from Flightradar24 for all flights on November 20th and March 30th 2018 for two different aircraft types, the Boeing 787-800 and Boeing 777-300ER. The reason for selecting these aircraft types is discussed in Section 3.2.1. By analysing flight trajectories retrieved from the Opensky network it was found that the nominal cruise altitude of a Boeing 777-300ER is in the range of 33,000 ft to 35,000 ft and the Boeing 787-800 in the range of 39,000 ft to 41,000ft. Because of this large difference in cruise altitudes it is expected that the climate impact will be different for both aircraft.

For the purpose of this research historical as-flown flight trajectories are used instead of generic trajectories between city pairs. The advantage of actual flight trajectories over generic trajectories is that by definition actual trajectories are a realistic representation of the global distribution of flights both in geographical and vertical direction. Furthermore, using actual trajectories enables to include the effect of wind since the exact time and location of the aircraft trajectories are known. The effect of wind has a large influence on the fuel consumption as will be shown in Section 3.6.2.

To acquire a data set which is representative of the global traffic pattern, all flights departing on the 20th of November and 30th of March 2018 were analyzed. Two different non consecutive days were selected with the purpose to include multiple weather situations with a different wind pattern. Furthermore it was chosen to use Flightradar24 data instead of Opensky data because of its better quality as described in Section 3.2.4. The quality difference originates from the higher global coverage of the Flightradar24 receiver network which results in a larger number of datapoints per trajectory and a larger set of complete flights.

3.3.1. Flight track parameters

The trajectory data consists of data for the aircraft geographical position (latitude, longitude), vertical position (altitude), groundspeed, flight direction, time of flight and callsign. The frequency of the available datapoints is generally close to one point per minute. Within this research the data for groundspeed and altitude are assumed to be constant between two datapoints and equal to the value of the first datapoint.

3.3.2. Criteria for a valid track

Flightradar24 generates flight tracks based on aircraft transmitted ADS-B data received by one of their 20,000 connected receivers. Due to the high frequency used (1090 MHz) the coverage from each receiver is limited to about 250-450 km in all directions [3]. This distance depends on the location, where the more blockage by for instance buildings, the smaller the coverage. Furthermore, the further away from the receiver an aircraft is flying, the higher it has to fly to be covered by the receiver. This is partly due to the mentioned blockage and because of the curvature of the Earth. As a result of this distance limit, the coverage over the oceans is limited which is the main cause for flight tracks having a part with missing data. The larger the part of the flight track with missing data, the larger the related uncertainties which will translate to inaccuracies in the results. These inaccuracies will not only be present for the part of the trajectory for which the data is missing but also for the rest of the track. This is because the fuel consumption is a driving factor determining the take-off weight of the aircraft which influences the fuel consumption and produced emissions throughout the flight. Therefore to ensure the tracks used for the study will result in accurate results several criteria have been formulated and are listed below. Track which do not comply to these criteria have been omitted.

[3] https://www.flightradar24.com/how-it-works

- **Start and end of cruise phase should be present**
  The first and last data point of the trajectory should have an altitude of less than 20,000 ft. This is to be certain that the entire cruise phase is present.

- **Cruise phase should have a minimal duration of 30 minutes**
  The track should have a cruise segment, defined as a level segment at or above 25,000 ft with a duration of a minimum of 30 minutes. This ensures that the trajectory contains a cruise phase for which the emissions can be determined.

- **Time of data loss should be minimal**
  The track should not have lost coverage for more than 4 consecutive hours of the flight. This is because between these hours there is a gap in the data which will require interpolation techniques to analyse this part of the track. Very large gaps will result in larger uncertainties which translate into inaccuracy of the results.

- **Data loss in combination with an altitude shift should be avoided**
  The track should not include a step climb larger than 1,000 ft in combination with a loss of coverage for more than 2 hours. If there has been an altitude shift in time of a gap in the data it is not possible to locate the exact moment where this altitude shift has taken place and will therefore result in inaccurate results. Especially since the main objective of the research is to find the optimal cruise altitude.

3.3.3. Handling gaps in data

As a consequence of the selection criteria it is possible for tracks with gaps in the data to be considered valid for analysis as long as the altitude difference at the end of this period with respect to the start is not too large. The problem with trajectories with missing data however is that the calculated emissions can not be accurately projected on a geographical location. It has been considered to make use of complete tracks exclusively however this would result in a large fraction of flights flying across the oceans to be disregarded which in turn leads to an inaccurate representation of global emissions. Therefore it was chosen to use an interpolation method to estimate flight trajectory data during a so called gap in the data.

To determine the flight performance of the aircraft and the corresponding emissions during a gap a linear interpolation method is used to estimate the geographical location of the aircraft during this time. This is done by assuming the aircraft followed the minimal distance between point one (P1) and two (P2) which is by definition the great circle distance. A visualization of both points is shown in Figure 3.4 where the great circle distance is indicated by length g. Based on the desired step size, the location of N intermediate points on this great circle are determined between points P1 and P2. This is done by first converting the GPS coordinates to Cartesian coordinates according to the equations below.

$$x = cos(lon) \cdot cos(lat) \tag{3.1}$$

$$y = sin(lon) \cdot cos(lat) \tag{3.2}$$

$$z = sin(lat) \tag{3.3}$$

A graphical visualization of the location of x,y and z is shown in Figure 3.3. Secondly, the angle ψ was determined between the begin and endpoint on the great circle according to equation 3.3.3. This angle is shown in Figure 3.4

$$\psi = arccos(x_A x_B + y_A y_B + z_A z_B) \tag{3.4}$$

The points i at angular distance ϕ from point P1 are found according to equations 3.5 to 3.7 where if $\phi = 0$ the point is located at point P1 and when $\phi = \psi$ the point is located at point P2. Both angles are depicted in Figure 3.4.

$$x_i = \frac{x_1 sin(\psi - \phi_i) + x_2 sin(\phi_i)}{sin(\psi)} \tag{3.5}$$

$$y_i = \frac{y_1 sin(\psi - \phi_i) + y_2 sin(\phi_i)}{sin(\psi)} \tag{3.6}$$

$$z_i = \frac{z_1 sin(\psi - \phi_i) + z_2 sin(\phi_i)}{sin(\psi)} \tag{3.7}$$

These Cartesian coordinates are converted back to GPS coordinates by using Equations 3.8 and 3.9.

$$lat = arcsin(z_i) \tag{3.8}$$

$$lon = arctan(y_i, x_i) \tag{3.9}$$

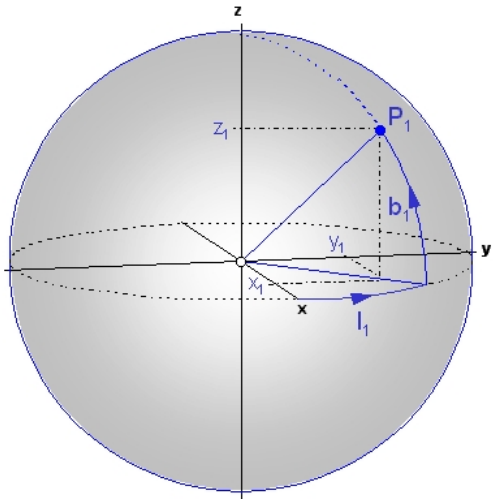

Figure 3.3: Schematic Figure showing point P1 and its conversion from GPS to Carthesian coordinates

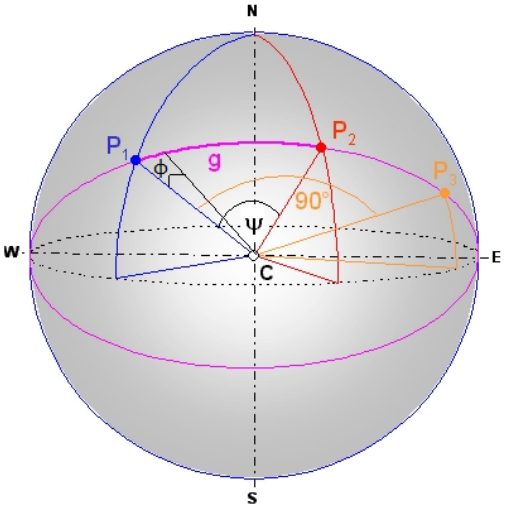

Figure 3.4: Schematic Figure showing the great circle distance between points P1 and P2 and the angle ψ between both points

To visualize the results of this interpolation Figure 3.5 is presented which shows a flight track crossing the Atlantic ocean from Paris to Chicago on November 20th. The original track is shown in red and shows a gap in data above the Atlantic ocean. The interpolated coordinates are shown in green which represent the great circle route connecting the first and second half of the trajectory. It should be noted that for illustrational purposes a distance of 40 kilometers was taken as spacing between the interpolated points. For the actual analysis this spacing is set equivalent to the spacing of the other data points.

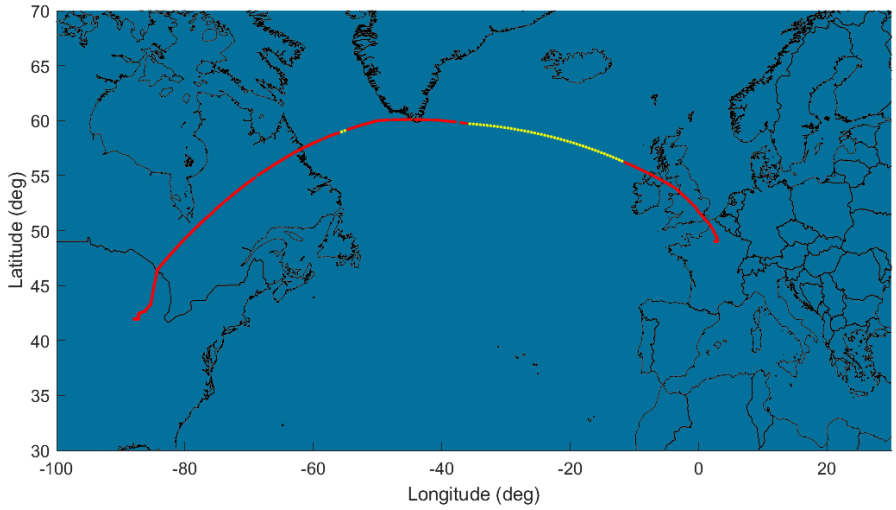

Figure 3.5: World map showing one interpolated flight trajectory from Paris to Chicago where the interpolated aircraft location is shown by the green dots

Besides the geographical location, the aircraft altitude is interpolated as well. For the altitude it is assumed that the aircraft will remain at the altitude at which it is flying at the start of the gap since there is no information available regarding any performed step climbs.

3.3.4. Selection of cruise segment

With the objective to find the produced emissions during the cruise phase of the flight, the first step is to distinguish the part of the flight which corresponds to this phase. A general flight consists of three phases, a climb, cruise and descent phase. The beginning of the cruise phase was taken as the first level segment above an altitude of 25,000 ft which lasted more than 10 minutes and the final level segment as the last level segment meeting the same criteria. Figure 3.6 displays an example of the altitude profile of a track where the segment selected as cruise phase is shown in blue.

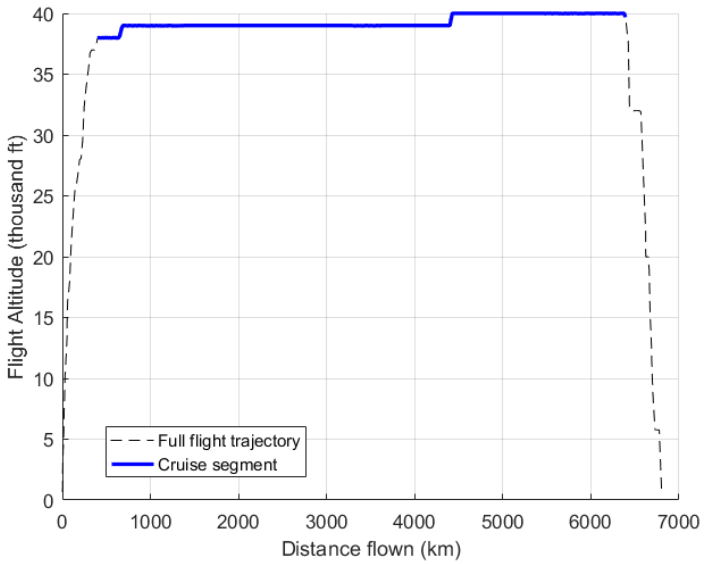

Figure 3.6: Visualization of cruise phase of flight track

3.3.5. Length cruise segments

The emissions during the cruise phase of the flight will be determined by discretizing the entire cruise segment into a finite number of smaller cruise segments. These cruise segments are defined as the segments in between the available data points. This results in an average segment length in the order of 15 kilometers which translates to a resolution of approximately 0.1 by 0.1 degrees. This is considered a small enough grid to determine the emissions. After the individual cruise segments are determined the emissions during these segments will be determined and will be accumulated at each available coordinate point.

To determine the emissions during each cruise segment, first the exact length of each segment is determined by assuming a great circle route is flown in between two location points (P1 and P2) such that a minimal distance is flown. A visualization of such a great circle route is shown in Figure 3.4. To find the distance between two coordinates on a great circle, the Haversine formula is used to find this distance d as shown in Equation 3.10.

$$d = 2r \cdot arcsin\left(\sqrt{sin^2\left(\frac{\phi_2 - \phi_1}{2}\right) + cos(\phi_1) \cdot cos(\phi_2) \cdot sin^2\left(\frac{\lambda_2 - \lambda_1}{2}\right)}\right) \tag{3.10}$$

In this equation the subscripts 1 and 2 indicate the two location points between which the distance is calculated. Furthermore, ϕ is the latitude, λ is the longitude and r is the radius of the Earth which assumed constant and equal to 6371 km. Here the aircraft height above the Earth surface is not taken into account since it is assumed negligible (in the order of 0.1%).

3.4. Aircraft performance data

Aircraft performance data is required to determine the instantaneous fuel consumption during every cruise segment. This performance data is provided by Lissys Piano-X which is commercial aircraft performance software. The performance data in Piano-X is derived from first principles based on aerodynamics, aircraft mass and engine characteristics and tuned using data from airlines and manufacturers [43]. Piano-X is widely used in other academic researches to determine emissions based on aircraft types and flight profiles [51],[16],[13] and [27]. Section 3.4.3 will further elaborate on the Piano-X performance model which includes the verification of the performance data. Figure 3.7 shows a flowchart indicating the input and output of the performance module. This section will elaborate on both.

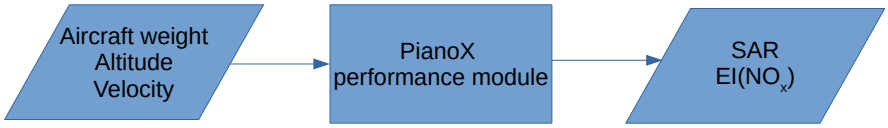

Figure 3.7: Flowchart of the Piano-X performance module

3.4.1. Specific air range

One of the functions of Piano-X is the instantaneous point performance module which allows to calculate the specific air range (SAR) at every point during cruise flight based on three input parameters; altitude, weight and velocity. The specific air range is the derivative of the distance flown with respect to the change in mass (fuel). Which can also be described as the air range per kilogram of fuel consumption. For the air range the Brequet range equation is considered, previously shown in Equation 1.1. However, the weight is substituted by mass (m) times acceleration (g) and the airspeed is substituted by the Mach number (M) and speed of sound (a). The resulting equation for air range (X) is shown in Equation 3.11.

$$X = \int_{m_2}^{m_1} \frac{M \cdot a}{g \cdot c_T} \frac{C_L}{C_D} \frac{dm}{m} \tag{3.11}$$

In this equation c_T is defined as the specific fuel consumption. By taking the derivative with respect to mass, Equation 3.12 is found for the specific air range [14].

$$SAR = \frac{dX}{dm} = \frac{M}{W}\left(\frac{L}{D}\right)\frac{a}{c_T} = f(W, M, h) \tag{3.12}$$

From Equation 3.12 it is observed that the SAR depends on the Mach number and instantaneous weight of the aircraft which are both inputs in the point performance module. Furthermore SAR depends on the value for lift over drag, which is determined based on the required value for lift coefficient which depends on the weight of the aircraft, velocity (Mach number) and altitude through density. Aerodynamic drag is calculated as a function of lift coefficient, Mach number and Reynolds number and tuned with actual lift over drag data whenever these are known. The aircraft fuel flow is determined based on the assumption of steady flight where thrust equals drag and from the fuel flow the specific fuel consumption is determined. Finally the speed of sound is determined based on the used input for altitude. As a result only three input values are required to determine the specific air range which are aircraft weight (W), Mach number (M) and flight altitude (h).

This specific air range however needs to be corrected for wind since the actual distance covered on the ground is a function of both airspeed and windspeed. This actual distance covered per

kilogram of fuel is defined as the specific ground range (SGR) which is found by multiplying the SAR by the ratio of groundspeed over airspeed as will be discussed in Section 3.6.

3.4.2. Emission index nitrogen oxides

In contrast to the emission index of CO_2, the emission index of nitrogen oxides (EI_{NO_x}) is not constant and depends mainly on the conditions in the combustion chamber which depend on the fuel flow. Piano-X determines this emission index based on tested engine characteristics for four conditions representative for idle, approach, climb-out and take-off which are found in the ICAO aircraft engine emissions databank [33]. The listed emission indices are provided by the engine manufacturers and the emissions indices during arbitrary flight conditions are derived by a method based on fuel flow (the Boeing 2 fuel flow method) [50].

3.4.3. Verification Piano-X performance data

Piano-X has been verified with Eurocontrols Base of Aircraft Data (BADA version 3.3) in the AERO2k project (Eyers 2004) [11] and in Jensen et al. (2005) [43] with BADA revision 3.6. Jensen found that Piano-X SAR contours showed reasonable agreement near the optimal cruise speed and altitude operating points. For these conditions it was found that the SAR calculated by PianoX is between 6% lower and 2% higher compared to BADA revision 3.6. However far away from the optimal speed and altitude PianoX showed stronger efficiency penalties mainly for high aircraft weights (no numbers are shown). Here it should be noted however that Jensen compared Piano-X to BADA Revision 3.6 which according to Jensen uses a simplified parametric approach for aerodynamic and propulsive performance which may reduce the accuracy of the model. Furthermore the specific aircraft types for which the comparison is performed are not presented. Secondly, Eyers compared the fuel flow rate calculated with Piano-X and BADA version 3.3 for 26 different aircraft types calculated for 10 different cruise altitudes and three aircraft weights. From this comparison it was found that as an average Piano-X predicts a 4.7% higher fuel consumption. It should be noted however that the specific aircraft types used in this study are not considered in this comparison and that the Piano-X version used for this comparison dates back to 2004.

Summarizing the results found by Eyers and Jensen it can be stated that overall Piano-X tends to calculate a higher fuel consumption (lower SAR) compared to BADA version 3.3 and 3.6. Additionally, the results presented by Jensen indicate that this difference increases when moving away from the optimal altitude. The differences however are considered to be acceptable and therefore Piano-X will be used to determine the aircraft performance in this work.

3.4.4. Regression analysis

Since the user interface of Piano-X does not allow it to be accessed from outside the tools environment by a numerical program it is not practical to determine the aircraft performance for every combination of Mach number, weight and altitude individually. For this reason it is chosen to perform a regression analysis for SAR and the emission index of NO_x based on a range of input values for flight conditions. The regression of the data makes it accessible for a numerical calculation program such as Matlab and estimates for SAR and EI_{NO_x} can be determined for every arbitrary flight condition.

More into detail it is chosen to perform an individual regression analysis for each flight level ranging from 20,000 ft to 43,000 ft based on input values for weight ranging from operational empty weight plus payload to maximum takeoff weight in steps of 10,000 kg. (Piano-X determines the aircraft weight based on the input value for mass in kg). This was done because aircraft fly at discrete flight levels which are separated by 1,000 ft [14] and are not allowed to

cruise in between flight levels since they need to be compliant to the minimum vertical separation standards. This makes it unnecessary to perform a regression analysis in the altitude dimension since aircraft performance at cruise altitudes in between flight levels is not of interest.

Considering the aircraft velocity, one constant Mach number will be used as input for the performance module in this study. This is based on the observation that the cruise Mach number for a specific aircraft type is contained in a very narrow band and constant throughout the flight. The data leading to this observation will be presented in Section 4.2. The reason why this cruise Mach number is contained in a narrow band is explained in Section 1.5.3 where it is stated that aircraft generally fly at the economically most profitable speed which is ECON speed and lies in between the maximum range cruise speed (MRC) and the long range cruise speed (LRC). For the Boeing 787-800 (abbreviated B788) the Mach number corresponding to these two operational limits are 0.833 and 0.846 [50] which indicates how narrow this range is. The three inputs for the Piano-X performance module (cruise Mach number, aircraft weight and altitude) will now be discussed seperately in more detail.

3.4.5. Cruise Mach number selection

To select the Mach number used for the regression analysis an average Mach number will be calculated from all calculated instantaneous Mach numbers for all trajectories. The calculation procedure to determine the instantaneous Mach number for each cruise segment will be described in Section 3.5.1. The respective average Mach number will be verified by comparing it to the values of MRC and LRC. Results of the Mach number analysis for both the B788 and the Boeing 777-300ER (abbreviated B77W) for the two different dates are discussed in Section 4.2.

It has been chosen to use an average calculated Mach number based instead of instantaneous Mach numbers because using instantaneous calculated Mach numbers are not expected to improve the quality of the calculation results. To assess the exact cruise Mach number during every instance of the flight would require to have very accurate values for groundspeed, windspeed and temperature which are all prone to fluctuations. Although data for windspeed and temperature is available from atmospheric data this is only present for a finite number of altitude levels based on a finite grid size which will require interpolation. Furthermore the data for wind is based on hourly estimates and does not capture the instantaneous fluctuations in wind speed and direction. Moreover, for tracks with gaps in the data there will not be any ground speed data available which will make finding the Mach number an estimate.

3.4.6. Correlation Mach number and cruise altitude

Besides the analysis of all instantaneous cruise Mach numbers, an analysis is performed to investigate whether there is any correlation between the flown Mach number and the cruise altitude. From this analysis it was found that airlines fly a certain Mach number independent of their respective cruise altitude throughout the operational altitude range. These results are presented and discussed in more detail in Section 3.5.1. Based on this observation it is assumed in this work that by shifting the trajectories up or down the flown Mach number will remain constant and equal to the found average Mach number of the original trajectories. Therefore the Mach number is kept constant for all scenarios in this study.

Flying a constant Mach number while lowering the cruise altitude in the troposphere however results in an increasing true airspeed (TAS) due to the increasing temperature and corresponding speed of sound. Furthermore, the dynamic pressure increases which is indicated by a higher equivalent airspeed (EAS). The equivalent airspeed is defined as the speed at sea level for which the dynamic loads are equivalent to the dynamic loads for the true airspeed at the

actual cruise altitude. This effect is present throughout the entire atmosphere and is indicated by the dashed constant Mach lines in Figure 3.8. As a result of these increased dynamic loads, the structural loads on the aircraft are increased. To ensure the dynamic loads stay within the safety margin of the aircraft there is the so called maximum operating velocity V_{MO} which is listed in the respective aircraft Type certificate datasheet published by the Federal Aviation Administration [4]. In order to not exceed the V_{MO} the aircraft velocity is reduced to the V_{MO} below altitudes at which flying a constant Mach number would yield an equivalent airspeed above the maximum operating airspeed. For both aircraft types the V_{MO} is retrieved from the Type certificate of the aircraft and yields an equivalent airspeed of 350 knots (KEAS) for the B788 and 330 KEAS for the B77W. Additionally for the B788 there is a second airspeed limit listed at 350 knots calibrated airspeed (KCAS) as shown in Figure 3.8. To give an example of the implications of this operating speed restriction, it is calculated that by reducing the cruise altitude of both aircraft to 20,000 ft, the operating cruise Mach numbers are reduced to 0.774 and 0.736 for the B788 and B77W respectively.

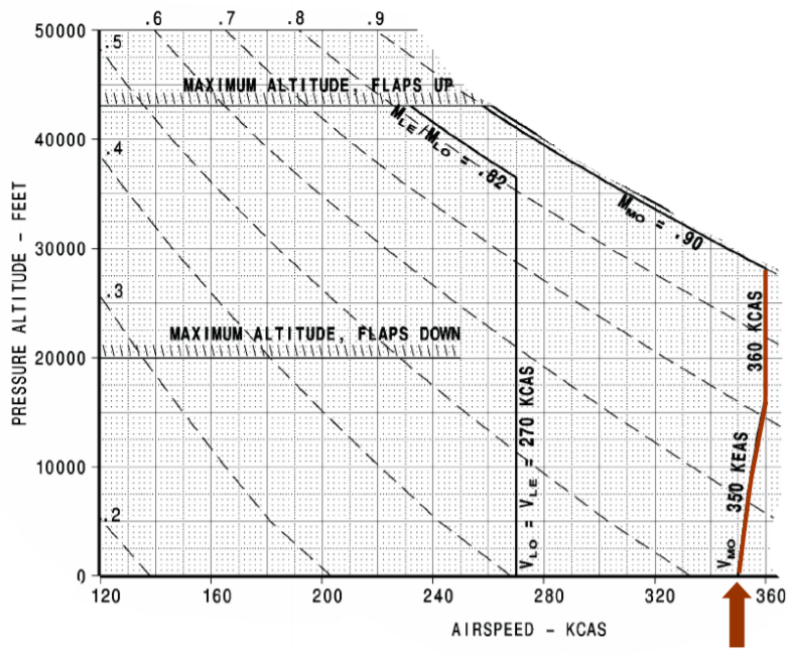

Figure 3.8: Boeing 787-800 Operational Flight Envelope with the maximum operating airspeed (V_{MO} = 350 KEAS and 360 KCAS) indicated by the red arrow [32]

3.4.7. Weight estimation

The second input parameter of the Piano-X point performance module is the instantaneous aircraft weight. At the start of the cruise phase this weight is the top of climb weight (TOCW) which is the take-off weight minus the fuel used to climb to the initial cruise altitude. For each consecutive cruise segment the aircraft weight is reduced by the fuel burned during the previous segment calculated by the aircraft performance tool.

The TOW of the aircraft for each flight is not disclosed by airlines and therefore remains unknown. The performance of the aircraft however is very dependent on the TOW where the larger the weight of the aircraft the higher the fuel consumption. Therefore, to accurately determine the fuel consumption and produced emissions, the TOW needs to be estimated based

[4] https://rgl.faa.gov/Regulatory_and_Guidance_Library/rgMakeModel.nsf/MainFrame?OpenFrameset

on the available known flight parameters which include the aircraft type, airline and flight distance. This is a crucial step in the performance calculation because if the TOW is overestimated, the fuel consumption during every cruise segment will be overestimated as well. The method which is used to estimate the TOW is described in this section.

The aircraft TOW is composed of the operational empty weight, OEW which is a constant and listed for each aircraft, the payload and the total fuel weight taken on board as summarized in Equation 3.13. All components will be discussed individually.

$$TOW = OEW + Payloadweight + Fuelweight \tag{3.13}$$

Operational empty weight

The aircraft operational empty weight (OEW) is build up of the manufacturers empty weight, standard items and operator items including the weight of the flight crew. According to Janes [42] the OEW is listed as 117,705 kg for the B787-800 and 167,825 kg for the B777-300ER respectively. In practice however the operational empty weight varies per airline due to for example a different cabin layout. This difference in OEW is not included in this study and will be included in the uncertainty analysis presented in Section 4.8.

Payload weight

The payload weight consists of the weight of the passengers taken on board, their luggage and any additional freight or cargo. These individual contributions are not known beforehand for each flight and therefore will be estimated. For this purpose the total payload weight is grouped into two contributions, the total passenger weight (including luggage) and the cargo weight. First of all, the total passenger weight is estimated based on three parameters:

1. The passenger capacity of the aircraft. This is how many seats are available on board the aircraft.

2. The passenger load factor. This is a measure of the occupancy rate, 100% being the aircraft has no empty seats.

3. The average weight of one passenger including luggage.

The passenger capacity of the aircraft in combination with the load factor yields the number of passengers which are assumed to be on board the aircraft. By multiplying the total number of passengers with the average weight of one passenger including luggage the total passenger payload is determined.

Considering the first parameter, the aircraft passenger capacity can vary significantly for one specific aircraft type since there are several seating configurations available. The Boeing 787-800 for example is typically flown in a 242 passenger configuration [42] however it can also be delivered in an all economy variant being able to carry up to 375 passengers and a low density option limiting the amount of passengers to 187 [42]. This difference in available seats is a result of the increased ratio of business class seats which take up more cabin space. The passenger capacity is found to be very dependent on the operating airline where for example an all economy version of a B777-300ER operated by Emirates is capable of carrying up to 427 passengers[5] where on the other hand All Nippon Airways operates a version that has a maximum capacity of 212 passengers[6]

[5] https://www.seatguru.com/airlines/Emirates_Airlines/Emirates_Airlines_Boeing_777-300_ER_2class.php

[6] https://www.seatguru.com/airlines/ANA/ANA_NH_Boeing_777-300ER_G.php

To account for this large difference in passenger capacity and to minimize the related uncertainties with respect to aircraft weight, the passenger capacity for each analyzed flight is based on the average capacity of the operating airline. The average passenger capacity of each operating airline is then calculated by taking into account all configurations of the specific aircraft type in their fleet. The data for aircraft passenger capacity for specific airlines was found in [67] and was crosschecked with data found on [1]. Furthermore, operations data for both aircraft types was obtained from the U.S. Department of Transportation Bureau of Transportation Statistics (BTS) Form 41 Schedule T-100. This data contains segment data including available seats, passengers transported, and freight reported for all carriers flying flying to or from the United States. The available seats data was used to verify the passenger capacities of the airlines flying to or from the U.S. found in references [67] and [1].

Secondly, the passenger load factor is determined based on the available seats and the transported passengers reported in The BTS T-100 data for 2018[7]. This resulted in an average passenger load factor of 82% for the flights operated with the B787-800 and a load factor of 81% for flights with the B777-300ER. Comparing these loadfactors to the 81% global average passenger load factor published by ICAO transport statistics of 2017 [37] shows good agreement.

The third and last parameter is the weight per passenger. According to the current guidelines presented by ICAO the internationally agreed recommended average passenger mass is 90 kg [35]. A survey in 2009 among IATA members however showed that 82% of the 28 carriers that replied agree that "for statistical purposes an average mass of 100 kg per passenger plus its checked baggage better reflects today's actual values" [35]. For this reason a conservative estimate of 95 kg is assumed as the average passenger mass in this research.

The second contribution to the total payload weight is the weight of the cargo. The cargo weight is estimated by using freight data from the BTS T-100 data which includes the total freight transported on each segment to or from the United states. The freight transported per flight was estimated by taking an average of the all freight transported with one aircraft type over a time span of one year (2018). As a result on average 10,600 kg and 5,900 kg of freight was transported with a B777-300ER and B787-800 respectively.

Since the payload weight is the largest uncertainty in calculating the take-off weight, an uncertainty analysis will be performed for this parameter which is discussed in Section 4.8.

Fuel weight

The fuel weight taken on board is composed of the fuel used during take-off, climb, descent, approach, reserve fuel and fuel burned during cruise as summarized in Equation 3.14. All components will be discussed separately in more detail.

$$F_{Total} = F_{take-off} + F_{climb} + F_{cruise} + F_{descent} + F_{approach} + F_{reserve} \tag{3.14}$$

First of all, the fuel used during climb is estimated based on the aircraft TOW and initial cruise altitude (ICA). These two parameters were chosen because they showed a large correlation with climb fuel in Piano-X. The relationship for climb fuel as function of TOW and ICA is retrieved by using data from Piano-X and using a regression analysis between the three parameters. A third parameter found to have a large correlation with the climb fuel is the climb distance. However calculated climb distances in Piano-X show a very narrow range (200-300km) whereas climb distances determined from the trajectory data show a significantly larger variance. Therefore it was not possible to perform a regression analysis based on this parameter since this would result in inaccurate results.

[7] https://www.transtats.bts.gov/Fields.asp

The fuel used during descent is determined through the same principle as for the climb fuel where a correlation was found between the descent fuel and TOW. Similar to the climb distance the descent distance showed to have a large correlation with descent fuel. However due to the same reason as discussed above, this parameter was found not suitable to be used in the regression analysis.

Take-off and approach fuel components are assumed constant as they are found to be constant per aircraft type in Piano-X.

Reserve fuel is assumed to be the minimum required reserve fuel which consists of contingency fuel, destination alternate fuel and final reserve fuel. Contingency fuel is the fuel required to compensate for unforeseen factors such as a lower than foreseen cruise altitude or factors related to weather such as strong headwinds and shall be five percent of the planned trip fuel [31]. Diversion fuel is the fuel required to fly to an alternate airport which is assumed to be 200 nautical miles away [50]. The final reserve fuel or holding fuel is the fuel which should be a minimum of 30 minutes flying time at 1500 ft over the airport at holding speed [31].

Finally the fuel burned during cruise is found by taking the sum of the fuel consumed of all cruise segments. The fuel consumed at each segment is found by combining the segment distance, the specific air range found from Piano-X and the wind data. This procedure is discussed in more detail in Section 3.6. The specific air range however depends on the instantaneous aircraft weight which is dependent on the TOW which is at this point still unknown. To solve this system an iterative process is build in Matlab which is schematically shown in Figure 3.9.

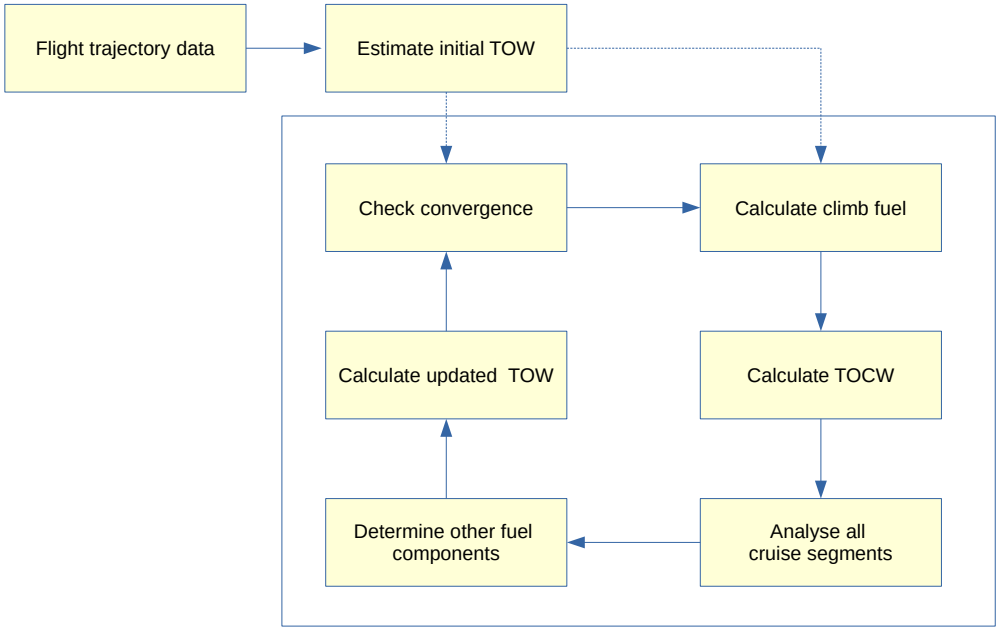

Figure 3.9: Flow diagram schematically displaying the iterative loop used to find the TOW

As a first step an initial TOW is estimated by summing the known contributions of the payload and operational empty weight and assuming a fuel load based on the total distance of the trajectory. Based on this initial TOW the climb fuel is calculated following the principle discussed above. By subtracting the climb fuel from the TOW the top of climb weight (TOCW) is calculated which is the starting weight of the cruise phase. Subsequently the fuel consumption during all individual cruise segments is calculated using the aircraft performance data and

using the the instantaneous weight of the aircraft as input. For each consecutive cruise segment this weight is reduced by the fuel consumption of the previous segment. The total cruise fuel consumption is then found by summing the fuel consumption of all cruise segments. As a next step the descent fuel and reserve fuel are calculated based on the TOW and total fuel consumption during cruise. Finally the updated TOW is found by summing all calculated fuel contributions, the payload and the OEW. This updated value for TOW is then compared with the estimated TOW to check if it is within the specified margin of 1 kg. If not the calculation is performed again however now by using the updated TOW. This process is repeated until the value for TOW converges and the calculated fuel burn corresponds to the value based on the actual TOW.

By implementing this approach the TOW of all trajectories converged between 3 and 10 iterations. Furthermore it was found that the TOW converged irrespective of whether the initial TOW is overestimated or underestimated which shows the method robust. As expected it was found that the required number of iterations became lower as the initial TOW was estimated closer to the final TOW. For this reason the initial estimate of the TOW is calculated based on the average found fuel load as function of the mission distance. For the B788 this is approximately 6 kg fuel per kilometre whereas for the B77W this was found to be 9 kg of fuel per kilometre. An example of the convergence history of one trajectory showing the convergence behaviour is presented in Figure 3.10 where the first iteration represents the initial TOW estimate. This trajectory corresponds to the analyzed trajectory discussed in Section 3.6.1

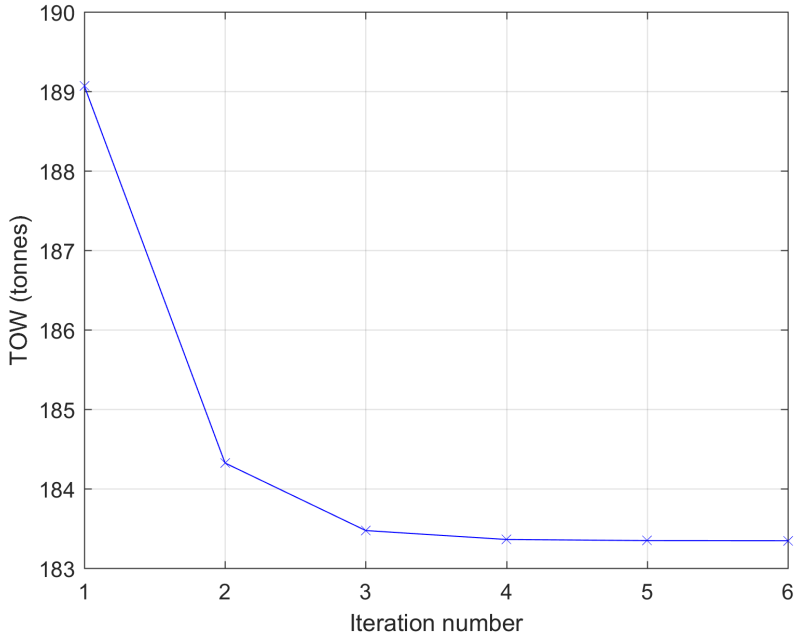

Figure 3.10: Example of TOW convergence history

3.4.8. Altitude selection

The final input parameter to determine the aircraft specific air range and NO_x emission index is the aircraft cruise altitude. For the base case where the altitude is not shifted the aircraft altitude is directly retrieved from the flight trajectory data. For the scenarios with a shifted trajectory the entire cruise segment of the flight is shifted an integer two thousand feet up or down. In this process the maximum attainable altitude is limited by the aircraft service ceiling of 43,100 ft. All altitudes above this altitude are lowered to the nearest flight level to the service ceiling which is 43,000 ft.

3.5. Atmospheric weather data

Global atmospheric weather data is retrieved from the European Centre for Medium-Range Weather Forecasts (ECMWF)[8]. This data was assembled by combining model data with observations from across the world into a globally complete and consistent data set. This reanalysis data is used for monitoring climate change as well as for other research. Reanalysis data contains estimates of atmospheric parameters including air temperature and wind velocity at various pressure altitudes. The specific data set used in this study is the fifth major global reanalysis produced by the ECMWF which is referred to as ERA5.

The ERA5 dataset provides 4D wind and temperature data on a 0.25 by 0.25 degree horizontal grid with 37 pressure altitude levels and a 1-hour temporal update cycle. This specific data set is chosen since it provides the highest available spatial and temporal resolution. The pressure levels range from 1000 hPa to 1 hPa however they are not equally spaced throughout the atmosphere. The available pressure levels in the region of interest are 150 hPa, 175 hPa, 200 hPa 225 hPa 250 hPa 300 hPa and 350 hPa. This corresponds to the flight levels of respectively 44,000 ft, 41,000 ft, 39,000 ft, 36,000 ft 34,000 ft, 30,000 ft and 25,000 ft at which the wind data is available. This leads to the observation that the wind and temperature data is not available for every flight level. Therefore to be able to accurately determine the wind and temperature throughout the entire operational cruise altitude range, a spatial linear interpolation in vertical direction was performed.

The wind data is provided in terms of the zonal velocity u, which is the component of the horizontal wind towards the east and the meridional velocity v which is the component of the horizontal wind towards the north.

The wind speed, direction and temperature at every instance during the flight is determined by using the aircraft trajectory data as input. Since the wind data is four dimensional this requires inputs for the aircraft latitude, longitude, altitude and time which are obtained from the flight trajectory data.

3.5.1. Airspeed and Mach number

The weather data is combined with the flight track data for two purposes. First of all wind data is used to convert groundspeed to airspeed which is required to determine the specific ground range (SGR). Furthermore airspeed (V_{air}) is required in combination with the speed of sound (a) to determine the cruise Mach number (M) through Equation 3.15 which is required to determine the average Mach number used for the regression analysis. In this Equation the speed of sound is calculated according to Equation 3.16 where the temperature retrieved from the atmospheric weather data is used as input. Furthemore γ is the ratio of specific heats which is 1.4 for air and R is the individual gas constant for dry air equal to 287.05.

$$M = \frac{V_{air}}{a} \tag{3.15}$$

$$a = \sqrt{\gamma RT} \tag{3.16}$$

[8] https://www.ecmwf.int/

The airspeed of the aircraft is determined by subtracting the wind component from the groundspeed obtained in the trajectory data. Since both the groundspeed and windspeed are vectors it is required to do this through vector addition. In this procedure the direction towards the east and north are defined as positive. Furthermore the component of the airspeed towards the east is defined as the x component and the component of the airspeed towards the north as the y component. The x and y components of the airspeed are found through Equations 3.17 and 3.18 by subtracting the groundspeed x and y components shown in Figure 3.11 by the x and y wind component. The wind component towards the east is called the zonal wind component denoted by u and the wind component towards the north is called the meridional wind component denoted by v. The zonal and meridional wind components u and v are visualized in Figure 3.12 and are retrieved from the atmospheric weather data.

$$V_{air_x} = V_{ground_x} - u \tag{3.17}$$

$$V_{air_y} = V_{ground_y} - v \tag{3.18}$$

The zonal (x) and meridional (y) components of the groundspeed are determined based on the direction of the aircraft where again the direction towards the east and north is defined as positive. For this analysis the aircraft direction, ψ is defined as its direction towards where the aircraft is moving (track angle). This is expressed in relation to the north on a compass and measured clockwise (towards the east is 90 degrees). This is done according to Figure 3.11 and Equations 3.19 and 3.20.

$$V_{ground_x} = sin(\psi) \cdot V_{ground} \tag{3.19}$$

$$V_{ground_y} = cos(\psi) \cdot V_{ground} \tag{3.20}$$

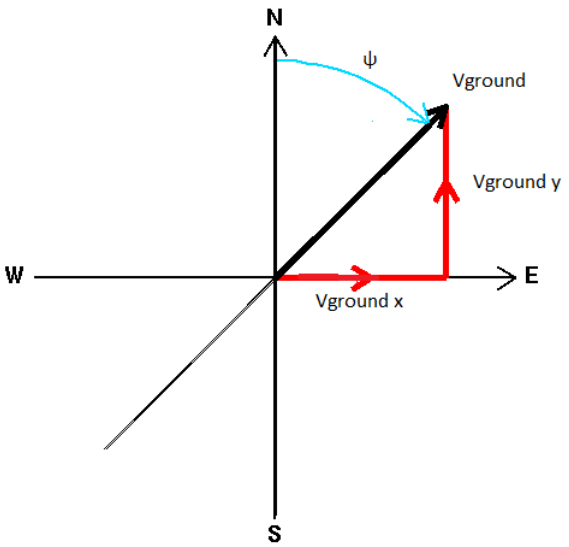

Figure 3.11: Zonal and meridional components of the groundspeed where ψ is the track angle

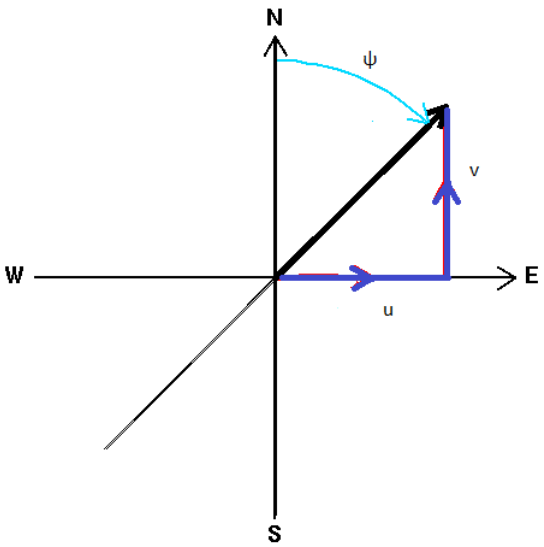

Figure 3.12: Zonal (towards the east) and meriodional (towards the north) components of the windspeed

Finally the Airspeed is found by combining the x and y component of the airspeed through equation 3.21

$$V_{air} = \sqrt{V_{air_x}^2 + V_{air_y}^2} \tag{3.21}$$

3.6. Fuel consumption and produced emissions

The fuel consumption and resulting emissions are determined by combining the aircraft performance data, the weather data and the trajectory data as shown in Figure 3.13. First of all to account for the effect of wind, the specific air range (SAR) determined in the performance module is converted to specific ground range (SGR) by multiplying with the ratio of groundspeed over airspeed according to Equation 3.22. Here the groundspeed is found in the trajectory data and the airspeed is derived by incorporating the weather data as discussed in Section 3.5.1. The fuel consumption for one segment is then determined by multiplying the cruise segment length calculated from the trajectory data, by the inverse of specific ground range according to Equation 3.23. The calculation of fuel consumption is repeated for each cruise segment.

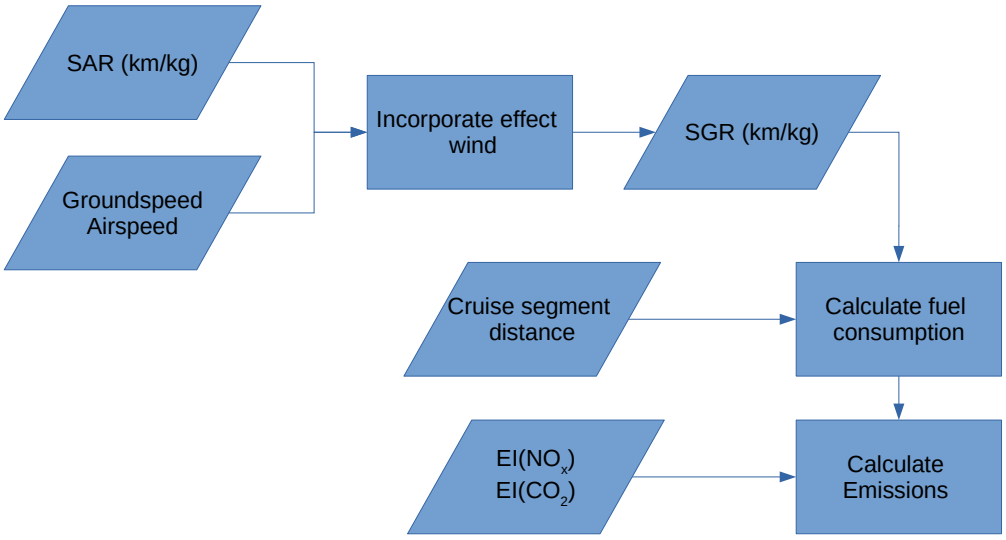

Figure 3.13: Flow diagram showing the calculation procedure of the fuel consumption and emissions per cruise segment

$$SGR = SAR \cdot \frac{V_{ground}}{V_{air}} \tag{3.22}$$

$$Fuel_{segment} = length_{segment} \cdot \frac{1}{SGR} \tag{3.23}$$

Finally the produced emissions of CO_2 and NO_x during every segment are determined by combining the fuel consumption with the specific emission indices of both pollutants. For CO_2 this emission index is constant, where for each kilogram of fuel 3.16 kilograms of CO_2 are produced. The emission index of NO_x on the other hand is an output of the Piano-X performance module as discussed in Section 3.4.2.

3.6.1. Verification of performance data for one analyzed trajectory

To verify the calculated fuel consumption and resulting emissions of one analyzed track, results obtained in this work are compared with simulation data of a similar trajectory in Piano-X. This Piano-X verification data is obtained by using the detailed flight profile function and specifying the same total flight distance and allowed flight levels as were found in the actual track. Furthermore the payload is set equal to the payload calculated for the actual trajectory which is slightly over 29,000 kg. With these inputs Piano-X simulates the entire flight and selects the cruise altitude out of the supplied range of cruise levels resulting in the lowest fuel consumption. As the flight progresses and the aircraft becomes lighter this can result in a step-climb if the supplied cruise levels allow it. As output, Piano-X supplies the total fuel consumption during cruise, climb, take-off, descent and reserve fuel and additionally presents the calculated resulting TOW. For this verification procedure the calculated fuel consumption in this work is based on the specific air range and does not include the effect of wind since this is not included in Piano-X either.

Out of the total set of tracks a representative track was selected which covered a total distance of 8,977 km. The selected flight was operated by a Boeing B787-800 from TUI and flew from London to Colombo as shown in Figure 3.14. The aircraft flew the first segment of the cruise phase at 39,000 ft after which it initiated at step-climb to 41,000 ft. This vertical profile occurred frequently in the dataset and is therefore considered representative as well.

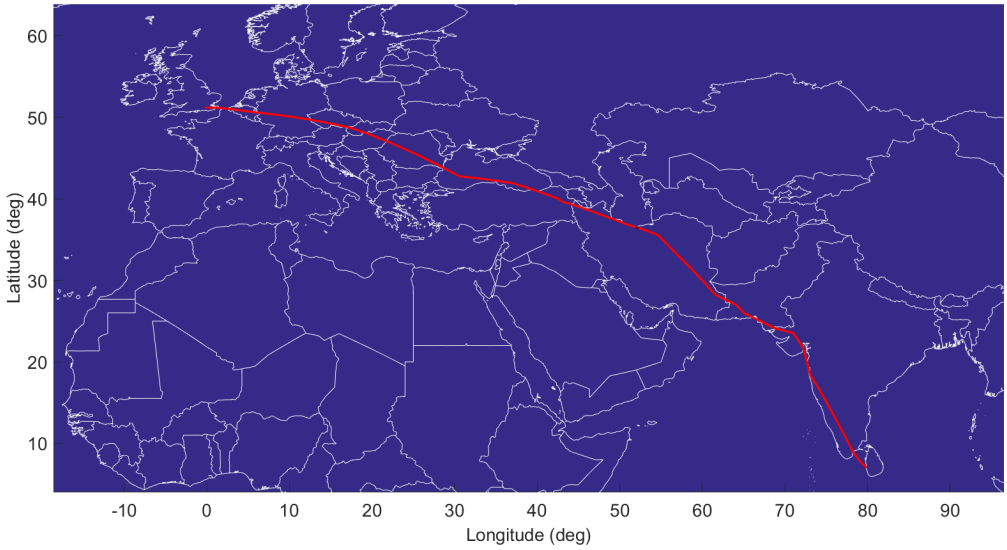

Figure 3.14: B787-800 flight trajectory from London to Colombo on November 20th shown in red.

A comparison of the vertical flight trajectories for the actual and the Piano-X verification flight is shown in Figure 3.15 where the flight altitude is plotted against the flown distance. By looking at the figure a few differences are observed where first of all the actual trajectory shown in blue has a slightly larger climb distance. This can be due to a smaller climb gradient or a reduced climb speed. Secondly, the actual trajectory starts to descend earlier and takes a longer distance to reach the ground. Although both differences are small, they result in a cruise segment distance which is smaller for the actual flown trajectory compared to the Piano-X verification trajectory. Finally the actual flown trajectory performs a step climb slightly earlier than the simulated Piano-X trajectory. The point where the Piano-X trajectory initiates a step climb however can not be specified as it is determined based on what results in a minimal fuel consumption. The same holds for the climb and descent profile for which Piano-X does not allow to alter the

climb or descent gradient. For this reason a closer match between the actual trajectory and the verification trajectory could not be attained.

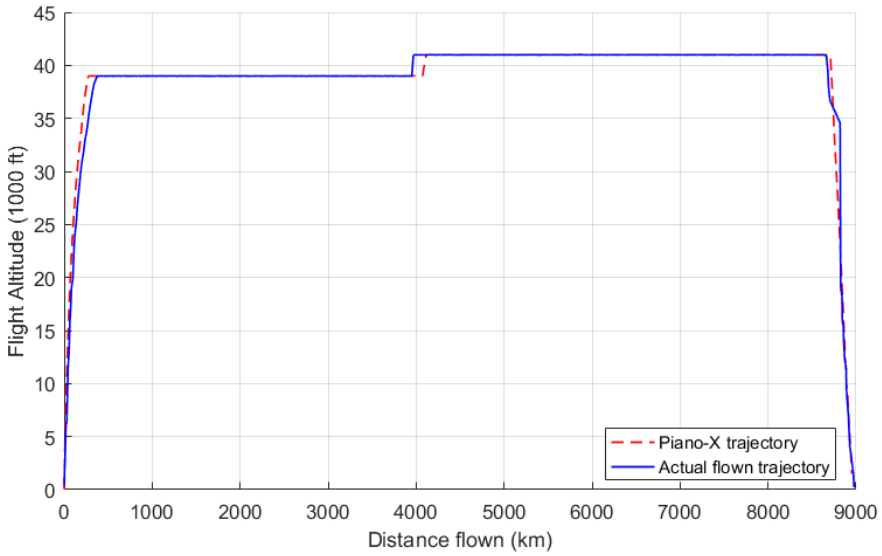

Figure 3.15: Altitude profile of the actual flown trajectory found in the data compared to a simulated verification trajectory with Piano-X

The resulting flight characteristics including the determined fuel consumption and TOW of the actual trajectory analyzed in this work and the Piano-X verification trajectory are presented in Table 3.1. For clarification, the values presented under This work are obtained by using the regression data retrieved from Piano-X and by summing the calculated fuel consumption during every individual cruise segment. Piano-X verification data on the other hand is obtained directly from Piano-X by simulating a complete trajectory covering the same total flight distance.

Flight characteristic	This work	Piano-X Verification	Difference (%)
Flight distance (km)	8,977	8,977	0
OEW (kg)	117,705 [42]	117,705	0
Payload (kg)	29,114	29,114	0
Cruise distance (km)	8,285	8,409	1.5
Cruise fuel consumption (kg)	43,024	43,820	1.8
Fuel per kilometre (kg)	5.19	5.21	0.38
Climb fuel (kg)	4,087	4,167	1.9
Descent fuel (kg)	394	420	6.2
Reserve fuel (kg)	6,977	7,136	2.2
Total fuel (kg)	54,985	56,046	1.9
TOW (kg)	201,804	202,865	0.52
CO_2 Emissions* (kg)	137,990	138,470	0.35
NO_x emissions* (kg)	487.2	490.7	0.71

Table 3.1: Calculated flight characteristics for a trajectory analyzed in this work compared to verification data obtained by simulating a complete trajectory in Piano-X. The difference with respect to the verification data is presented in the last column. *CO_2 and NO_x emissions are scaled up to account for the higher cruise distance of the verification trajectory.

Table 3.1 indicates that although the total flight distance is set equal, there is a significant difference in cruise distance of 124 kilometres originating from the difference in climb and descent distance. The larger cruise phase of the Piano-X trajectory partially justifies the 1.8 % higher fuel consumption during cruise. By taking this difference in cruise distance into account and comparing the fuel consumption per kilometre flown, both flights are in good agreement with a difference of less than 0.5%. This small difference is suspected to originate from the difference in calculation procedure where in this work the fuel required to climb from 39,000 ft to 41,000 ft is not considered whereas Piano-X does take this into account as it defines the cruise fuel consumption from initial cruise altitude (ICA) to ICA. The resulting difference in emissions however is small and therefore considered sufficiently accurate.

A direct effect of the lower cruise fuel consumption for the trajectory analyzed in this work is observed in the TOW which is approximately 1000 kg lighter. As a result of this lighter aircraft a lower climb fuel is calculated as well as a lower reserve fuel. These differences however are considered to be acceptable since they are an direct consequence of the difference in cruise distance. The difference in descent fuel is larger, however since the absolute difference is small this is acceptable as well. The lower TOW calculated in this work contributes to the lower fuel consumption during cruise as well. Finally, comparing the emissions of CO_2 and NO_x scaled up to the higher amount of kilometres for the verification trajectory, shows good agreement with a difference less than 1%. All in all the results are considered sufficiently accurate and thereby the calculation procedure for the aircraft performance data including emissions is verified.

3.6.2. Verification of weatherdata for two analyzed trajectories

To quantify the effect of wind on aircraft performance and emissions two flights are analyzed between Paris and Washington operated by a Boeing B787-800 from United Airlines on March 30th 2018. These specific flights where chosen since they cross the Atlantic ocean where they will be subjected to the strong jetstream. This is expected to have a large impact on the fuel consumption of both trajectories. Furthermore flights were chosen for which the data loss was minimal. Figure 3.16 shows the two trajectories in red where the segment with a dataloss is indicated by the dashed segment. In this figure the northern trajectory (B) is the flight from Washington to Paris and trajectory A is the flight from Paris to Washington. Additionally the green dotted line represents the shortest distance between the two cities which is the great circle route.

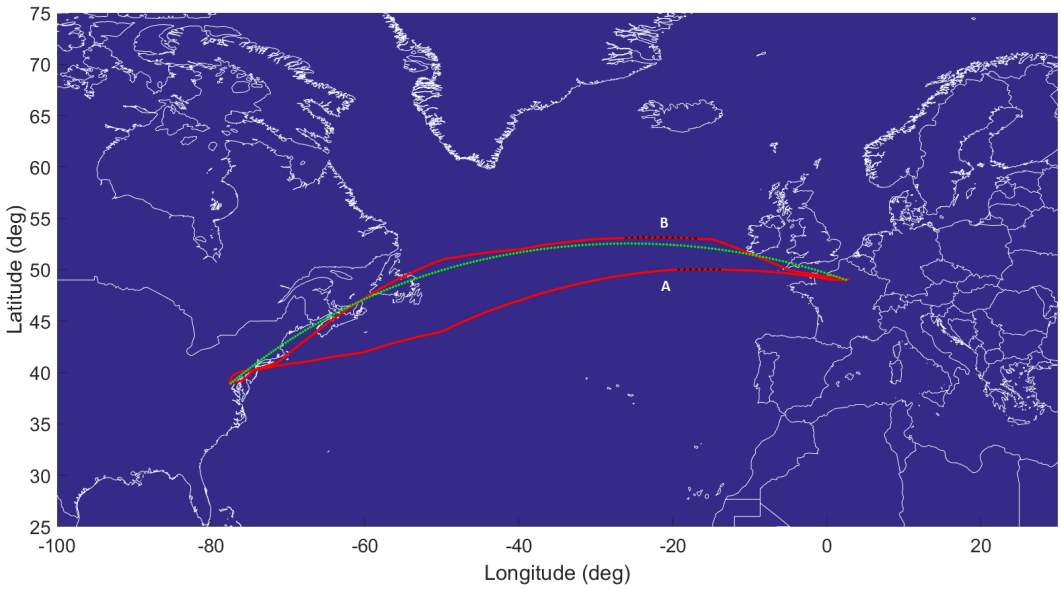

Figure 3.16: Flight A from Paris to Washington and flight B from Washington to Paris on March 30th

Comparing both flights it is observed that the trajectory of flight B is located closer to the great circle route. For this reason the total flown distance is shorter, 6329 km compared to 6446 km for the track from Paris to Washington. A reason for this deviation from the shortest route is found when looking at the prevailing wind pattern at the time of flight A as depicted in Figure 3.17. Here the absolute wind velocity is shown in combination with the wind direction indicated by the arrows. The arrows show that the wind direction is towards the east which results in a continuous headwind. Moreover it is suspected that by deviating from the shortest route, this flight attempts to avoid the region where the wind velocity is highest to minimize the resulting time and fuel penalty.

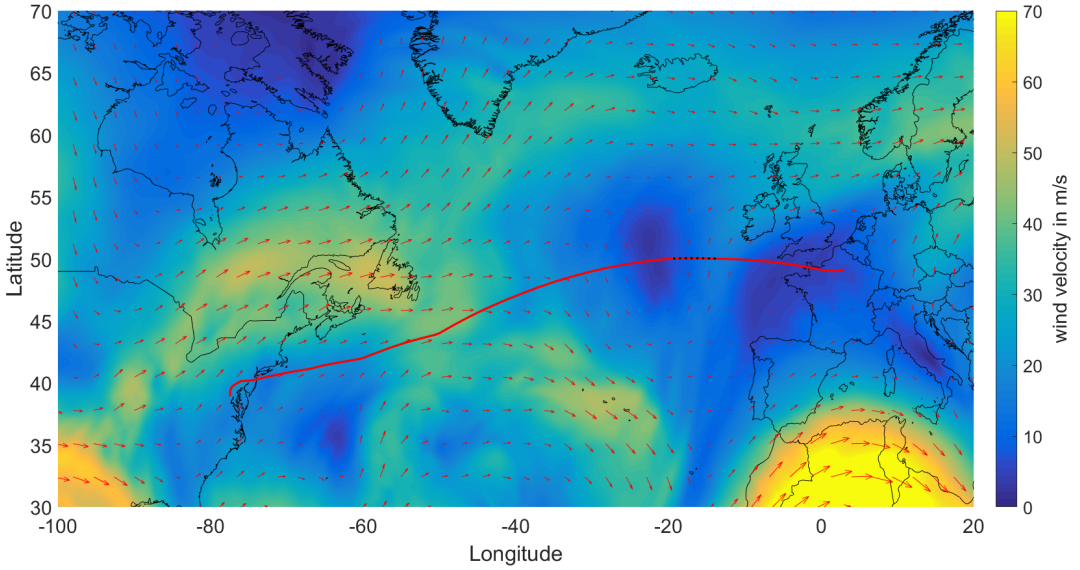

Figure 3.17: Flight A from Paris to Washington with prevailing wind pattern

By looking at the wind pattern for flight B from Washington to Paris it is observed that this trajectory follows a path for which the wind velocity is most favourable. This will effectively reduce the flying time and result in a lower total fuel consumption.

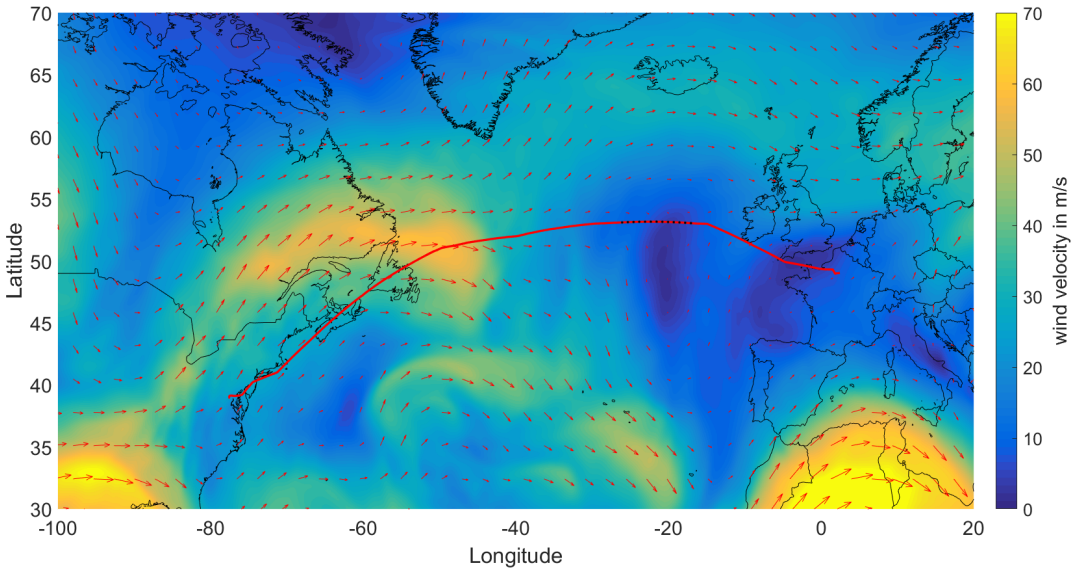

Figure 3.18: Flight B from Washington to Paris with prevailing wind pattern

The effect of wind is most prominent when looking at the groundspeed of both flights. Figures 3.19a and 3.19b show the groundspeed as function of flight time during the cruise phase in red. Furthermore, the airspeed and Mach number are shown by the blue line and dashed black line respectively and are calculated based on the method stated in Section 3.5.1. From Figure 3.19a it is observed that the continuous headwind experienced by flight A results in a groundspeed which is lower than the calculated airspeed shown in blue. For flight B the groundspeed is higher than the airspeed due to the favourable wind conditions. As a result the cruise time is approximately one hour shorter.

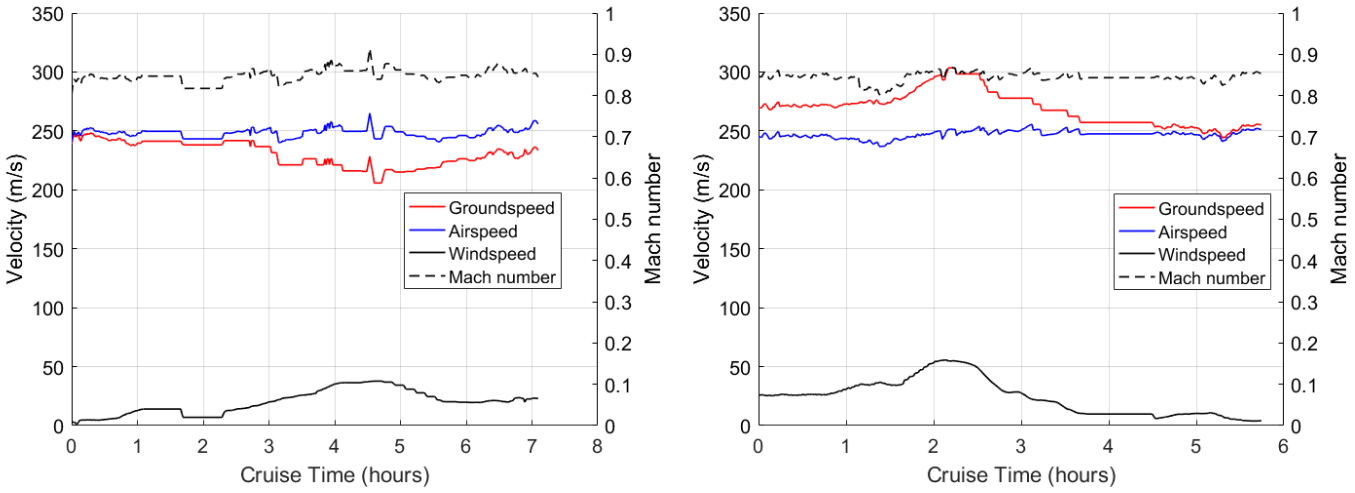

(a) Flight A

(b) Flight B

Figure 3.19: Groundspeed in relation to airspeed and Mach number for flights A and B

Figures 3.19a and 3.19b show that the groundspeed of both trajectories changes in magnitude throughout the flight which is due to the effect of wind. The airspeed on the other hand is more or less constant and equal for both flights and is around 250 m/s. This translates to a Mach number of approximately 0.84 which lies inside the MRC and LRC Mach numbers discussed in Section 3.4.5. Furthermore the calculated Mach number throughout both flights is relatively constant as well. Small but high frequency fluctuations in airspeed and Mach number do persist however these originate from fluctuations in wind velocity or gusts which are not captured in the weather data and are therefore inevitable.

Considering the magnitude of the windspeed depicted by the solid black line, one can see that for flight B (Figure 3.19b) a maximum wind velocity of approximately 60 m/s is found which is corresponds to the yellow color in Figure 3.18. Furthermore it is observed that for this specific trajectory the groundspeed can be approximated by adding the windspeed curve to the airspeed curve. This indicates that the wind direction is aligned to the flight direction which is conform the wind direction as depicted in Figure 3.18.

As a consequence of the higher groundspeed of flight B the flight time is approximately one hour shorter which is observed by comparing the cruise time of both flights in Figures 3.19a and 3.19b. This higher groundspeed results in a higher specific ground range (the ground distance covered for one kilogram of fuel) which reduces the fuel consumption for the flight. This is observed in Table 3.2 which shows the calculated fuel consumption, take-off weight and other characteristics of both flights for a calculation which includes the effect of wind and a calculation disregarding effect of wind which assumes the SGR is equal to the SAR. This is to exclude other parameters which might influence the fuel consumption such as the cruise altitude.

By comparing the fuel consumption during cruise of flight A and B it is observed that flight B consumes significantly less fuel, 24,970 kg compared to 29,482 kg for flight A. This 15% difference shows the large effect of the wind pattern on the fuel consumption. As a result the total fuel weight taken on board is lower and as a consequence the TOW is lower as well.

Flight characteristic	Flight A (no wind)	Flight A (wind)	Flight B (no wind)	Flight B (wind)
TOW (kg)	180,004	182,502	181,102	178,445
Flight distance (km)	6,446	6,446	6,329	6,329
Cruise distance (km)	5,538	5,538	5,546	5,546
Cruise altitude (ft)	40,000	40,000	39,000	39,000
Total fuel weight (kg)	38,348	40,846	39,446	36.789
Cruise fuel consumption (kg)	27,136	29,482	27,465	24,970

Table 3.2: Flight characteristics of flight A and B including and excluding the effect of wind

If only the effect of wind on one trajectory is considered, the fuel consumption of flight A is increased by 9% compared to the no wind case whereas the fuel consumption of flight B is decreased by 9% with respect to the no wind case. Comparing flight A with flight B for the no wind case a small difference in fuel consumption is found as well. This can be attributed to the difference in cruise altitude of both trajectories where flight A cruises at 40,000 ft and flight B cruises at 39,000 ft as shown in the vertical profiles of both tracks depicted in Figures 3.20 and 3.21. By simulating both flights in Piano-X it can be found that for the respective flight conditions flying at 40,000 ft results in a higher specific air range and therefore results in less fuel consumption which justifies the found difference.

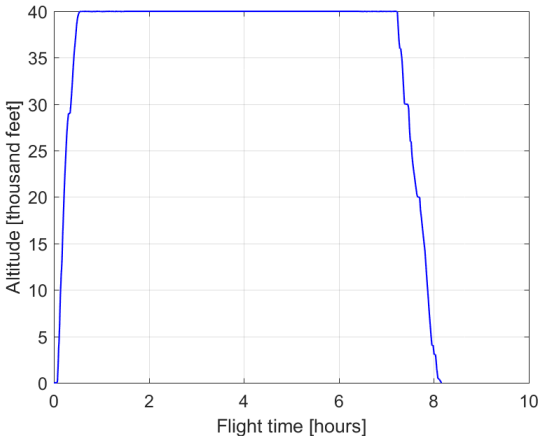

Figure 3.20: Altitude profile flight A

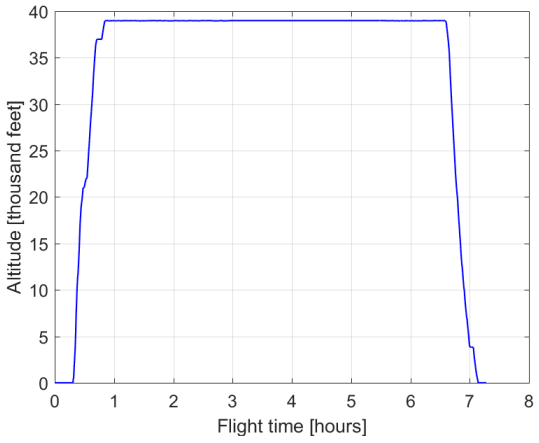

Figure 3.21: Altitude profile flight B

3.7. AirClim climate response model

In this work, the climate response model AirClim will be used to calculate the climate impact of different emission scenarios.

AirClim is a climate response model which can be used as an efficient assessment tool to evaluate the climate impact of numerous air traffic scenarios including the effect of changes in cruise altitude. AirClim is developed by Grewe and Stenke (2008) [22] and is based on the linear response model from Sausen and Schumann 2000 [63]. However in contrast to Sausen and Schumann the climate response to emissions is dependent on the altitude and location of the emissions. The model has recently been expanded by Dahlmann [7] where among other things the effect of contrail cirrus was included. AirClim combines the input of air traffic emission data with pre-calculated climate sensitivity data and calculates the evolution of atmospheric concentration changes, radiative forcings and surface temperature changes [9].

The pre-calculated climate sensitivity data is atmospheric response data to localised and normalised emissions of NO_x and H_2O into idealized regions. For each of these idealized regions, a climate-chemistry simulation is performed with the state of the art climate chemistry model ECHAM4.L39(DLR)/CHEM-ATTILA, from now abbreviated as E39/CA [22] to obtain the climate response data as a result of the normalized emission input [7]. This pre-calculated response data consist of both atmospheric concentration changes as well as radiative forcings of ozone, methane and water vapor all of which are called emission response functions [9]. For contrail cirrus, ECHAM4-CCMod [5] is used [9]. AirClim combines the precalculated, altitude and latitude dependent emission response functions with emission data in order to calculate atmospheric composition changes, radiative forcings and near surface temperature changes [9]. This is done by decomposing the 3D emission inventory into contributions from the localised emission regions which then translate in a linear combination of the response pattern [26]. A schematic of the working of the model is presented in Figure 3.22.

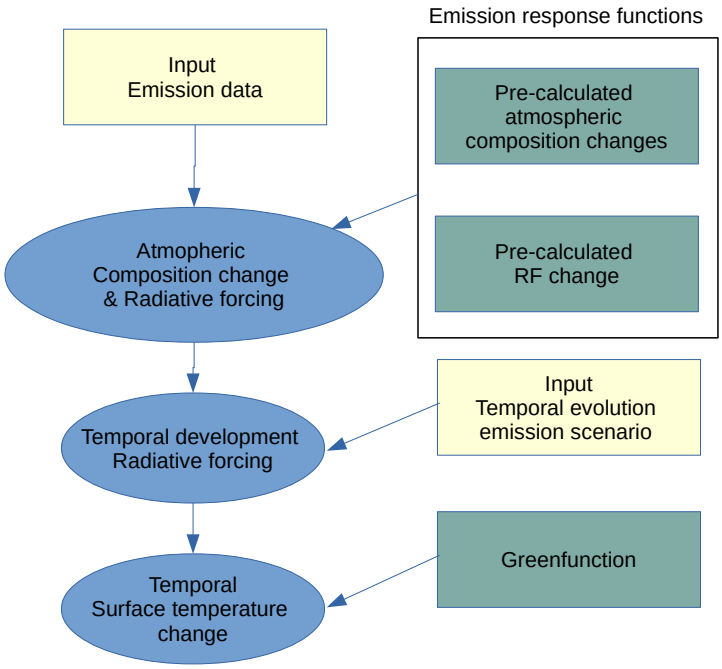

Figure 3.22: Flow chart showing the working principle of the AirClim model

In principle the model can be divided into two main parts: The linear combination, which combines the emission response functions with the emission input to find the changes in atmospheric composition and radiative forcing. And the response model which calculates the temporal development of the radiative forcing and temperature response. All relevant steps will be discussed in the next sections.

3.7.1. Defining the emission input

To determine the climate impact of an air traffic scenario, AirClim requires an emission scenario as input. This input consists of two components, the input emission data and a temporal evolution scenario. The input emission data is defined as the input emission inventory which is a three dimensional geographical distribution of fuel consumption, NO_x emissions and kilometres flown representative for a certain moment in time. This input is 3D since it consists of a latitude, longitude and altitude dimension. In this study this input is generated according to the procedure described Section 3.6 and will further be elaborated upon in Section 4.7.1.

To verify the climate model results, the standard emission inventories referred to as AERO2k, Quantify and TRADEOFF will be used as input. These emission inventories represent the total global emissions of air traffic for one specific year and are developed and used as emission input by a variety of other studies which makes them suitable for verification. The inventories differ in terms of total amount of fuel consumption and distance flown because they are representative of a different year and are assembled based on different traffic data. Table 3.3 shows the most relevant characteristics of these different global emission inventories. Additional information regarding the origin and characteristics of these emission inventories such as the geographical distribution over the globe can be found in Appendix C.

Inventory	Reference year	Fuel (Tg)	NO_x (Tg_N)	Distance (10^9 km)	Vertical resolution (ft)
AERO2k	2002	176	0.68	33.2	1,000
Quantify	2000	214	0.85	30.5	2,000
TRADEOFF	2000	154	0.60	25.4	2,000

Table 3.3: Overview of the characteristics of the AERO2k, Quantify and TRADEOFF emission inventories

The second component of the emission input is the emission temporal evolution scenario. Since the objective of AirClim is to assess the climate impact over a period of time it is necessary to assume a certain temporal development of this emission scenario considering the development of air traffic emissions in the past and future. This temporal evolution will be used to scale the input emission data in time. In this work the same scenario will be used as in Frömming et al. (2012) [16] where aviation fuel usage from 1940 to 1995 is taken from Sausen and Schumann (2000) [63] based on data from the International Energy Agency (IEA). For future emissions, the IPCC Fa1 scenario (Penner et al. 1999) [57] is used. In this scenario the emissions in 2015 follow the NASA forecast by Baughcum et al. (1998) [3]. Furthermore for 2050 emissions are those predicted by the ICAO Forecasting and Economic Support Group (FESG) by assuming mid range economic growth and a corresponding annual growth rate of fuel consumption of 1.7% (scenario FSEGa) [70]. Thereafter this scenario is extended up to 2100 by assuming a medium growth rates of 1% annually [63]. Figure 3.23 gives an overview of this emission scenario. Furthermore it should be noted that the growth rates are assumed to be globally homogeneous. Finally a scenario is assumed for the background concentrations of CO_2 and methane according to the Representative Concentration Pathway (RCP) 8.5 scenario from the IPCC [41]. These background concentrations are of influence for the climate impact of the perturbations of CO_2 and CH_4 as will be discussed in Section 3.7.4.

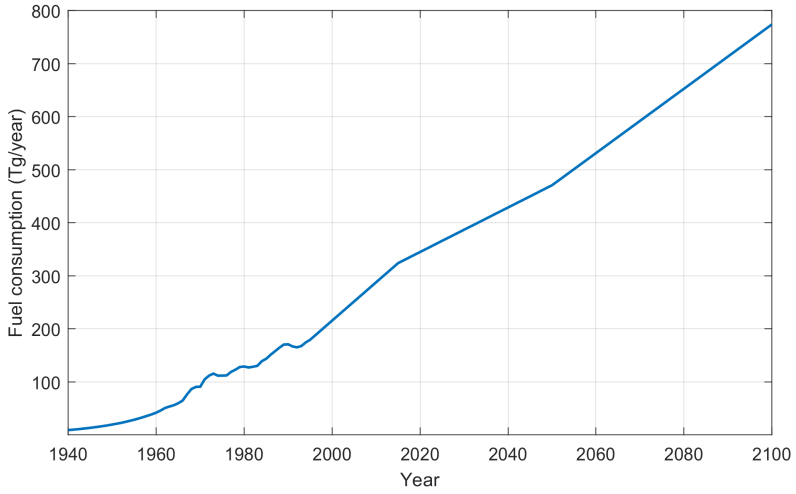

Figure 3.23: Temporal development of fuel consumption according to data from Sausen and Schumann [63], Baughcum et al. [3], the IEA and assuming an Fa1 future growth scenario according to [57]

3.7.2. Emission response functions

The atmospheric composition changes and resulting radiative forcing are a function of both the emission and the sensitivity of the atmosphere to these emissions. This sensitivity is dependent on the emission location and is captured in the emission response functions determined by simulations with a climate chemistry model E39/CA. First of all, to be able to address the local atmospheric sensitivity which is a function of altitude and latitude, 84 idealized emission regions (boxes) were determined (7 latitude bands and 12 altitude ranges). These regions are shown in Figure 3.24 (Fichter 2009) [12]. Here it can be seen that the idealized regions are more concentrated in the northern mid latitudes at pressure levels above 300 hPa. This is because cruise altitudes for most subsonic aircraft are located between 300 hPa and 200 hPa [9] as can be seen from the traffic distribution shown by the grey shaded contour. Furthermore the vertical resolution varies as well and has a resolution of roughly 1 kilometer [9].

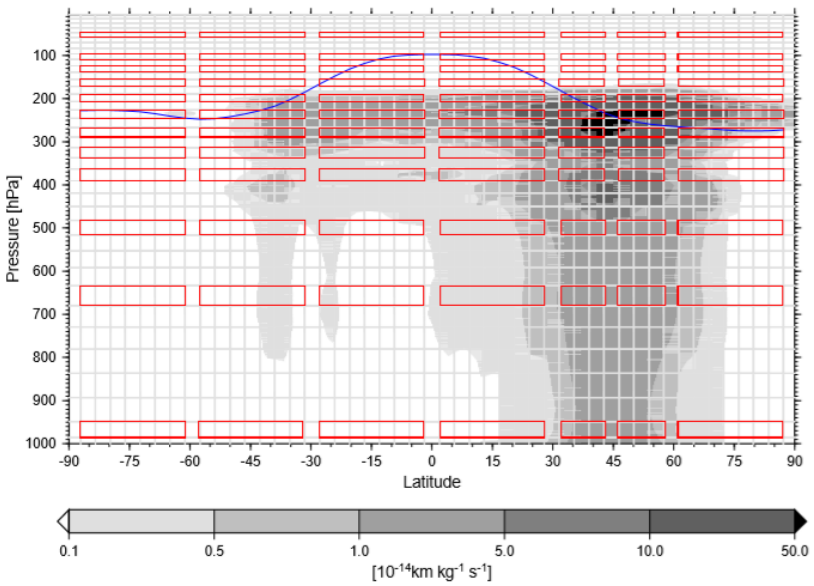

Figure 3.24: Location of the idealized emission regions shown by the red boxes. The grey shaded areas shows the present day air traffic density in kilometres per second per kilogram of air. Figure taken from [12]

Within each of these idealized emission regions, zonally homogeneous unified aircraft emissions in terms of fuel, NO_x and flown kilometres are added to a background air traffic inventory [12]. These unified emissions and flown kilometres are shown Table 3.4. For each of these 84 idealized emission regions a climate-chemical simulation was performed with E39/CA in which these emissions were emitted in addition to the background emissions of the base case scenario. This base case simulation was performed which includes state-of the art emissions for all categories such as industry, biomass burning and air traffic [9]. The resulting change in corresponding concentrations and radiative forcing compared to the base case simulation (without the idealized emissions) are used as emission response functions and are a measure of the dependency of radiative forcings to the location and altitude of the emissions.

Fuel (10^{-13} kgkg$^{-1}s^{-1}$)	NO_x (10^{-16}kgkg$^{-1}s^{-1}$	H_2O (10^{-13} kgkg$^{-1}s^{-1}$)	Distance (10^{-14} kmkg$^{-1}s^{-1}$)
1.0	4.5	1.25	1.8

Table 3.4: Normalised emissions into the idealized regions as used for the idealized scenario simulations. Numbers taken from [12]. Unit is kilograms of emission per second into one kilogram of air

3.7.3. Atmospheric Concentration change of climate forcing components

To determine the concentration change of the climate forcing components of CO_2, O_3, H_2O and CH_4 as a result of the produced emissions, a distinction is made between forcing components which are not affected by the emission location and forcing components which are affected by the location of the emissions. Only the latter will make use of the emission response functions.

Carbon Dioxide

One forcing component which is not affected by the emission location is CO_2. Due to its average atmospheric lifetime in the order of 100 years, the emissions will be homogeneously distributed through the atmosphere making them independent of the emission location [7]. The temporal development of the atmospheric concentration of CO_2 is calculated according to the same method as in Sausen and Schumann [63] through a response function with different lifetimes, representing the different decomposition processes of CO_2. This response function is shown in Equation 3.24

$$\Delta C^{CO_2}(t) = \int_{t_0}^{t} G_C(t-t')E(t')dt' \tag{3.24}$$

In this equation E(t) is the temporal development of the CO_2 emission converted into volume mixing ratio per year and $G_C(t)$ is a climate impulse response function (Green function) calculated according to Equation 3.25 [63]. This climate impulse response function represents the climate response at time t to a unit emission at time t [29]. In this Equation τ_j is the e-folding time of mode j where the equilibrium response of mode j to a unit forcing is $a_j\tau_j$ [63]. These parameters were found by Hasselmann et al. (1997) [29] as shown in Table 3.5 where they are chosen such that the concentration change of CO_2 approximates the concentration change simulated with a carbon-cycle model (Maier-Reimer and Hasselmann, 1987).

$$G_C(t) = \sum_{j=0}^{5} \alpha_j e^{-t/\tau_j} \tag{3.25}$$

j	1	2	3	4	5
α_j (ppbv/Tg(C))	0.142	0.241	0.323	0.206	0.088
τ_j (year)	∞	313.8	79.8	18.8	1.7

Table 3.5: Coefficients of the impulse response function G_C shown in Equation 3.25 taken from Fichter (2009)[12]

Ozone and water vapor

Due to the relatively short lifetime of ozone and water vapor in the main emission regions of aircraft (in the order of weeks for ozone [49] and up to one month for water vapor [22]), the concentration changes of these forcing components are dependent on both the emission quantity as well as location. For this reason the concentration changes of these components are determined by a linear combination of the aforementioned precalculated emission response functions with the air traffic emissions [12] according to Equation 3.26 [7].

$$\Delta C^{spec} = \frac{1}{T}\int_0^T \frac{E^{spec}(x,t)}{X} \sum_{k=1}^{4} \frac{\epsilon_k(t)\Delta C_{id}^{spec}(i_k,j_k)}{M(i_k,j_k)} dt \tag{3.26}$$

For the time at which the emissions are present, the concentration changes are calculated by multiplying the zonal mean emission at a certain location and time $E^{spec}(x,t)$ in (kg/s) by the global precalculated concentration change of the idealized emission region (the emission response functions denoted by $\Delta C_{id}^{spec}(i_k,j_k)$ in (kg/kg) and integrating over the period in which the emissions take place. The dimensions i and j represent the latitude and pressure level corresponding to region k. A total of four emission response functions are linearly combined where $\epsilon_k(t)$ is the weighing factor of the individual response functions. The individual weighing factors are calculated in accordance with the respective distance of the emission location to the idealized emission region in order to interpolate between the emission regions. Furthermore in this Equation X is the magnitude of the unified emission (in kg/kg air) and $M(i_k,j_k)$ the mass of the idealized emission region in kg.

To determine the temporal development of the global concentration change ΔC_{spec} of O_3 and H_2O a linear differential equation is used as shown in Equation 3.27.

$$\frac{d}{dt}\Delta C^{spec} = P(t) - \frac{\Delta C^{spec}}{\tau_{spec}} \tag{3.27}$$

$$P(t) = s \cdot E(t) \tag{3.28}$$

In this Equation τ_{spec} is the lifetime of the individual species and P(t) (Equation 3.28) is a production term proportional to the emission development of the corresponding emission, E(t) where CO_2 is used for the concentration of H_2O and the emission of NO_x is used for the concentration of O_3. Furthermore a constant s is chosen in such a way that the solution of the differential equation at the time t + the lifetime of the respective species, τ_{spec} agrees with the change in concentration found in Equation 3.26. The time t + τ_{spec} is used since the change in concentration is calculated for a state of equilibrium which sets after a certain time.

Methane

For methane a different calculation method is used because the lifetime of methane is significantly longer than the model simulation duration of three years [7]. For methane the temporal evolution of the concentration change is calculated using the difference between two linear differential equations, Equation 3.29 for the background concentration, $C_0^{CH_4}$ and Equation 3.30 for the perturbation ($C^{CH_4} = C_0^{CH_4} + \Delta C^{CH_4}$)

$$\frac{d}{dt}C_0^{CH_4} = P(t) - \frac{C_0^{CH_4}}{\tau_{CH_4}} \tag{3.29}$$

$$\frac{d}{dt}C^{CH_4} = P(t) - \frac{C^{CH_4}}{\tau_{CH_4}(1+\delta)} \tag{3.30}$$

In these equations τ_{CH_4} is the lifetime of a methane perturbation which is 12 years and δ is the relative change of the lifetime due to the change of the OH concentration by the NO_x emission. The relative change of the lifetime δ is calculated by using and emission response function according to Equation 3.26 where the emission of NO_x is used as E^{spec}. Combining both equations results in the temporal development of the methane concentration change, Equation 3.31.

$$\frac{d}{dt}\Delta C^{CH_4} = \frac{\delta}{1+\delta}\cdot\frac{C_0^{CH_4}}{\tau_{CH_4}} - \frac{1}{1+\delta}\cdot\frac{C^{CH_4}}{\tau_{CH_4}(1+\delta)} \tag{3.31}$$

Contrail Cirrus

For contrail cirrus the term describing the measure of quantity is the coverage rather than the concentration. This contrail coverage however is non linearly dependent on the amount of flown kilometres and therefore it is not possible to determine the coverage as a linear function of the emission input. Instead, a parametrization was developed by Dahlmann (2012) [7] based on simulations with the climate model ECHAM4-CCMod (Burkhardt and Kärcher, 2011)[5] to find a relationship between the two.

To find the relationship between the flown kilometres and the degree of contrail coverage, a measure of the flown kilometres in a contrail sensitive area is determined which is defined as the contrail-flight distance density (CFDD) [9]. In AirClim, the CFDD is calculated by summing the distance flown in a grid box weighed with the average probability of the conditions in this box to satisty the Schmidt-Appleman criterion (p_{SAC}) and summing it over all pressure levels. This is shown in Equation 3.32 where i is the geographical latitude, j the longitude and k the pressure level. In this procedure the average probability to fulfill the Schmidt-Appleman criterion is retrieved from the climate model simulations with the climate model ECHAM4-CCMod (Burkhardt and Kärcher, 2011) [5].

$$CFDD(i,j) = \sum_k \left(\frac{FlownDistance(i,j,k)}{GridboxArea(i,j)} \cdot p_{SAC}(i,j,k) \right) \tag{3.32}$$

As a next step, for every box which overlaps between 200 and 250 hPa the fractional area of ice super saturation (ISS) and the contrail coverage with an optical thickness higher than 0.02 in the short wave (cccov) are calculated with the climate model to establish a relationship between the contrail coverage, contrail-flight distance density and ISS. By fitting this climate model data, the response function was found as shown in Equation 3.33 calculating the degree of coverage for each grid box as function of CFDD. From this data it was found that the degree of coverage increases with contrail-flight distance density until saturation is encountered where saturation value depends on the ice supersaturation frequency. This relationship is shown in Figure 3.25.

$$cccov(i,j) = 0.128 \cdot ISS(i,j) \cdot arctan\left(97.7 \cdot \frac{CFDD(i,j)}{ISS(i,j)}\right) \tag{3.33}$$

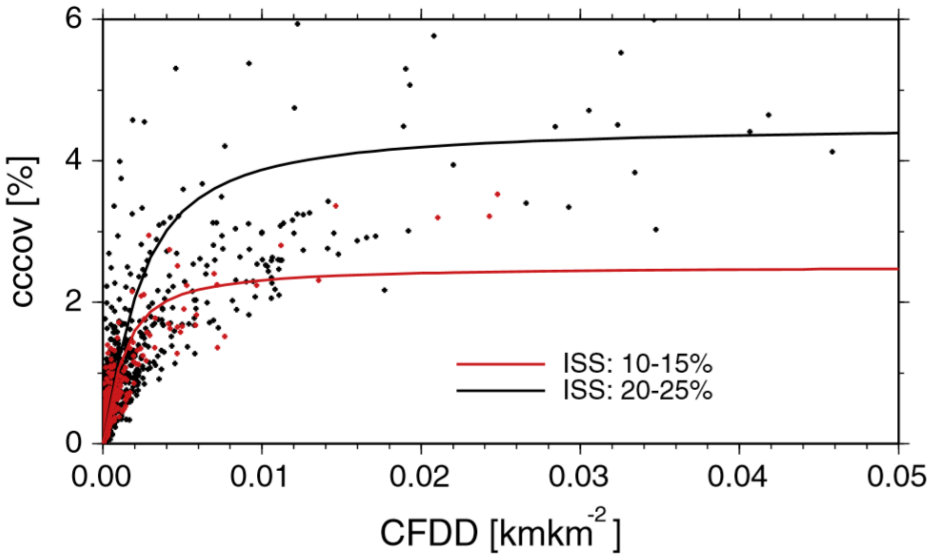

Figure 3.25: Correlation between the contrail-flight distance density (CFDD) and contrail coverage (cccov) for two different regimes of ice super saturation. Data is used from ECHAM4-CCMod and lines represent the best fit. Figure taken from Dahlmann et al. (2016)[9]

Thereafter the global coverage is determined by taking the area weighed coverage average of the individual grid boxes. To find the temporal evolution of global the contrail coverage the contrail kilometre density (CFDD) is scaled with the temporal emission development where in this case the parameter of interest is the flown kilometres.

3.7.4. Calculating radiative forcings

Similar to their atmospheric concentration changes, the radiative forcings of O_3 and H_2O are calculated by linearly combining the air traffic emissions with the precalculated emission response functions according to Equation 3.34 [12]. However for this case the response functions are the precalculated global mean radiative forcings associated with the perturbations from the idealized scenarios [12] denoted by $RF_{id}(i_k, j_k)$. Furthermore $E(l_m, p_n)$ is the zonal mean emission at latitude l_m and pressure level p_n and the total radiative forcing is the summed contribution of all emissions at latitudes m and pressure levels n.

$$RF = \sum_{m,n} \frac{1}{t} \int_{t0}^{t} \frac{E(l_m, p_n)(t)}{X} \sum_{k=1}^{4} \frac{\epsilon_k(t) RF_{id}(i_k, j_k)}{M(i_k, j_k)} dt \tag{3.34}$$

For CO_2 on the other hand, the radiative forcing is calculated with Equation 3.35 according to the IPCC [40] and is only dependent on the logarithm of the concentration change of CO_2. In this equation $C_0^{CO_2}$ is the back ground CO_2 concentration in the atmosphere (in ppm) and the total concentration is defined as $C^{CO_2} = C_0^{CO_2} + \Delta C^{CO_2}$ where ΔC^{CO_2} is the change in concentration due to the aircraft emissions.

$$RF(t) = \alpha_{CO_2} \cdot ln \frac{C^{CO_2}(t)}{C_0^{CO_2}(t)} \tag{3.35}$$

And where $\alpha_{CO_2} = 5.35\ Wm^{-2}$ based on radiative transfer calculations with three-dimensional meteorological input data (Myhre et al 1998b) [56]. Due to its dependency on the logarithm of the relative concentration change, the radiative forcing of an increment in CO_2 concentration has a smaller effect at higher background CO_2 concentrations [63].

The radiative forcing of methane is calculated according to the IPCC [40] as well (Equation 3.36) and is a function of the concentration change where α_{CH_4} = 0.0036 Wm^{-2}, M = C^{CH_4} (the concentration of methane), M_0 = $C_0^{CH_4}$ (the background concentration of methane) and N = C^{NO_2} (the concentration of NO_2) all in ppb. Furthermore, f(M,N) is found according to Equation 3.37.

$$RF(t) = \alpha_{CH_4}(\sqrt{M} - \sqrt{M_0}) - f(M,N) - f(M_0,N)) \tag{3.36}$$

$$f(M,N) = 0.47ln[1 + 2.01 \cdot 10^{-5}(MN)^{0.75} + 5.31 \cdot 10^{-15}M(MN)^{1.52}] \tag{3.37}$$

The temporal evolution of the radiative forcing is calculated by by following the same procedure as discussed in this section while updating the emissions in Equation 3.34 and the flown kilometres in Equation 3.32. For this step it is necessary to assume a temporal development of the used emission input. Furthermore, as indicated by Equations 3.35 and 3.36 the radiative forcings of CO_2 and methane are both a function of the background concentration of the respective species. Therefore to calculate the temporal development of these radiative forcings the temporal development of their respective background concentrations needs to be assumed as well.

The radiative forcing from contrail cirrus is calculated by applying the linear relationship found between global contrail coverage and radiative forcing according to simulations from Burkhardt and Kärcher (Figure 3.26). This linear relationship is shown in Equation 3.38 where the radiative forcing is in Wm^{-2}.

$$RF = 14.9 \cdot \overline{cccov} \tag{3.38}$$

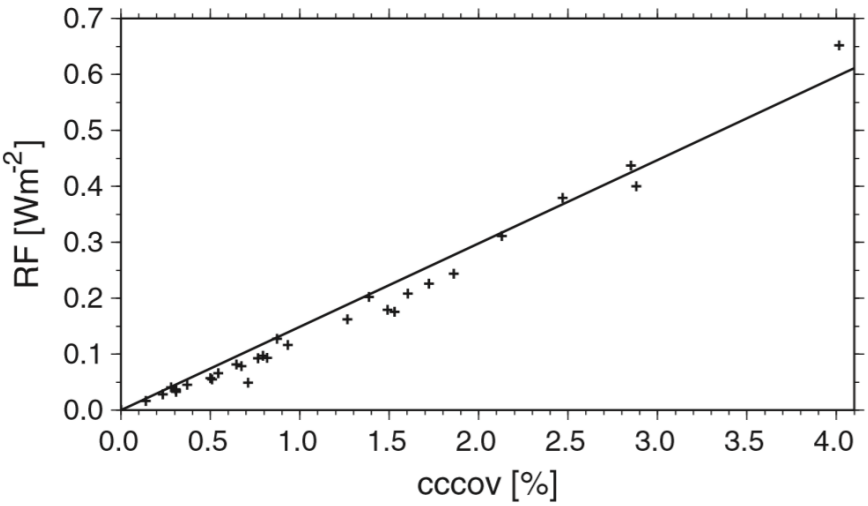

Figure 3.26: Correlation between radiative forcing and contrail coverage (cccov) with an optical dept of 0.02. Climate model data is indicated by the crosses and line represents the best (linear) fit. Figure taken from Dahlmann et al. (2016)[9]

This response function was recently refined by Grewe et al. (2016) [23] to include additional latitudinal dependencies. The updated function is shown in Equation 3.39 where $h(lat)$ is the additional latitude dependency of the radiative forcing shown in Equation 3.40 and $f(lat)$ is a shift of the contrail coverage towards the equator shown in Equation 3.41.

$$RF(lat) = 14.9 \cdot \overline{cccov} \cdot h(lat) \cdot f(lat) \tag{3.39}$$

$$h(lat) = 0.24 \cdot cos\left(\frac{\pi lat}{23}\right) + 1.00 \tag{3.40}$$

$$f(lat) = 0.86 \cdot cos\left(\frac{\pi lat}{50}\right) + 1.62 \tag{3.41}$$

The radiative forcing of primary mode ozone (the decrease in ozone production due to the decrease in methane) is calculated as a linear function of the radiative forcing of methane as in Equation 3.42. This relation was established based on simulations with E39/CA.

$$RF(O_3^{pm}) = 0.29 \cdot RF(CH_4) \tag{3.42}$$

3.7.5. Calculating surface temperature change

The temperature response as function of the radiative forcing is calculated by following the same approach as in Sausen and Schumann [63] according to Equation 3.43 where G(t) is the Green function of the temperature response found by Equation 3.44. This function was fitted to reproduce the performance of a global atmosphere-ocean circulation model to determine the parameters $\alpha = \frac{2.246K}{36.8y}$ and $\tau = 36.8$ years.

$$\Delta T_{spec}(t) = \int_{t_0}^{t} G(t-t')RF^*_{spec}(t')\,dt' \tag{3.43}$$

$$G(t) = \alpha e^{-t/\tau} \tag{3.44}$$

Furthermore RF^*_{spec} is the radiative forcing of a forcing component normalised to the radiative forcing of CO_2 found by Equation 3.45. In this equation λ_{spec} is the climate sensitivity parameter which indicates how strong the climate responds to a normalised perturbation.

$$RF^*_{spec}(t) = RF_{spec} \cdot \lambda_{spec} \tag{3.45}$$

3.7.6. Verification of the climate model results

To verify that the climate model is used correctly, the model results first needs to be verified and validated with results found in literature. Since the model is build up from several calculation steps, the verification process is split into three parts: The calculation of the radiative forcings of all forcings components, the temperature response over time and the sensitivity of the climate impact to changes in altitude. All three verification steps will be discussed separately in the next sections.

Radiative forcings

First of all, the procedure for calculating the radiative forcings will be verified by comparing calculated radiative forcings for the three standard emission inventories to results presented by Dahlmann (2012) [7] and Fichter (2009) [12]. The three standard emission inventories, Quantify, AERO2k and TRADEOFF are identical to the emission input of Dahlmann and Fichter and were acquired by personal communication with Prof. Grewe. All three emission inventories have different characteristics as discussed in Section 3.7.1 which result in a different climate impact. For this reason it is of additional value to verify the model with multiple inputs. The fuel consumption, emissions of NO_x and flown distance of the three emission inventories are summarised in Table 3.3. Other relevant characteristics of the inventories such as the latitudinal and altitudinal distribution of the fuel consumption are presented in Appendix C. Comparing these distributions to the distributions shown in [9] shows good agreement verifying that the emission inventories used in this work are identical to the ones used in [7] and [12].

To verify the radiative forcings from the Quantify and AERO2k emission inventories the work from Dahlmann will be used as reference whereas the work from Fichter will be used to verify the radiative forcings from the TRADEOFF inventory. Results from Dahlmann include calculated radiative forcings of CO_2, H_2O, O_3, CH_4, O_3^{pm} and contrail cirrus for the years 2002 and 2005. These results were obtained by using the AirClim response model which make them very suitable for comparison. Results from Fichter include radiative forcing values CO_2, H_2O, O_3 and CH_4 for the TRADEOFF inventory for the year 2000 calculated with both AirClim and the climate chemistry model E39/CA. Section 3.7.7 will elaborate on the difference between these results acquired with AirClim and E39/CA.

A comparison of the radiative forcings found in this work to the work of Dahlmann and Fichter is shown in Tables 3.6, 3.7 and 3.8. For the historical and future development of the emissions the scenario was used as described in Section 3.7.1 which is consistent with the scenario used by Dahlmann and Fichter.

Emission inventory	Forcing component	This work	Dahlmann[7]	% Difference
Quantify (2000)	CO_2	23.96	23.9	0.3
Quantify (2005)	CO_2	27.43	27.4	0.1
	H_2O	2.47	2.4	2.9
	O_3	30.91	31.1	0.6
	CH_4	-8.72	-13.0	32.9
	O_3^{pm}	-2.51	-3.8	33.9
	Contrail cirrus	48.0	41	17

Table 3.6: Calculated radiative forcings for the Quantify emission inventory in mW/m^2 compared to results presented by Dahlmann [7]. Differences are calculated based on the original numbers before rounding off.

Emission inventory	Forcing component	This work	Dahlmann[7]	% Difference
AERO2k (2002)	O_3	20.5	20.7	1.0
	CH_4	-7.72	-9.8	22.2
	O_3^{pm}	-2.2	-2.7	18.5
	Contrail cirrus	38.53	34.2	12.6

Table 3.7: Calculated radiative forcings for the AERO2k emission inventory in mW/m^2 compared to results presented by Dahlmann [7]. Differences are calculated based on the original numbers before rounding off.

Emission inventory	Forcing component	This work	Fichter[12]	% Difference
TRADEOFF (2000)	CO_2	23.44	23.4	0.2
	H_2O	1.79	1.6	24.4
	O_3	22.38	22.4	0.1
	CH_4	-6.75	-6.9	2.2

Table 3.8: Calculated radiative forcings for the TRADEOFF emission inventory in mW/m^2 compared to results presented by Fichter [12]. Differences are calculated based on the original numbers before rounding off.

Table 3.6 shows that the CO_2 forcings calculated in this work for the Quantify inventory in 2000 and 2005 are in agreement with the results presented by Dahlmann [7]. Furthermore the CO_2 forcing from the TRADEOFF inventory shown in Table 3.8 corresponds to the forcing found by Fichter. This indicates that the historic emission scenario is used correctly as the radiative forcing of CO_2 is a function of the accumulation of CO_2 over the years due to its long lifetime [12]. Dahlmann does not present radiative forcings of CO_2 and H_2O for the AERO2k inventory and are therefore not shown for this work either.

Comparing the radiative forcing from ozone shows good agreement for all three emission inventories. This indicates that the climate sensitivity to the vertical distribution of the emissions of NO_x is modeled correctly since all three emission inventories have a different vertical distribution as shown in Appendix C.

For the radiative forcings of methane a 33% difference is found for both AERO2k and Quantify emission inventories by comparing the calculated radiative forcings with results presented by Dahlmann. The forcing of methane calculated for the TRADEOFF inventory on the other hand corresponds well to the forcing calculated by Fichter.

The difference in radiative forcings for primary mode ozone is a direct effect of the difference in forcings of methane since the forcing from primary mode ozone is calculated as a factor of the methane forcing as shown in Equation 3.42.

The calculated radiative forcings of water vapor show good agreement for both the TRADEOFF emission inventory as well as the Quantify inventory.

Finally the forcing of contrail cirrus is higher compared to the forcing calculated by Dahlmann for both the Quantify and AERO2k emission inventories. This difference was found to be the result of the refined modeling of the contrail forcing as discussed in Section 3.7.4. An additional latitudinal dependency of the contrail coverage and forcing was implemented by Grewe et al. (2016) [23] and was not yet included in the AirClim version of Dahlmann [7]. Results from Grewe et al. (2016) [23] showed that by incorporating additional latitude effect, a forcing of 38.63 mW/m^2 is calculated in comparison to the 34.2 presented by Dahlmann. This updated value is in agreement with the forcing found in this study.

All in all it can be concluded that the radiative forcing values in this work are in agreement with those presented by Dahlmann and Fichter and thereby this part of the model is verified. Small

differences can be attributed to rounding differences and a possible difference in background CH_4 scenario used by Dahlmann which would explain the differences in methane forcing.

Temporal response of radiative forcing and temperature change

To verify that the emissions are correctly scaled in time and that the climate sensitivity parameters are assumed correctly, the temporal response of the temperature change and radiative forcing is calculated and verified with results found by Fichter [12]. Similar to Fichter the TRADEOFF emission inventory is used and emission are scaled in time according to the Fa1 emission scenario as shown in Figure 3.23. Furthermore, the background CO_2 concentration is assumed similar to the one presented in Sausen and Schumann [63].

The calculated temporal development of the radiative forcings and temperature change of all forcing components are shown in Figures 3.27 and 3.28 respectively. These are directly comparable to the results obtained by Fichter which are shown in Figures 3.29 and 3.30. Fichter calculates the response based on both the simulations performed E39/CA represented by the solid line and data calculated with AirClim which are represented by the dashed line. In this comparison the latter is of interest since these results are calculated with the same model.

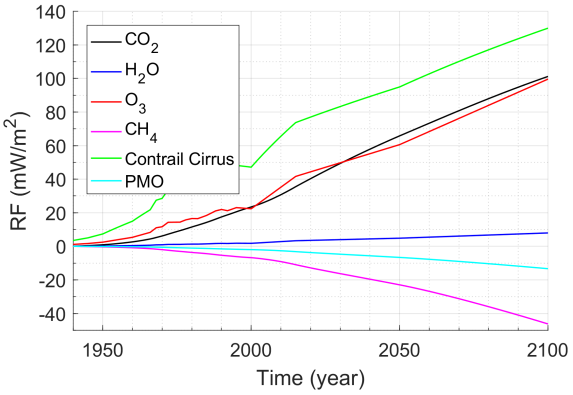

Figure 3.27: Temporal development of the calculated radiative forcing response for the individual forcing components

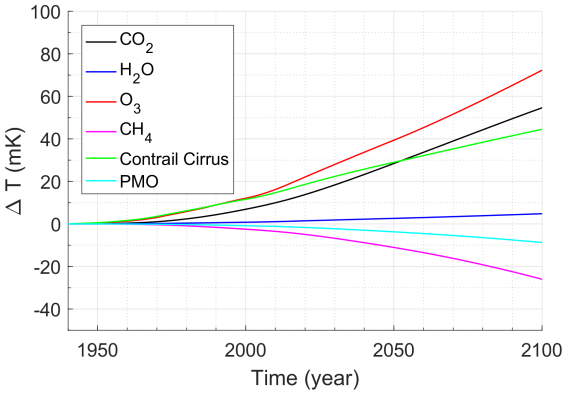

Figure 3.28: Temporal development of the calculated temperature change for the individual forcing components

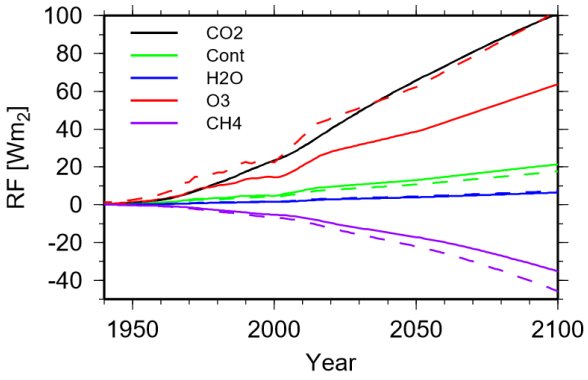

Figure 3.29: Temporal development of the radiative forcing response for the individual forcing components presented by Fichter [12]

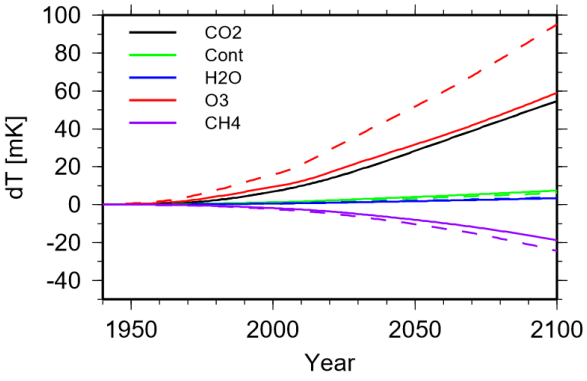

Figure 3.30: Temporal development of the temperature change for the individual forcing components presented by Fichter [12]

By comparing the radiative forcings results obtained in this work shown in Figure 3.27 with results presented by Fichter shown in Figure 3.29 it is observed that the radiative forcing of

all forcing components continuously increase in magnitude. This is due to the increasing fuel consumption of the Fa1 scenario. The magnitude of the forcings of CO_2, O_3, O_3^{pm}, H_2O and CH_4 show good agreement with the forcings calculated by Fichter as presented in Figure 3.29 (dashed lines). In contrast to the work from Fichter a significantly larger contribution to the radiative forcing is calculated for contrail cirrus (green). This is because Fichter only considers the radiative forcing of linear contrails which is roughly nine times smaller in magnitude compared to contrail cirrus [5].

The calculated temperature response shown in Figure 3.28 follows the same trend as found for the radiative forcings shown in Figure 3.27. The temperature response however shows a smoother development compared to the calculated radiative forcings due to the longer response times of the deep ocean [12]. The relative magnitude of the temperature response of the individual species on the other hand shows a different behaviour compared to the radiative forcings. These differences originate from the variations in the climate sensitivity parameters of the individual species. Comparing the temperature response as function of the individual forcing components of Figures 3.28 and 3.28 shows good agreement as well.

Climate sensitivity to changes in cruise altitude

Since the major focus of this work is the assessment of the change in climate impact as function of changes in cruise altitude, it is important to verify the climate impact sensitivity of AirClim with respect to the emission altitude. This verification will be performed by comparing the calculated climate impact for different cruise altitude scenarios with data presented by Fichter [12].

Fichter analyzed the effect of global flight altitude changes by comparing the climate impact of the TRADEOFF base case scenario to the climate impact of alternative scenarios with relocated flight altitudes. These alternative scenarios range from +2000 ft to -6000 ft in steps of 2000 ft and were developed within the EU FP5 Project TRADEOFF. More information regarding the origin and development of these scenarios is presented in Appendix C. The climate impact as function of the 5 scenarios (1 base case and 4 relocated scenarios) is quantified in terms of radiative forcing in the years 2000 and 2100. Similar to this work, the work from Fichter uses AirClim to calculate the radiative forcing differences for the short term forcing components (contrails, ozone and water vapor) in the year 2000 with respect to the base case scenario. For the long term forcings of methane and CO_2 differences in radiative forcings are calculated for the year 2100 based on radiative forcings calculated with E39/CA for the base year 2000 and using AirClim to calculate the temporal development.

Figure 3.31 shows the comparison of the calculated radiative forcing difference with respect to the base case for each individual forcing component calculated in this work and presented by Fichter. Similar to the data presented by Fichter, differences in short term forcings are calculated for the year 2000 and differences in long term forcings are calculated for 2100. As the magnitude of the differences in forcings will differ due to the different time scale, the resulting differences are presented in terms of a percentage. The data to generate Figures 3.31 a-c is shown in Appendix D Tables D.1 and D.2 and the data corresponding to Figures 3.31 d-e is presented in Tables D.4 and D.5.

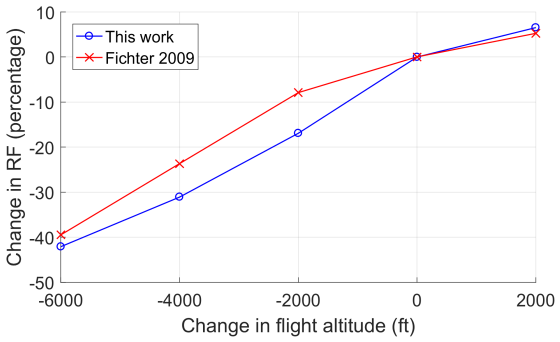

(a) Contrails (Cirrus)

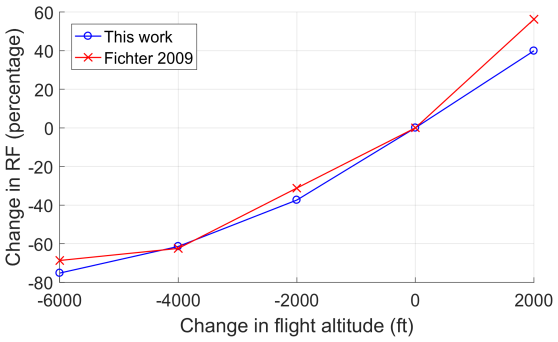

(b) Water vapor, (H_2O)

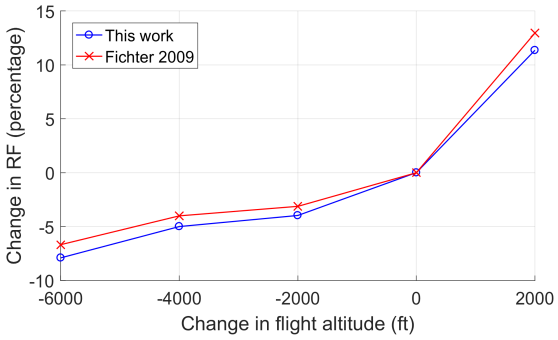

(c) Ozone, (O_3)

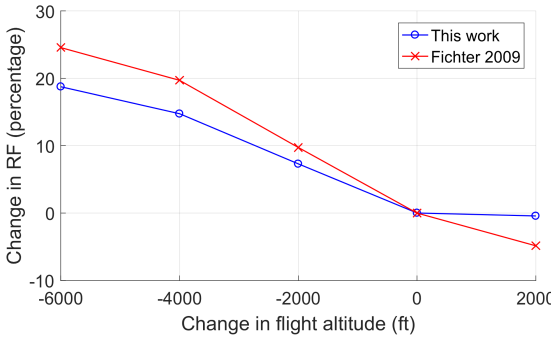

(d) Methane, (CH_4)

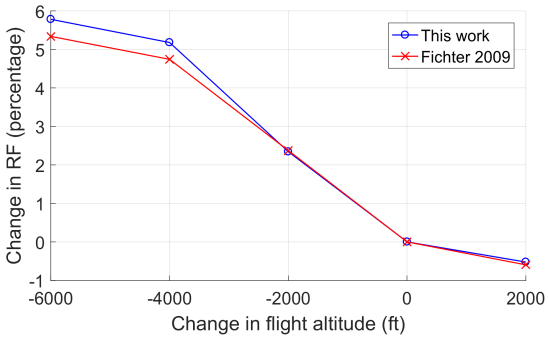

(e) Carbon dioxide (CO_2)

Figure 3.31: Radiative forcing differences with respect to the base case from contrail Cirrus, H_2O and O_3 calculated for the year 2000 and CO_2, CH_4 for the year 2100 through a displacement of flight altitudes by 2000 ft up, 2000 ft down, 4000 ft down and 6000 ft down.

From Figures 3.31 a-e it is observed that the climate response as function of the difference in emission altitude calculated in this work follows the same trend as the results found by Fichter. Radiative forcings from contrail cirrus, ozone and water vapor decrease with a decreasing emission altitude whereas the radiative forcing of CO_2 increases with decreasing emission altitude. For methane a lower flight altitude results in a radiative forcing which increases in magnitude (it becomes more negative).

By analyzing the differences of the short term forcings more closely it is observed that that the forcing magnitude for contrail cirrus, water vapor and ozone is in agreement with results presented by Fichter. Small differences are observed for water vapor which can be attributed to rounding errors in combination with the small magnitude of the forcing (in the order of 2 mWm^{-2}). For ozone differences of a few percent are observed which are considered sufficiently accurate. For contrails Fichter calculates a lower difference compared to the base case

for the -2000 ft and -4000 ft scenarios. This can be attributed to two factors. First of all, Fichter calculates radiative forcings of linear contrails whereas this work calculates the forcings of contrail cirrus. Secondly, the work from Fichter did not include the additional latitudinal dependency for calculating the contrail coverage and resulting forcing. As previously shown in Figure 2.4 the potential contrail coverage shows a strong dependency on the emission altitude in combination with latitude. Therefore this reason is suspected to be the most probable cause for the small difference in contrail forcing reduction shown in Figure 3.31c

Analysing the differences between the long term forcings it is observed that the forcings of CO_2 correspond very well to the results from Fichter where the differences are less than 1%. For methane however larger differences are present. In this work the magnitude of the radiative forcing change for this component is calculated to be smaller compared to Fichter. This difference can be attributed to the calculation procedure where Fichter calculated the forcings differences of the long term components based on forcing values originating from the E39/CA climate chemistry model. As will be shown in Section 3.7.7 the magnitude of the radiative forcings of ozone and methane are significantly larger calculated with AirClim compared to E39/CA and due to this magnitude difference the climate sensitivity to altitude changes is suspected to be different as well. Especially for methane since the forcing is dependent on the background concentration.

3.7.7. Comparison AirClim with other climate models

Since AirClim is a climate response model and does not model all atmospheric processes individually, it is important to validate the AirClim output with results obtained with a more complex climate chemistry model. Dahlmann [7] performed this validation by comparing the radiative forcings values calculated for the year 2005 for the Quantify inventory shown in Table 3.6 to results found by Lee et al. (2010) [49] and Sausen et al. (2005) (not shown). From this comparison it was found that the results obtained with AirClim showed good agreement with results presented in literature.

Furthermore, Fichter analyzed the difference between AirClim results and results obtained with the complex climate chemistry model E39/CA. These results include radiative forcings for all forcing components calculated for the year 2000 with the TRADEOFF emission inventory. The results of the comparison by Fichter are shown in Table 3.9. In this table the forcing from linear contrails is left out since in the current AirClim version this part is no longer present.

Forcing component	E39/CA	AirClim	Difference
CO_2	-	23.4	-
H_2O	1.5	1.6	6
O_3	14.9	22.4	50
CH_4	-5.4	-6.9	28

Table 3.9: Radiative forcing mWm^{-2} in 2000 calculated with the TRADEOFF inventory with E39/CA and AirClim [12]

From this comparison Fichter concluded that the global mean radiative forcing of water vapor agrees well between both models. For ozone and methane higher values were obtained by AirClim compared to E39/CA. According to Dahlmann reasons for this could be the lower spatial resolution of AirClim and non-linearities [9]. Fichter states these differences can be explained by the non-linearities in the chemistry which occur if the NO_x emissions of the real inventory are considerably different in magnitude from the unified NO_x emissions in the idealized regions at the same location. This non-linear effect is caused by the non-linear dependency of

the ozone production per emitted NO_x molecule on the background NO_x shown in Figure 2.3. which indicates that there is a range of background NO_x concentrations where the production of ozone reaches a maximum. Since the actual NO_x emissions of the real inventory can vary significantly from the unified NO_x emissions in the idealized regions, this can results in large variations in the perturbation of the background NO_x and consequently a large deviation in the production of ozone per emitted NO_x molecule [12].

The difference in methane forcing is attributed to atmospheric non-linearities as well where the OH production through air traffic NO_x is similar to ozone non-linearly dependent on the NO_x background mixing ratio and the relation of the unified NO_x emission to the real air traffic NO_x emissions.

Considering the radiative forcing of contrail cirrus the work from Dahlmann showed that forcings calculated with AirClim showed reasonable agreement with calculations performed with the complex climate model ECHAM4-CCMod. Although the contrail coverage was calculated to be identical, the radiative forcing from contrail cirrus was underestimated by 9% [9]. In the most recent AirClim version used for this work this difference was reduced to below 1% by implementing additional latitudinal relation between contrail forcing and coverage as was found by Grewe et al. [23].

To validate the climate sensitivity with respect to changes in emission altitude modeled with AirClim, Fichter analyzed the difference in radiative forcing between AirClim and E39/CA for the TRADEOFF scenarios with a difference in cruise altitude. This was done for the year 2000 for the short term forcing components of ozone, water vapor and contrails. These results are shown in Figures 3.32a, 3.32b and 3.32c and originate from the data presented in Appendix D Tables D.2 and D.3.

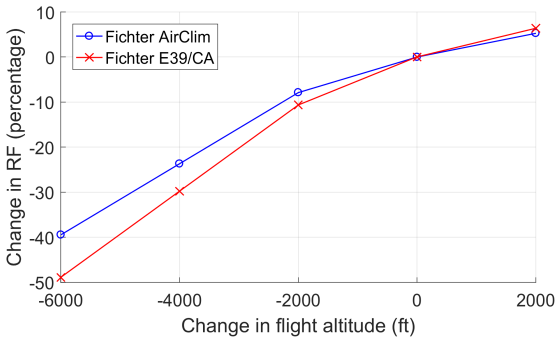

(a) Contrail cirrus (Contrails)

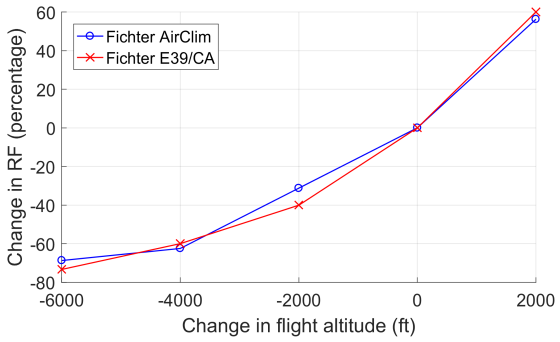

(b) Water vapor, (H_2O)

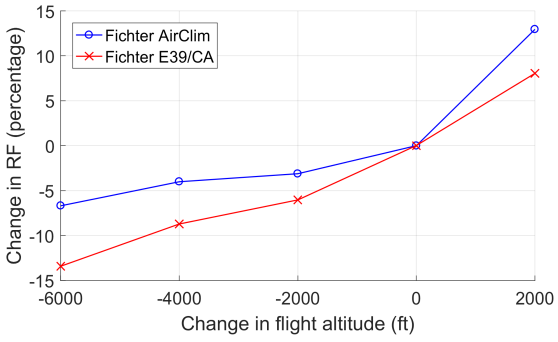

(c) Ozone (O_3)

Figure 3.32: Radiative forcing differences with respect to the base case from Contrail Cirrus, H_2O and O_3 calculated for the year 2000 with AirClim and E39/CA. Data originates from Fichter (2009) [12]

Comparing the results from the two different models Fichter states that the pattern of the induced perturbations is well reproduced. However absolute differences for the contrail and ozone forcing are again due to the non-linear effects. Contrail forcing being dependent on the background contrail and cloud coverage and ozone forcing depending on the background NO_x mixing ratios, both of which can not be fully captured by the linear approach. Additionally the coarser AirClim grid compared to E39/CA causes differences in the response pattern [12].

4

Results

4.1. Flight trajectory characteristics

In this section the characteristics of the assembled trajectory datasets are presented for which the climate impact will be assessed. This will give an indication of the size and distribution of the dataset which will make it comparable to other emission inventories. First of all an overview is shown of the number of found trajectories and their geographical distribution around the globe. Secondly the characteristics of the dataset will be shown in the form of the altitudinal and latitudinal distributions of the calculated fuel consumption. This is of importance since the climate impact of aviation is not only dependent on the quantity of the emissions but on the emission location as well.

4.1.1. Overview assembled trajectory data

Based on the procedure described in Section 3.3 a total set of 3457 flight trajectories was acquired from Flightradar24 of which 1187 B787-800 and 2270 B777-300ER trajectories. From this data set approximately 80% of the tracks were selected to be valid for further analysis based on the criteria outlined in Section 3.3.2. As a result, Table 4.1 shows an overview of the four assembled datasets used for the climate impact analysis. For further in text reference the two aircraft types are abbreviated to B788 and B77W.

Aircraft	20 November	30 March	Total
B787-800	464	454	918
B777-300ER	923	897	1820

Table 4.1: Overview of the total number of trajectories of the individual datasets used for further analysis

The selected trajectories for the B788 and B77W on November 20th are geographically visualized in Figures 4.1 and 4.2. Trajectories are only plotted for one day since the difference in geographical distribution on a daily basis is minimal.

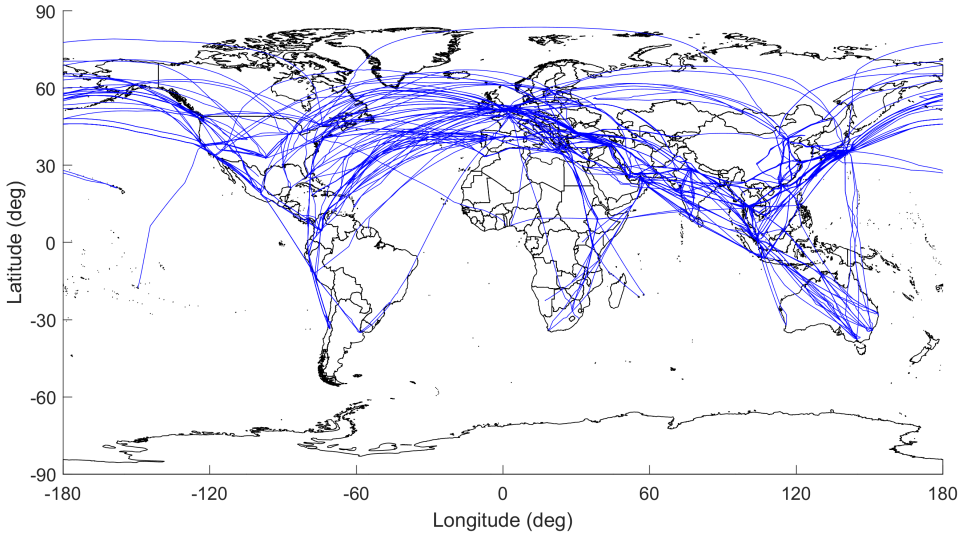

Figure 4.1: Geographical distribution of flown trajectories on November 20th for the assembled B788 dataset in this study

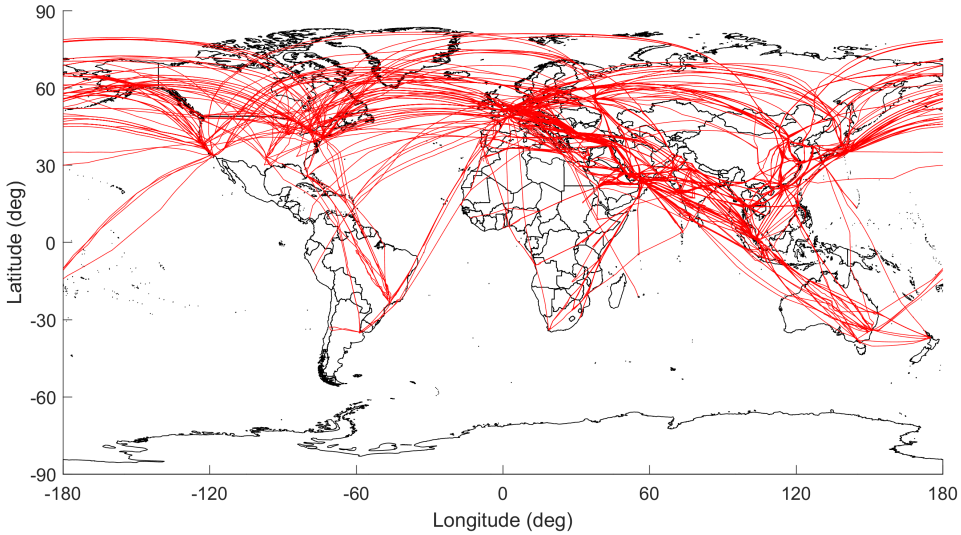

Figure 4.2: Geographical distribution of flown trajectories on November 20th for the assembled B77W dataset in this study

From the traffic distribution over the globe it is observed that for both aircraft types most of the traffic is located in the northern hemisphere which is similar to the AERO2k inventory constructed by Eyers [11] for the year 2002 (not shown). Furthermore the dominant share of air traffic is located in North America, Europe, the Middle East and Southeast Asia which corresponds to the most recent traffic numbers reported by ICAO [1]. This geographical distribution is different compared to the AERO2k inventory where most traffic was located in Europe and North America. This indicates the strong development of air traffic growth in Southeast Asia and the Middle East over the past decades.

[1] `https://www.icao.int/annual-report-2017/Documents/Annual.Report.2017_Air%20Transport%20Statistics.pdf`

4.1.2. Latitudinal distribution of fuel consumption

To analyze the geographical distribution of the found trajectories in more detail, a latitudinal distribution of the calculated fuel consumption for both aircraft types is shown in Figure 4.3 where the B788 distribution is shown in blue and the B77W distribution is shown in red. The latitudinal distribution of emissions is of importance since the emission response functions used by AirClim are dependent on the emission location including latitude. In Figure 4.3 the trajectories for both analyzed days (20 November and 30 March) are included. Additionally the latitudinal distribution of the TRADEOFF inventory is shown by the black dashed line.

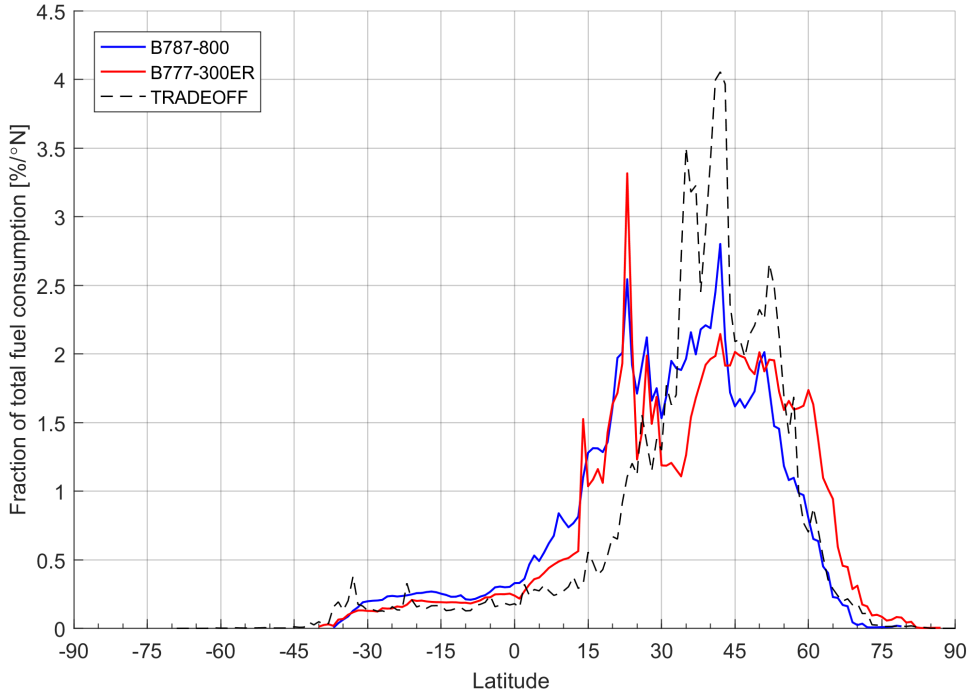

Figure 4.3: Latitudinal distribution of calculated fuel consumption for the assembled B788 dataset (shown in blue) and the B77W dataset (shown in red). Additionally the TRADEOFF latitudinal distribution (black dashed) is shown as reference

From the latitudinal distribution of the found trajectories it is observed that for both aircraft types most traffic is located at a latitude between 15 degrees and 60 degrees north. This is a relatively broad bandwidth compared to the standard emission inventories discussed in Section 3.7.1. The TRADEOFF inventory for example shows a bandwidth more concentrated between 30 and 60 degrees north. The increase in traffic between 15 and 30 degrees latitude can be attributed to the increasing traffic in the Middle East and Southeast Asia as discussed in the last section.

Analyzing the two latitudinal distributions more closely, two pair of coinciding peaks are observed at 23 and 40 degrees latitude for both aircraft types. The first and largest peak at 23 degrees north is due to the United Arab Emirates and Hong Kong being located close to this latitude. Furthermore especially the Boeing 777-300ER dataset shows to have a high concentration of fuel consumption at 23 degrees. This can be attributed to the large fraction of flights (approximately 25%) being operated by Emirates which has a base hub at Dubai airport. The second peak at 40 degrees latitude is consistent with the peaks in the TRADEOFF, Quantify and AERO2k dataset as shown in Appendix C2 and originates mainly from the traffic between Europe and North America and traffic to and from Beijing.

4.1.3. Altitudinal distribution of fuel consumption

As the emission altitude has a large effect on the climate impact of air traffic, the difference in emission altitude is analysed for the two different aircraft types and shown in Figure 4.4.

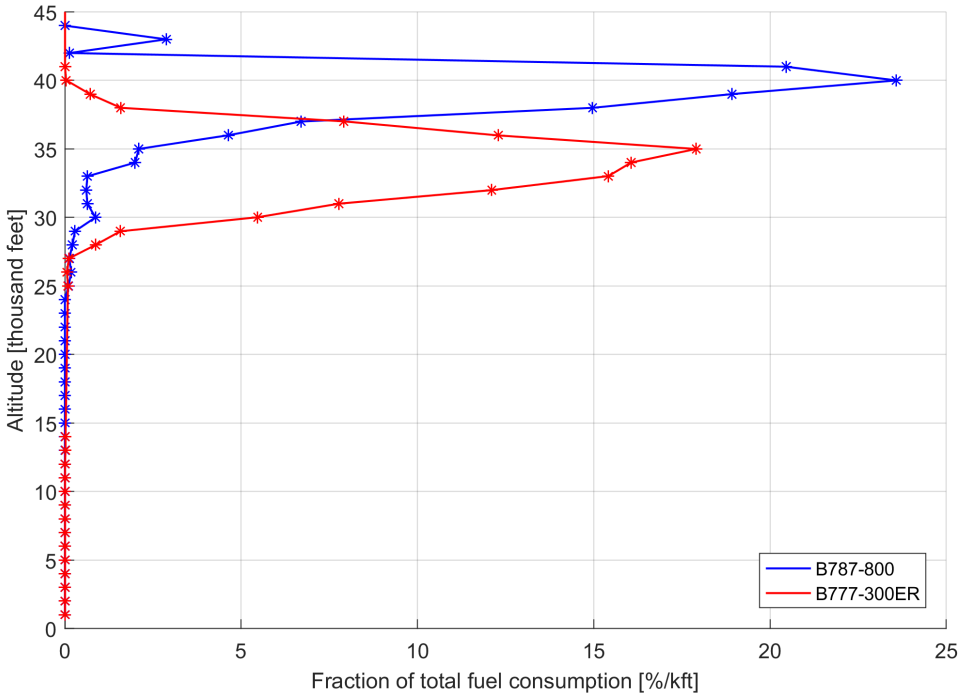

Figure 4.4: Altitudinal distribution of fuel consumption for the assembled B788 dataset (shown in blue) and the B77W dataset (shown in red).

Figure 4.4 shows the altitudinal distribution of the calculated fuel consumption for the analysed B788 dataset in blue and B77W dataset in red. The consumed fuel of both aircraft types shows a large variation in altitude where the B788 shows a peak around 40,000 ft and the B77W shows a peak at around 34,000 ft. These findings are similar to the altitudinal distributions found with the Opensky trajectory data discussed in Section 3.2.4. It should be noted however that the Opensky analysis is based on flown kilometers and not on consumed fuel.

By summing the contribution of the three most frequently flown altitudes for the two different aircraft types it is found that the B788 consumes 63.9% of its total fuel in an altitude range from 39,000 ft to 41,000 ft whereas the B77W consumes 49.3% between 33,000 ft and 35,000 ft. These two altitude ranges are 6,000 ft (approximately 2 kilometers) apart which is significant.

For both aircraft the calculated fuel consumption is zero below an altitude of 25,000 ft. This is because this study only considers the cruise phase with a lowermost altitude of 25,000 ft as outlined in Section 3.3. Fuel consumption during climb and descent are not shown in this figure since emissions during cruise and climb will not be considered for the climate impact assessment. The contribution of the climb and descent phase to the total fuel consumption is calculated only to estimate the aircraft TOW.

4.2. Mach number analysis

Results of the Mach number analysis for both the B788 and the B77W analysed trajectories for the two different dates are shown in Appendix B1 in the form of histograms. From these results it is observed that the data follows a normal distribution and the range of calculated Mach numbers is fairly narrow from approximately 0.80 to 0.86 for both aircraft types. This justifies the assumption that both aircraft are generally operated between MRC and LRC as stated in Section 4.4.4. Interestingly the distributions for each aircraft type show the same characteristics for the two different days where both the mean Mach number and the standard deviation are very similar. This indicates that the results are independent of the weather situation which shows that the used method is robust. Based on these results, mean Mach numbers of 0.844 and 0.830 were found for the B788 and B77W respectively. For this reason these have been used as input for the Piano-X performance module.

To investigate whether there is any correlation between the flown Mach number and the cruise altitude a second analysis was performed. Results of this analysis are presented in Appendix B2 in the form of a scatter plot where all blue points indicate a calculated instantaneous Mach number. Furthermore the red line indicates the average Mach number for each altitude level. From this trendline it is observed that for the B788 the average Mach number is constant and independent of cruise altitude for the range of altitudes from 34,000 to 43,000 ft. Similar results are found for the B77W where the altitude range for which the Mach number is constant ranges from 28,000 to 39,000ft. Both altitude ranges extend over nearly the full operational altitude range of both aircraft types as presented in Figure 4.4.

The found results indicate that airlines fly a certain Mach number independent of their respective cruise altitude. Below these altitude ranges the average Mach number does fluctuate where the overall trend is that the Mach number decreases for altitudes below 34,000 ft for the B788 and below 28,000 ft for the B77W. It should be noted however that the number of data points and corresponding distance flown at these altitudes is only a small fraction of the total dataset as can be seen in Figure 4.4 which makes these results statistically less significant. A probable cause for this overall lower Mach number at these low altitudes is due to aircraft flying a short cruise segment. In some cases it is therefore not worthwhile to accelerate up to a high cruise Mach numbers. A second reason is the increasing equivalent airspeed encountered when flying lower at a constant Mach number as shown in Figure 3.8.

4.3. Results regression analysis

This section presents the results of the regression analysis based on the output performance data of the Piano-X performance module including the specific air range and the NO_x emission index.

4.3.1. Specific air range vs altitude for constant weight

To analyse the performance in terms of range for the two aircraft types as function of the cruise altitude and weight, the specific air range (SAR) is plotted against cruise altitude for a constant aircraft weight ranging from operational empty weight (OEW) + payload + 10% fuel load to OEW + payload + 90% fuel load as can be seen in Figures 4.5a and 4.5b. In this analysis 100% fuel load is defined as the maximum amount of fuel which can be taken onboard considering the aircraft specific MTOW limit and average payload weight listed in Table 4.2.

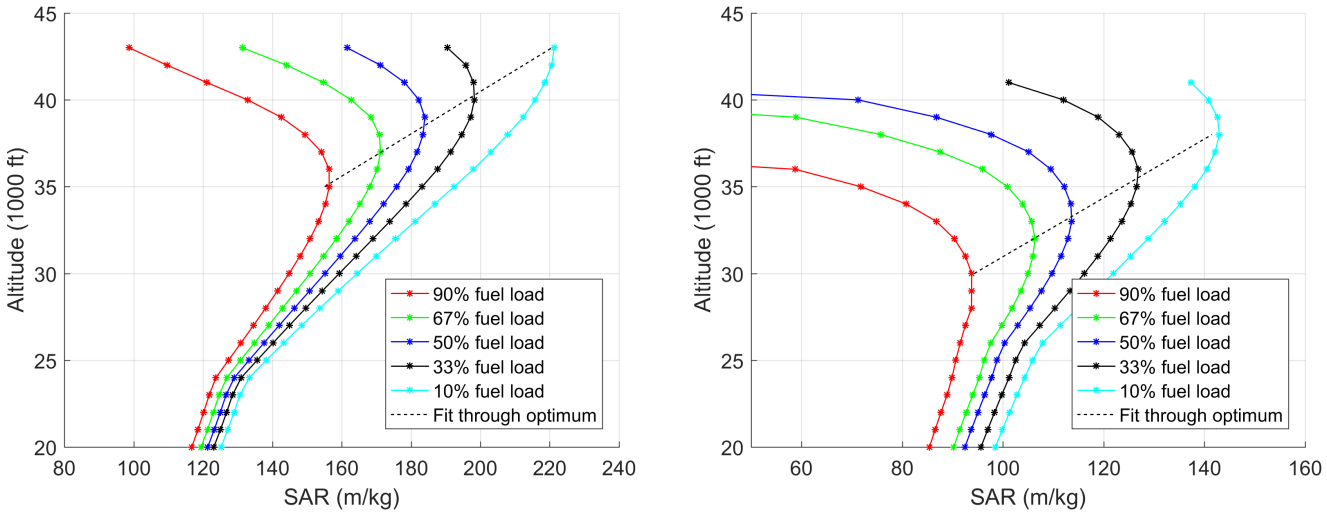

(a) B788

(b) B77W

Figure 4.5: Specific air range (SAR) as function of altitude for constant weight for the B788 and B77W aircraft types. Results for five different aircraft weights are shown ranging from 10% fuel load to 90% fuel load.

From Figures 4.5a and 4.5b it is observed that the SAR is highly dependent on the cruise altitude and a clear optimum can be found depending on the aircraft weight. Flying above or below this optimum altitude yields a decrease in specific air range and therefore a higher fuel consumption. Furthermore the altitude for which the optimum specific air range is obtained increases when the aircraft becomes lighter as indicated by the dotted line. This is because a lighter aircraft requires less lift to be in equilibrium and therefore can fly at a higher cruise altitude without compromising the optimum value for lift coefficient. This effectively results in a lower drag due to the reduced air density. As a consequence of this higher optimum cruise altitude with decreasing weight, aircraft perform regular step climbs to higher cruise altitudes. Secondly it is observed that the SAR decreases faster when flying above the optimum altitude compared to flying at a lower altitude than optimum. This is an important observation regarding the proposed altitude shifts where the performance data suggests that lowering the flight altitude will result in a lower penalty in fuel consumption compared to flying at a higher cruise altitude.

Furthermore, for both aircraft types the SAR decreases almost linearly with decreasing altitude from the optimum altitude to the altitude at which the transition takes place from constant Mach number to constant equivalent airspeed. This transition point from constant Mach to constant equivalent airspeed is indicated by the kink in the SAR plots and is located around 24,000 ft for the B788 and 26,000 ft for the B77W.

Below these altitudes the SAR decreases slower with altitude because the Mach number and true airspeed decrease as the equivalent airspeed is kept constant while lowering the flight altitude.

By looking at the individual aircraft types it is observed that the B788 has an optimum cruise altitude at 35,000 ft for an almost fully loaded aircraft which increases to 43,000 ft for an aircraft with only 10% fuel left. Furthermore it is observed that when the fuel load is less than 50% the optimum cruise altitude increases to 39,000 ft and higher. From the found altitude distribution shown in Figure 4.4 it is observed that the largest share of fuel emissions are located around 40,000 feet which indicates that if the aircraft would have flown fuel optimal, most flown kilometers would be flown with a fuel load in the range from 10% to 50%. This will be discussed in more detail in Section 4.6.1.

For the B77W it is observed that the optimum altitude ranges from 30,000 ft for an almost fully loaded aircraft to 39,000 ft for an empty aircraft. From the found altitude distributions it is observed that the largest share of kilometers are flown around 35,000 ft. By assuming the aircraft is operated close to its optimum SAR this which would indicate that most flown kilometers would be flown with a fuel load in the range from 33% to 50%.

4.3.2. Nitrogen oxide emission index vs altitude for constant weight

Similar to the specific air range, the effect of aircraft weight and cruise altitude is analysed with respect to the NO_x emission index. Figures 4.6a and 4.6b show the results of this analysis.

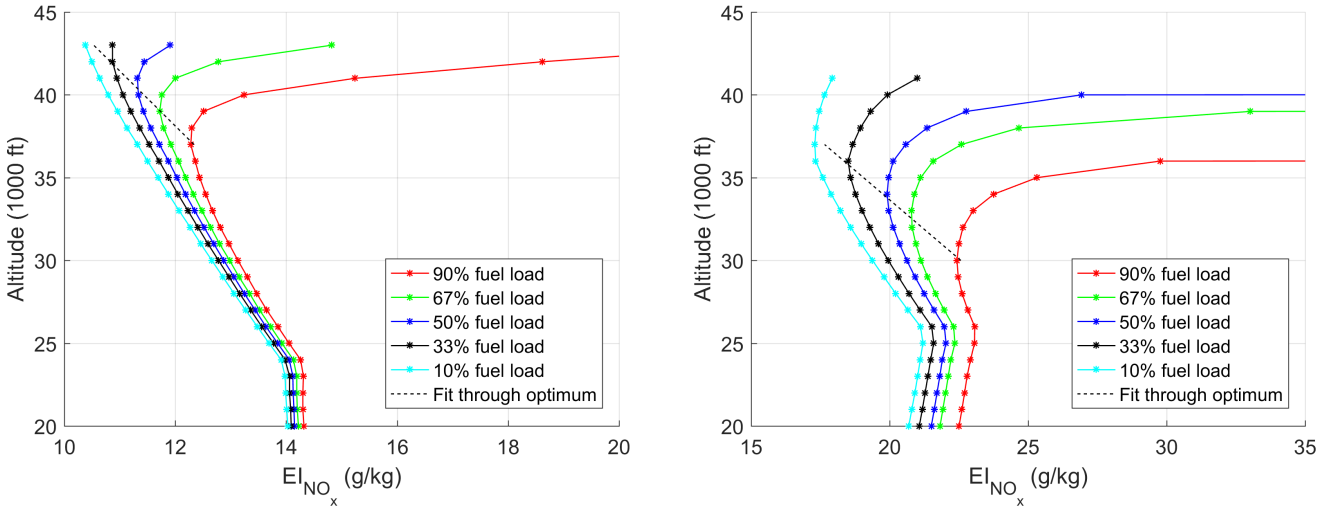

(a) B788

(b) B77W

Figure 4.6: NO_x emission index EI_{NO_x} as function of altitude for constant weight for the B788 and B77W aircraft types. Results for five different aircraft weights are shown ranging from 10% fuel load to 90% fuel load.

Figures 4.6a and 4.6b show that the NO_x emission index strongly depends on cruise altitude and aircraft weight. Similar to the results found for the specific air range, the optimum NO_x emission index is attained at a higher cruise altitude when the weight reduces. This is indicated by the dotted line where in this case the optimum emission index is defined as the lowest one. As a consequence, by initiating a step climb to attain the optimum SAR, the emission index is positively influenced as well.

Similar to the results for the specific air range, a kink in the performance plots can be observed around 24,000 ft for the B788 and around 26,000 ft for the B77W. This is again due to the transition from constant Mach number to constant equivalent airspeed as discussed in Section 4.4.6. Furthermore it is observed that for some combinations of TOW and cruise altitude, the NO_x emission index follows an asymptotic curve and increases to values beyond of the plotted range. This behaviour is observed for the SAR as well and the reason for this is that the aircraft is too heavy to cruise at the specific cruise altitude and is flying in an off-design condition. These combinations of aircraft weight and altitude can be disregarded since large upward altitude shifts will not be considered in this study.

4.4. Aircraft parameters

To determine the aircraft performance and emissions during cruise of each analysed trajectory, this study uses the aircraft parameters as presented in Table 4.2. The parameters stated under assumptions are a result of the method discussed in Sections 3.4.5 and 3.4.7. All other parameters are taken from Janes [42].

Parameter	**B787-800**	**B777-300ER**
Weights and Range		
Maximum take-off weight (kg)	227,930	351,535
Operating empty weight (kg)	117,705	167,825
Maximum zero fuel weight (kg)	161,025	237,680
Fuel capacity (usable) (kg)	101,015	145,535
Maximum range (km)	14,816	14,593
Assumptions		
Cruise Mach number	0.844	0.830
Average passenger capacity	242	355
Weight per passenger(kg)	95	95
Passenger load factor (%)	82	81
Cargo carried per flight (kg)	5,900	10,600
Average payload per flight (kg)	25,000	38,000

Table 4.2: Aircraft parameters used in this work

It should be noted that the listed passenger capacity and payload are average values calculated for the assembled dataset. As mentioned in Section 4.4.6, the actual number of passengers carried per flight and the corresponding payload weight depends on the airline.

4.5. Fuel consumption during cruise

Based on the calculation procedure discussed in Section 3.6 the fuel consumption during the cruise phase is calculated for each trajectory. This is done based on the specific air range (SAR) as well as the specific ground range (SGR) to analyse the effect of wind. The resulting cruise fuel consumption without the effect of wind is shown in Figures 4.7a and 4.7b for the B788 and B77W respectively where the calculated fuel consumption for each trajectory is represented by a blue dot. To show the general trend, a curve is fitted through the data shown by the green line. Additionally a linear dashed black line is shown to emphasize the behaviour of the trend-line. Furthermore, for the purpose of verification, complete trajectories with a varying cruise altitude are simulated in Piano-X of which the cruise fuel consumption is shown by the red crosses. This data verification data is only retrieved for the B788 aircraft and is found according to the same method elaborated upon in Section 3.6.1

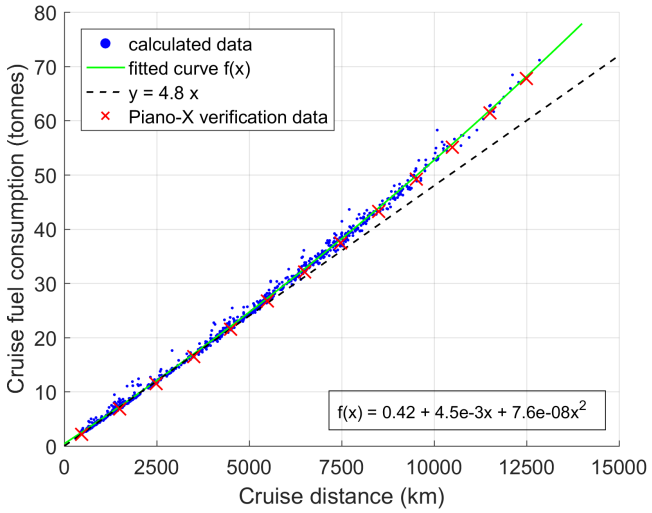

(a) B788 (excluding wind)

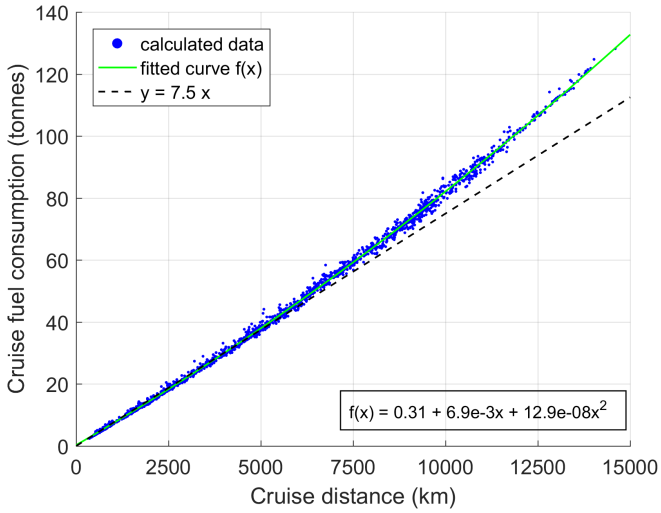

(b) B77W (excluding wind)

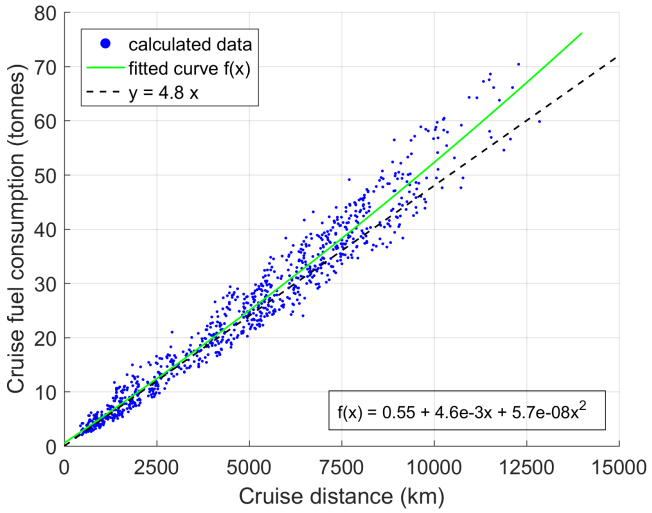

(c) B788 (including wind)

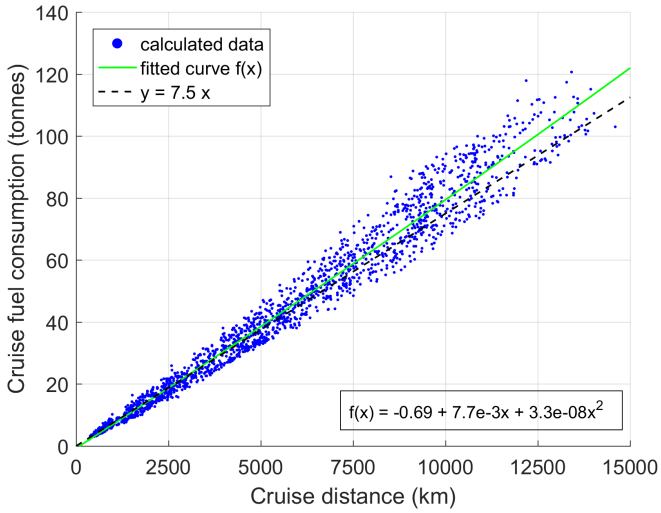

(d) B77W (including wind)

Figure 4.7: Cruise fuel consumption as function of cruise distance for all B788 and B77W flights calculated excluding and including the influence of wind. Each blue dot represents one trajectory.

From Figures 4.7a and 4.7b it is observed that as the cruise distance increases, the cruise fuel consumption increases as well. This relation however is not linear as the data points tend to follow a second order polynomial fitted curve shown in green of which the equation is shown at the bottom of the plot. Comparing this fitted curve to the plotted straight line in black, it is observed that the larger the cruise distance the more the data points move away from the linear curve. This indicates that the fuel consumption per distance flown is higher for long haul flights. The reason for this is that the total fuel carried on board for a long distance flight is higher which increases the weight of the aircraft which leads to a higher fuel consumption throughout the flight. This is due to the relation between SAR and aircraft weight as shown in Figures 4.5a and 4.5b. Finally, the calculated fuel consumption for all tracks is verified by comparing the found trend in green to the fuel data retrieved from Piano-X shown by the red crosses. Comparing the verification data to the fitted curve shows good agreement.

By looking at the vertical spread in fuel consumption it is observed that the calculated fuel consumption for one specific flight distance can vary slightly. The reason for this is that the estimated payload weight of both aircraft types can vary significantly from 20,000 kg to 32,000 kg for the B788 and from 29,000 kg to 46,000 kg for the B77W. This is due to the varying passenger capacity per airline. As the fuel consumption is dependent on the weight of the aircraft this will cause differences in the calculated total fuel consumption. The effect of varying payload on the fuel consumption is discussed in more detail in Section 4.8.2. Additionally, for some outliers with a high calculated fuel consumption an atypical altitudinal profile was found (not shown). For example, a B788 trajectory was found which covered a cruise distance of almost 8,000 km while remaining at 34,000 ft for the entire flight. A reason for the aircraft to remain at this lower less fuel efficient cruise altitude can be to minimize the effect of a headwind.

Figures 4.7c and 4.7d show the calculated fuel consumption based on the specific ground range which incorporates the effect of wind. The cruise fuel consumption follows the same trend as observed for the case without wind however a larger spread is observed. This larger spread can be attributed to the significant impact of the windspeed on fuel consumption as already indicated in Section 3.6.2. Furthermore, as the cruise distance increases this spread grows larger due to the longer time these trajectories are subjected to the prevailing wind pattern.

4.6. Aircraft Take-off weight and instantaneous weight

As discussed in Section 3.4.7 the take-off weight (TOW) is calculated by summing the aircraft OEW, fuel load and payload and this process is iterated until the value for TOW converges. Figures 4.8a and 4.8b present the resulting aircraft TOW for all trajectories for the analysis neglecting the effect of wind. Furthermore Figures 4.8c and 4.8d show the result of the analysis by including the effect of wind. The calculated TOW values are presented as blue dots and a green line is fitted through the data points to show the overall trend. Furthermore the red horizontal line represents the aircraft MTOW as presented in Table 4.2. Finally, the verification data as shown by the red crosses is retrieved for the B788 by simulating complete trajectories with a varying cruise distance in Piano-X. This was done according to same method as discussed in Section 3.6.1 and assuming an average payload weight of 25,000 kg.

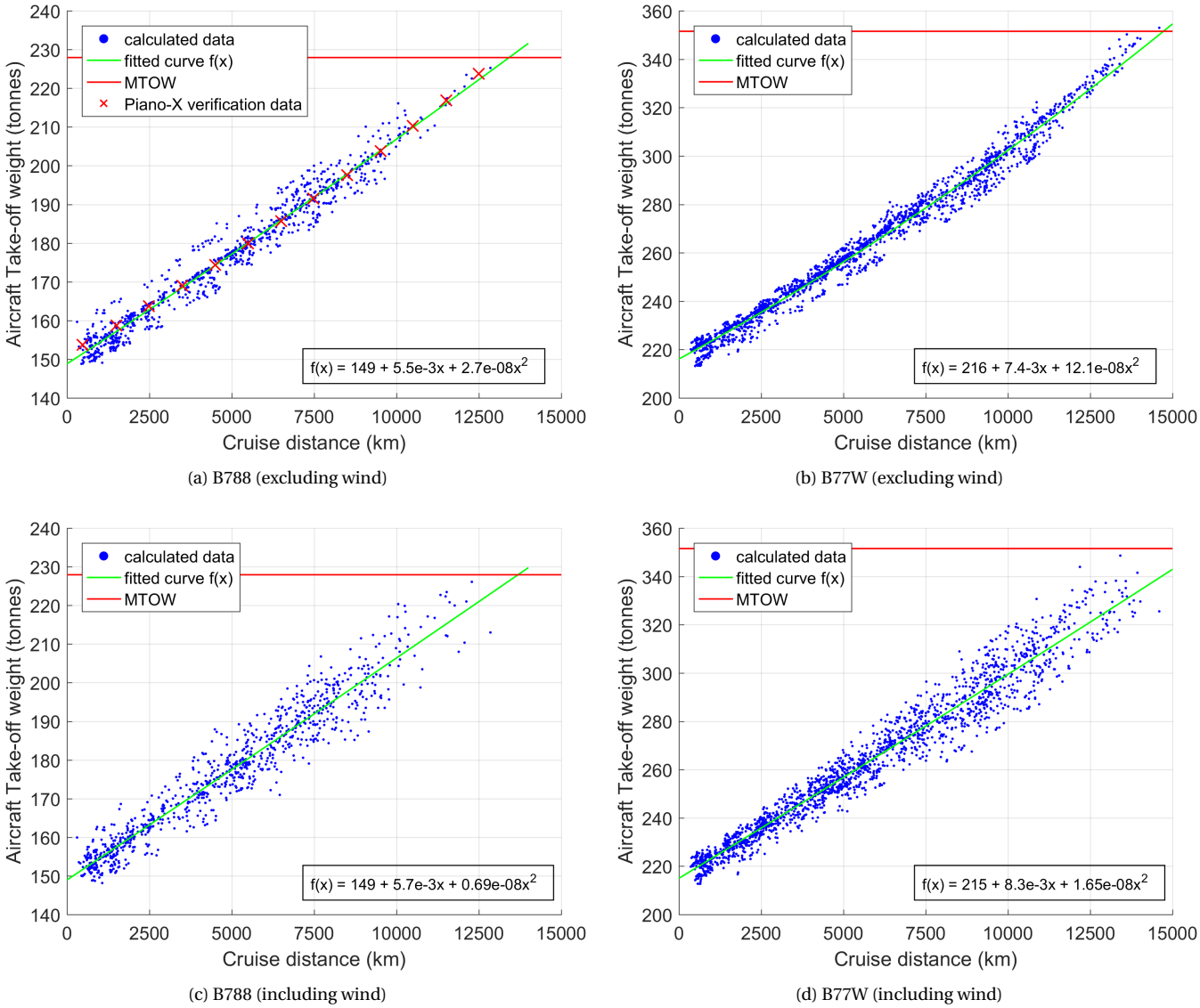

(a) B788 (excluding wind)

(b) B77W (excluding wind)

(c) B788 (including wind)

(d) B77W (including wind)

Figure 4.8: Take-off weight as function of cruise distance for all B788 and B77W trajectories for the case including and excluding the influence of wind

From Figures 4.8a and 4.8b it is observed that the TOW increases with cruise distance due to the increasing fuel weight. A larger vertical spread is found due to the variance in payload weight which can be up to 12,000 kg for the B788 and 17,000 kg for the B77W. Comparing the found trend to the Piano-X verification data shows good agreement. Furthermore all trajectories except one have a calculated TOW lower than the MTOW. This is an acceptable result considering the uncertainty in payload weight. As shown in Table 4.2 the maximum range of both aircraft is 14,816 km for the B788 (with 250 passengers) and 14,593 km (no conditions listed) [42]. This corresponds well to the found combination of TOW and maximum cruise distance shown in the figures where the maximum range is approached closely when the aircraft is at its MTOW. (It should be noted however that this is cruise distance and not total distance). This indicates that the aircraft could not have flown further under the assumed conditions.

When incorporating the effect of wind as shown in Figures 4.8c and 4.8d the spread in TOW increases due to the larger spread in fuel consumption observed from Figures 4.7c and 4.7d. Furthermore it is observed that for the largest cruise distances the TOW decreases compared to the results found for the TOW analysis in the no wind case. This indicates that these long trajectories were subjected to a beneficial wind pattern increasing their specific ground range and thereby reducing their fuel consumption. For this reason they are able to fly the long distance without exceeding the MTOW limit.

4.6.1. Aircraft instantaneous weight

Figures 4.9a and 4.9b show the calculated instantaneous aircraft weight for all cruise segments of all analysed trajectories. Both aircraft show the same characteristic distribution which is skewed to the right (positive skewness). The reason for this is that in principle all flights reach their destination with the same minimum required fuel left in the tanks whereas only a limited amount of long haul flights will start with a full tank. Furthermore the aircraft spend most of their time with a fuel load between 10 and 50%. This fuel load confirms the assumption stated in Section 4.3. It should be noted however that these fuel loads are determined based on an average payload of 25,000 kg for the B788 and 38,000 kg for the B77W. The minimal payload however was found to be 20,000 kg and 29,000 kg for both aircraft respectively. For this reason the fuel load can decrease below 10%.

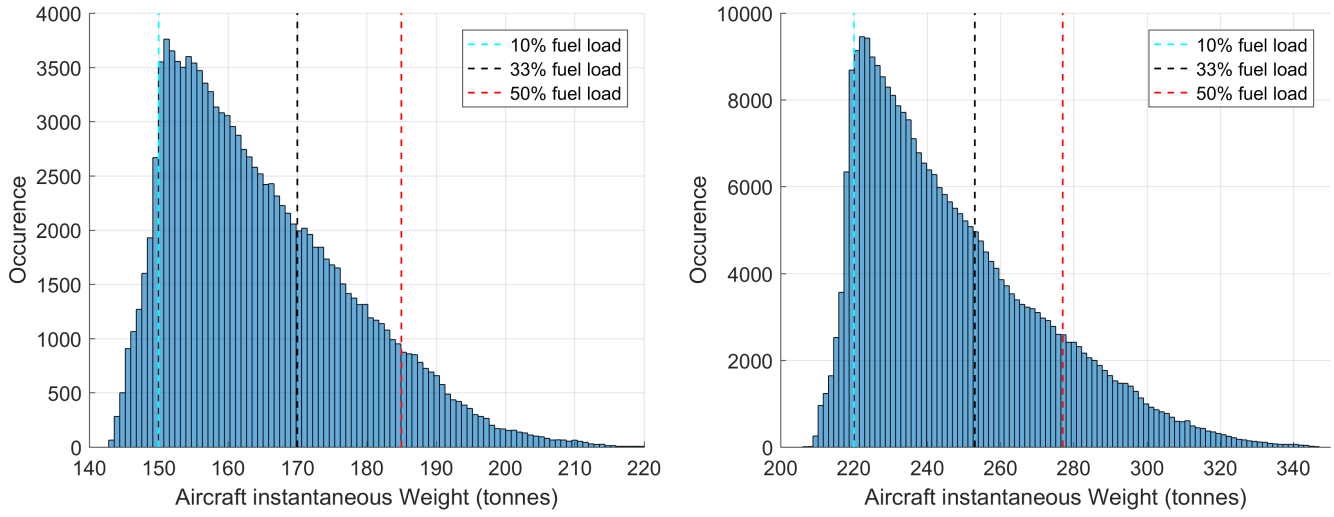

(a) B788

(b) B77W

Figure 4.9: Distribution of instantaneous aircraft weight for all B788 and B77W trajectories excluding the influence of wind. Vertical lines are shown to indicate the aircraft weight corresponding to a 10, 33 and 50% fuel load

4.7. Climate impact assessment

In this section the results of the climate impact assessment for the analysed trajectories will be presented. First the climate impact of the base case for both aircraft types will be determined for which the trajectories retain their original flown cruise altitude as found in the trajectory data. Thereafter the climate impact of seven alternative scenarios is evaluated where the cruise altitude is shifted up by 2000 ft and down by 2000, 4000, 6000, 10000, 14000 and 18000 ft. For these alternative scenarios the aircraft performance and corresponding emissions are reevaluated resulting in different emission inventories.

4.7.1. Emission inventories Base case

Table 4.3 shows an overview of the calculated total fuel consumption and NO_x emissions of the B788 and B77W data sets for the original cruise altitude scenario. These two datasets form the basis to determine the climate impact of the base case. These two inventories however represent a significantly smaller quantity of emissions and flown kilometers compared to the global air traffic pattern which is represented for example by the TRADEOFF inventory as shown in Table 4.4. As a consequence of this smaller emission quantity, saturation effects which are present for the atmospheric concentration of CO_2 and the coverage of contrails is not accurately represented if these unaltered inventories are used as input for the climate response model. For this reason the B787 and B77W emission inventories are normalised with respect to the amount of flown kilometers by scaling the flown kilometers to that of the TRADEOFF inventory. Furthermore the emissions of CO_2 and NO_x are scaled by the same factor to account for the increase in flown kilometers. The emission inventories resulting from this scaling process are shown in Table 4.4 and are representative of a global fleet. Moreover, by normalizing the emission inventories with respect to flown kilometers, it can be analyzed which aircraft type has a larger climate impact per flown kilometer. This will be done in Section 4.7.2.

Emission inventory	Flights	Fuel (10^6 kg)	NO_x (10^3 kg)	EI_{NO_x} (g/kg)*	Distance (10^6 km)
B788 (base case)	464	11.0	123.0	11.2	2.17
B77W (base case)	923	39.9	744.3	18.6	5.19

Table 4.3: Overview of the original emission inventory characteristics. *EI_{NO_x} is the calculated fleet average NO_x emission index of all analysed trajectories corresponding to the emission inventory

Emission inventory	Fuel (Tg)	NO_x (Tg_N)	EI_{NO_x} (g/kg)*	Distance (10^9 km)
B788 (base case scaled)	128	0.44	11.2	25.4
B77W (base case scaled)	194	1.10	18.6	25.4
TRADEOFF	154	0.60	12.8	25.4

Table 4.4: Overview of the scaled emission inventory characteristics where both inventories are scaled to the TRADEOFF flown kilometers. *EI_{NO_x} is the calculated fleet average NO_x emission index

By comparing the scaled base case B788 and B77W emission inventories a significant difference in fuel consumption and produced emissions per kilometre is observed between the two aircraft types. Quantifying this difference, the B77W consumes approximately 50% more fuel per kilometre compared to the B788 (7.7 kg vs 5.0 kg). Furthermore, the B77W produces nearly 2.5 times as much NO_x which is due to its higher emission index in combination with the higher fuel consumption. The reason for this higher fuel consumption is due to the difference in size of the two aircraft types where the B77W is larger and less fuel efficient per kilometre flown. This can also be observed in the SAR plots shown in Figure 5.5.

4.7.2. Climate impact Base case

The climate impact of the base case of the two aircraft types is evaluated with the AirClim climate response model. This is done by using the scaled B788 and B77W emission inventories presented in Table 4.4 as input. Furthermore, the same historic and future emission scenario is assumed as used for the TRADEOFF scenario which is elaborated upon in Section 3.7.1. Results of the temporal development of the radiative forcings are shown in Figures 4.10a and 4.10b. Furthermore the resulting temperature change is presented in Figure 4.11a 4.11b. Absolute numbers corresponding to the radiative forcing and temperature change for the individual forcing components in the year 2100 are presented in Tables 4.5 and 4.6.

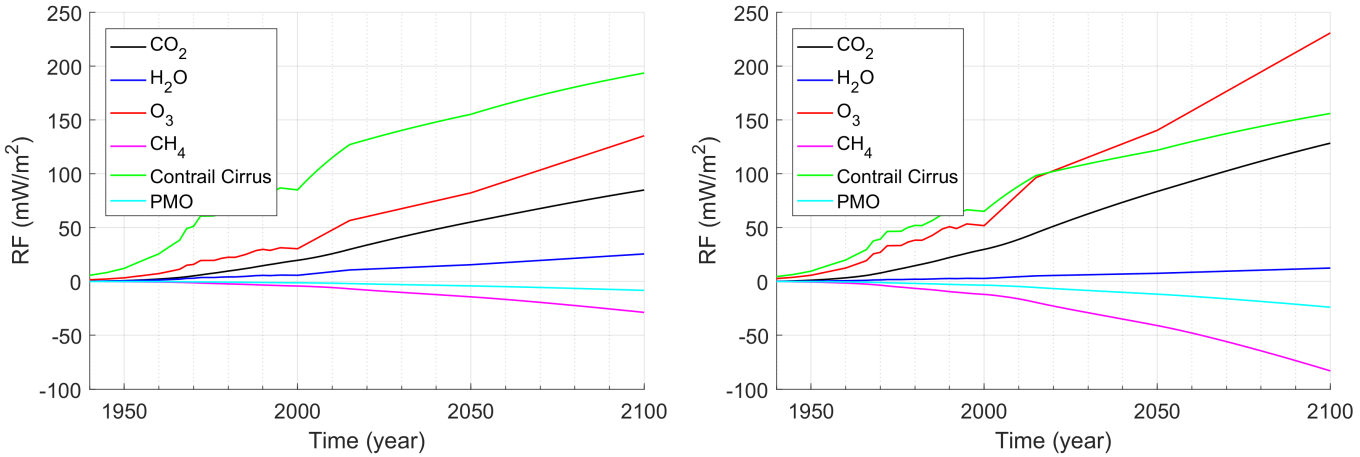

(a) B788 (b) B77W

Figure 4.10: Temporal development of the calculated radiative forcing (in mW/m^2) for the scaled base case B77W and B788 inventories. Different lines indicate the contribution of the different forcing components.

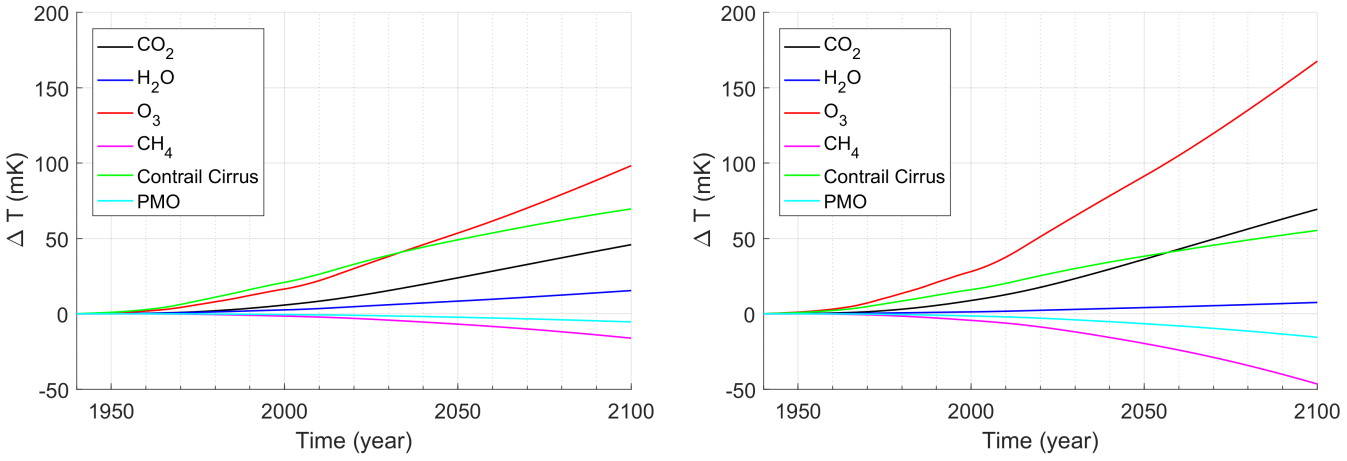

(a) B788 (b) B77W

Figure 4.11: Temporal development of the calculated temperature change (in mK) for the scaled base case B77W and B788 inventories. Different lines indicate the contribution of the different forcing components.

Emission inventory	Contrails	H_2O	O_3	CH_4	O_3^{pm}	CO_2	Total
B788 (base case scaled)	193.6	25.6	135.3	-28.7	-8.3	84.9	402.4
B77W (base case scaled)	156.0	12.5	230.8	-83.0	-23.9	128.4	420.8
Difference (%)	-19.4	-51.2	+70.6	+189.2	+188.0	+51.2	+4.6

Table 4.5: Global mean net radiative forcing (mW/m^2) for the scaled B788 and B77W emission inventories in the year 2100. Difference is defined as the percentage difference of the B77W inventory with respect to the B788 inventory.

Emission inventory	Contrails	H_2O	O_3	CH_4	O_3^{pm}	CO_2	Total
B788 (base case scaled)	69.6	15.4	98.3	-16.2	-5.4	45.8	207.5
B77W (base case scaled)	55.3	7.5	167.6	-46.6	-15.6	69.4	237.6
Difference (%)	-20.5	-51.3	+70.5	+187.7	+188.9	+51.5	+14.5

Table 4.6: Global mean net temperature change (mK) for the scaled B788 and B77W emission inventories in the year 2100. Difference is defined as the percentual difference of the B77W inventory with respect to the B788 inventory.

By analyzing the radiative forcing results of Figure 4.10, it is observed that the forcings of CO_2, O_3, CH_4 and O_3^{pm} are larger in magnitude for the B77W inventory. This observation is supported by Table 4.5 which shows the absolute radiative forcing values for the year 2100 and shows the relative differences between the B788 and B77W forcing strengths. The main reason for these forcing components to be larger for the B77W is the larger fuel consumption and corresponding emissions shown in Table 4.4. As a result of the higher fuel consumption, the CO_2 emission is larger resulting in a larger CO_2 forcing. Furthermore the larger emission of NO_x results in a larger ozone production and consequently a larger ozone forcing. Additionally the larger emission of NO_x induces the destruction of methane which reduces the methane forcing and additionally results in a lower ozone production which is incorporated in the larger negative O_3^{pm} forcing. A second reason for the difference in magnitude of the forcings of O_3, CH_4 is the effect of the emission altitude. This effect will be discussed in more detail in Section 4.7.3.

For contrail cirrus, Figure 4.11 shows that the B788 inventory is responsible for a larger forcing compared to the B77W inventory. This is explained by looking at the potential contrail coverage as function of altitude and latitude as shown in Figure 2.4. As discussed in Section 2.4.1 the dotted lines in Figure 2.4 indicate the region where most aircraft cruise, between 34,000 and 39,000 ft. Within this altitude band, the B77W is located close to the lower dotted line whereas the B788 cruises slightly above the top dotted line. Comparing the potential contrail coverage of both cruise altitudes it is observed that the B788 flies in a region where there is an overall higher potential of contrail formation which in turn results in a higher contrail forcing. Here it should be noted that there is little traffic in the polar regions as shown in Figure 4.3 and therefore the very dark regions at the polar latitudes are not considered for arriving at this observation. Additionally, since the contrail coverage depends on the emission latitude as well, the different latitudinal distribution of the two aircraft types might contribute to the difference in contrail forcing. Although this effect is not analyzed in detail in this research, Section 4.7.6 will briefly discuss the effect of the different latitudinal distribution of both inventories on the climate impact of contrails.

For the forcing of water vapor, the B788 inventory shows a larger forcing which is due to the higher emission altitude. At a higher emission altitude the water vapor has a longer lifetime resulting in a higher forcing as discussed in Section 2.4. This effect is dominant compared to the effect of the larger emission quantity of the B77W inventory.

The resulting temperature response shown in Figure 4.11 shows a similar trend as for the radiative forcings. A difference is observed by looking at the relative contribution of the contrail cirrus and ozone temperature response where in terms of temperature change, the ozone contribution is larger compared to contrail cirrus. This is due to the higher climate sensitivity parameter of ozone compared to contrail cirrus as discussed in Section 2.3.

Contribution to total climate impact

To analyse the relative contribution of the individual forcing components to the total climate impact of the two different aircraft types, Figures 4.12a and 4.12b are presented. These figures show a chart with the climate impact contribution quantified in temperature change of CO_2, NO_x, H_2O and contrail cirrus for both aircraft types and is based on the temperature change shown in Table 4.6. In these charts, the contribution of NO_x includes the combined effect of the induced forcing of O_3, the reduction of the forcing of CH_4 and the effect of O_3^{pm}.

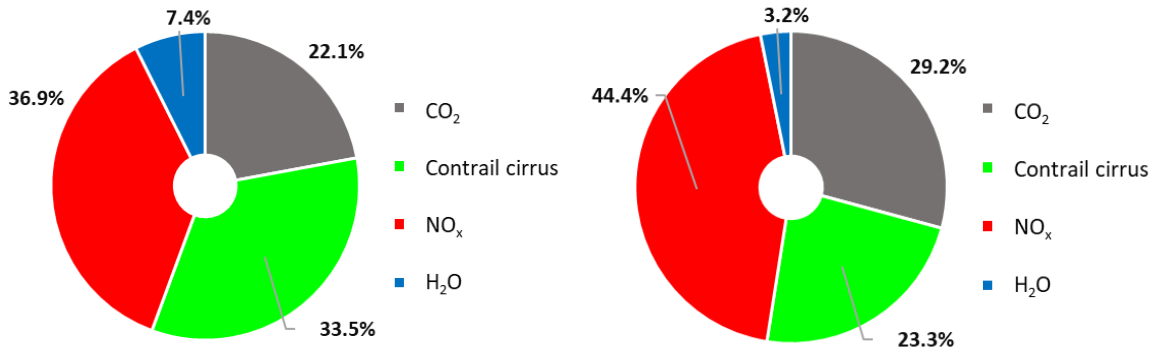

(a) B788

(b) B77W

Figure 4.12: Relative climate impact contribution of the emissions of CO_2, H_2O and NO_x for the two aircraft types in the year 2100

From Figures 4.12a and 4.12b it is observed that there is a significant difference in the contribution of the individual emission species to the total climate impact per aircraft type. First of all, for the B788 the emission of water vapor (shown in blue) has a larger climate impact compared to the B77W. Additionally, the forcing of contrail cirrus induced by the emissions of water vapor (green) is higher for the B788 as well. Considering the total effect of water vapor the relative contribution adds up to 41.2% for the B788 and 26.5% for the B77W. Secondly, the contribution of the emission of NO_x is larger for the B77W compared tot he B788 (44% compared to 37%) which indicates that the increase in temperature as a result of ozone is larger than the reduction effect of methane. Finally, the contribution of CO_2 is larger for the B77W as well (29% compared to 22%) , due to the larger fuel consumption and emissions.

In summary, the main reason for difference in climate impact of the emissions of H_2O is the emission altitude whereas for CO_2 and NO_x is the difference in emission quantity. However, Tables 4.5 and 4.6 indicate there is an effect of the emission location on the climate impact of NO_x as well. This is indicated by the varying differences where the increase in ozone is approximately 70% and the increase in methane forcing almost triples. To analyze this effect, not only the flown kilometers are normalized to the TRADEOFF inventory, but the fuel consumption and the emissions of NO_x are normalised as well. By doing this, the only difference between the two inventories is the emission location. Results of this analysis are presented in the next section.

4.7.3. Base case normalised emissions

To analyse the difference in climate impact of the two aircraft types as function of only the difference in emission location, all emission inventory parameters are normalized to the TRADEOFF inventory. This entails that the flown kilometers, fuel consumption and emission of NO_x of both the B788 and B77W inventories are equal and scaled to the TRADEOFF inventory. Furthermore, the same historic and future emission scenario as used for the TRADEOFF scenario as discussed in Section 3.7.1 is used. Results of the temporal development of the radiative forcing and temperature increase for the individual forcing components is presented in Figures 4.13 and 4.14.

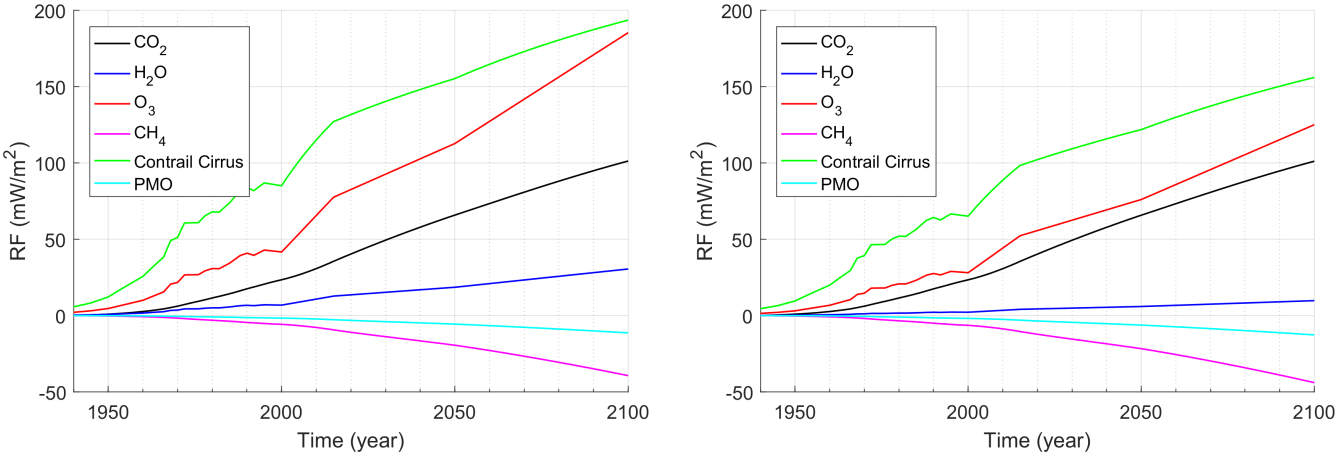

(a) B788

(b) B77W

Figure 4.13: Temporal development of the calculated radiative forcing (in mW/m^2) for the normalised B788 and B77W base case inventories. Different lines indicate the contribution of the different forcing components.

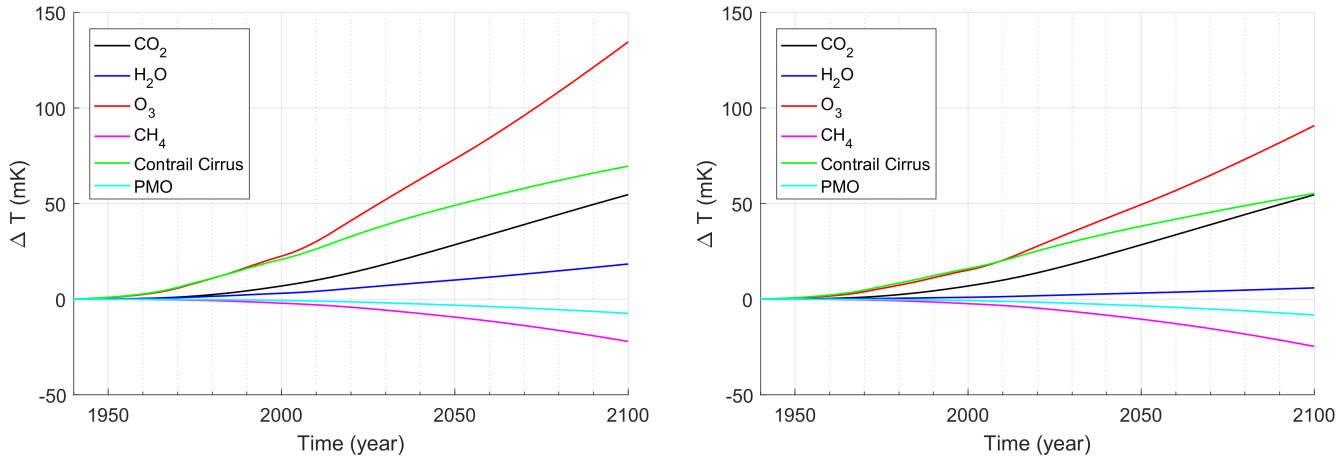

(a) B788

(b) B77W

Figure 4.14: Temporal development of the calculated temperature change (in mK) for the normalised B788 and B77W base case inventories. Different lines indicate the contribution of the different forcing components.

From Figures 4.13 and 4.14 it is observed that by noralising all emissions to the TRADEOFF inventory, the climate impact of CO_2 is the same for both inventories. The reason for this is that the forcing of CO_2 is not dependent on the emission location.

For contrail cirrus the results obtained are the same as the results obtained in Section 4.7.2 due to the flown kilometers are equal. Furthermore, for H_2O it is observed that the B788 has a larger climate impact. This is due to the higher emission altitude as discussed in the previous section.

In contrast to the results shown in Section 4.7.2, the climate impact of ozone is larger for the B788 inventory compared to the B77W inventory. Since the NO_x emission quantity is normalised, this difference can be attributed to the different emission location. Due to the longer residence time of the emissions of NO_x at high altitudes this results in a net increase in O_3 production and a higher forcing. For the forcing of methane it is observed that similar to the results obtained in Section 4.7.2 the B77W inventory shows a larger impact. The difference in magnitude however is smaller in this analysis which indicates that although the emission location does have an effect on the methane forcing, the effect of the quantity of NO_x emissions is dominant. The reason why the methane forcing is larger for the B77W in this analysis is that a lower emission altitude results in NO_x mixing ratios to increase which increases the overall OH mixing ratios for lower flight altitudes resulting in a reduction of methane lifetime and consequently a more negative forcing.

By comparing both results to the temporal response of the TRADEOFF base case as depicted in Figure 3.27 and 3.28 a few differences are observed as well. For both the B788 and B77W radiative forcings of O_3 and contrail cirrus are larger compared to the results found for the TRADEOFF inventory. For the B788 this is as expected due to the significantly higher cruise altitude. Due to the longer residence time of the emissions of NO_x at high altitudes and the higher potential contrail coverage this results in a larger impact of contrails and ozone. For the B77W however this is not expected since it shows the same peak in emissions at 35,000 ft. The TRADEOFF inventory however shows larger emissions at lower altitudes because the climb and descent phase are included in this data set. As a result a significant part of the emissions is emitted below the more climate sensitive region. The inventories constructed in this study on the other hand only consider emissions at cruise altitude which explains the higher climate impact of the B77W inventory compared to the TRADEOFF inventory.

4.7.4. Emission inventories Alternative scenarios

As discussed in Section 3.4.8 alternative emission inventories are developed by constructing traffic scenarios with a shift in cruise altitude with respect to the base case. In this process the fuel consumption as well as the NO_x emissions are recalculated based on the changed aircraft performance as function of the relocated cruise altitude. Tables 4.7 and 4.8 show an overview of the resulting emission inventories with a relocated altitude for the B788 and B77W respectively. Similar to the alternative TRADEOFF scenarios these tables include the shifted altitude profiles of 2000 ft up, 2000 ft down, 4000 ft down and 6000 ft down. Additionally, scenarios with an altitude shift of 1000 ft up, 10000 ft down, 14000 ft down and 18000 ft down are presented. Furthermore the percentage of flights for which the calculated TOW exceeds the maximum takeoff weight is indicated.

B788 Scenario	Fuel consumption (10^6 kg)	NO_x emissions (10^6 kg)	EI_{NO_x} (g/kg)	Flown distance (10^6 km)	Flights above MTOW (%)
Base + 2000 ft	10.96	0.120	10.95	2.17	0
Base + 1000 ft	10.92	0.121	11.07	2.17	0
Base case	11.00	0.123	11.19	2.17	0
Base -2000 ft	11.30	0.130	11.50	2.17	0
Base - 4000 ft	11.81	0.140	11.85	2.17	< 1
Base - 6000 ft	12.45	0.152	12.21	2.17	< 1
Base -10000 ft	14.01	0.182	12.99	2.17	2.7
Base - 14000 ft	15.82	0.217	13.72	2.17	4.7
Base - 18000 ft	17.26	0.243	14.08	2.17	7.2

Table 4.7: Constructed emission inventories for the B788 base case scenario and scenarios with flight altitude changes. *Percentage of flights for which the penalty in fuel consumption causes a TOW which exceeds the maximum take-off weight.

B77W Scenario	Fuel consumption (10^6 kg)	NO_x emissions (10^6 kg)	EI_{NO_x} (g/kg)	Flown distance (10^6 km)	Flights above MTOW* (%)
Base + 2000 ft	39.38	0.726	18.44	5.19	< 1
Base + 1000 ft	39.49	0.730	18.49	5.19	< 1
Base case	39.94	0.744	18.63	5.19	< 1
Base -2000 ft	41.40	0.794	19.18	5.19	< 1
Base - 4000 ft	43.44	0.863	19.87	5.19	< 1
Base - 6000 ft	45.79	0.942	20.57	5.19	< 1
Base -10000 ft	50.27	1.075	21.38	5.19	2.4
Base - 14000 ft	53.40	1.130	21.16	5.19	3.7
Base - 18000 ft	55.14	1.156	20.96	5.19	4.2

Table 4.8: Constructed emission inventories for the B77W base case scenario and scenarios with flight altitude changes. *Percentage of flights for which the penalty in fuel consumption causes a TOW which exceeds the maximum take-off weight.

From the results presented in Tables 4.7 and 4.8 it is observed that for both aircraft types the fuel consumption increases when the cruise altitude is shifted down. This indicates that there is a penalty in emissions when the altitude is lowered. Furthermore the fuel consumption slightly decreases when the altitude is shifted 2000 ft up. Combining both observations indicates that overall, the analysed aircraft have flown slightly below but close to their fuel optimal cruise altitude. To analyse this in more detail an additional scenario is constructed with a relocated altitude 1000 ft above the base case. For the B788 this results in an even lower fuel consumption indicating that the optimum cruise altitude with respect to fuel consumption is 1000 ft higher than the base case. For the B77W however the 2000 ft higher scenario remains the optimal scenario in terms of fuel consumption. To confirm that this is the optimum an additional scenario was constructed at 3000 ft above the base case (not shown). This resulted in a higher fuel consumption than the base case indicating that the +2000 ft scenario is the fuel optimal scenario for the B77W inventory.

Similar results are found for the emissions of NO_x which follow the same pattern although they show a stronger increase with decreasing cruise altitude. This can be attributed to the higher fuel consumption in combination with the increasing NO_x emission index with decreasing altitude as shown in Tables 4.7 and 4.8. This latter effect was previously observed in Figures 4.6a and 4.6b where an increase of EI_{NO_x} was found with decreasing altitude. Due to this twofold dependency, the emissions of NO_x increase faster compared to the fuel consumption.

The increase in fuel consumption and NO_x emissions due to the shift in cruise altitude is visualized in Figure 4.15 which shows the relative difference of fuel consumption and NO_x emissions of the alternative scenarios with respect to the base case for both the B788 and B77W inventories. Furthermore as reference the difference of the TRADEOFF scenarios with respect to the base case is plotted in black.

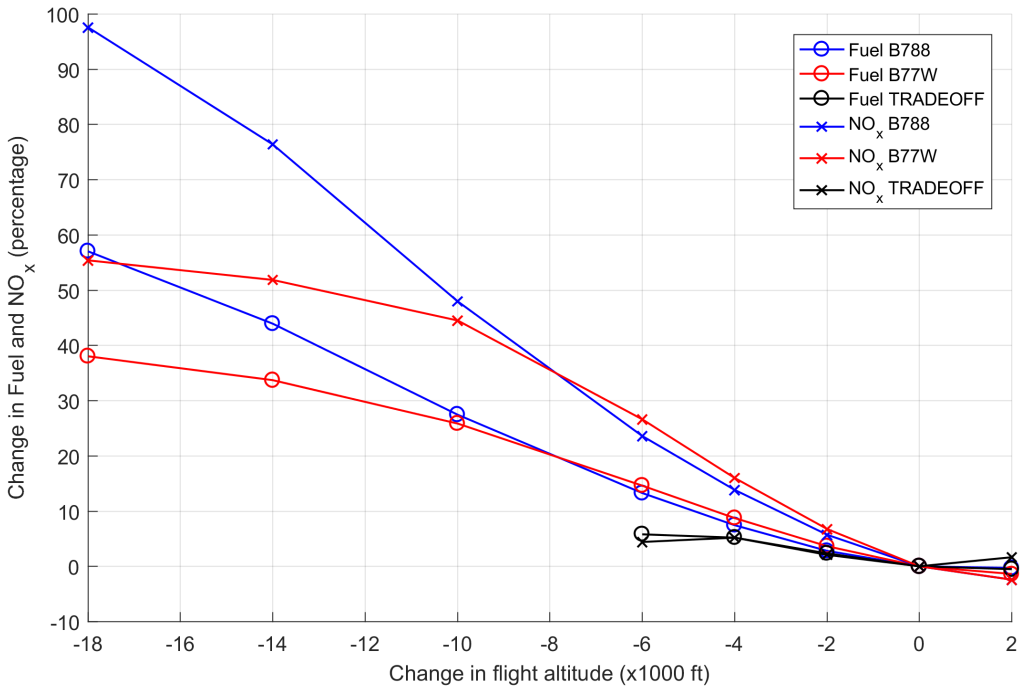

Figure 4.15: Change in fuel consumption and NO_x emissions as function of a relocated altitude profile for the B788, B77W and TRADEOFF emission inventories relative to the base case

From Figure 4.15 it is observed that for altitude shifts from +2000 to -6000 ft the B788 and B77W inventories show a similar trend although the penalty in fuel consumption and NO_x emissions for the B77W inventory is slightly larger compared to the B788 inventory. Comparing the B788 and B77W inventories to the TRADEOFF inventory shows an even larger difference where the relative increase in fuel consumption for the TRADEOFF inventory is significantly lower. For an altitude shift of 6000 ft down the increase in fuel consumption (and corresponding fuel costs) is 6% for the TRADEOFF inventory, 13% for the B788 inventory and 14% for the B77W inventory. The main reason for this difference is the average cruise distance of the trajectories analyzed in the respective inventories. Research by Poll [58] states that for a given trajectory, the penalty in fuel consumption is a strong function of the flight distance where the larger the distance, the larger the penalty for a given shift in cruise altitude. For an altitude shift of 4000 ft down from the optimum altitude, Poll found a penalty in fuel consumption ranging from 2% for short haul flights with a cruise distance shorter than 2800 km to 9% for long haul flights with a cruise distance larger than 5500 km. This 9% fuel penalty is in agreement with the calculated penalty in fuel consumption for the B788 and B77W inventories.

Since the focus of this work is on aircraft types which typically perform long haul flights, the average flight distance for the analyzed B788 and B77W inventories is significantly larger than the average flight distance of the TRADEOFF inventory. To have an indication of this difference, the average cruise distance of the TRADEOFF inventory is estimated by using data from the MIT data project which contains flight segment data for all American carriers for 2018 [2]. From this data an average flight distance of 1950 km was found which is considered a reasonable indication of the average flown distance in the TRADEOFF inventory. Comparing this to the average cruise distance calculated in this work of 5400 km and 6200 km for the B788 and the B77W respectively indicates a large difference and explains the large difference in fuel penalty.

As discussed, the emissions of NO_x are more affected by the altitude shifts compared to the fuel consumption for the B788 and B77W inventories. This effect is less apparent for the TRADEOFF inventory where the penalty in fuel consumption is approximately equal to the penalty in NO_x emissions when shifting the cruise altitude. This indicates that the average emission index of NO_x is modeled approximately constant with altitude. Only a small difference is found for the two extreme scenarios where the NO_x increase is slightly higher at +2000 ft. According to Gauss et al. (2006) [19] the reason for this is that aircraft types that can fly 2000 ft higher have a larger EI_{NO_x} at this altitude. Furthermore for the -6000 ft case the listed EI_{NO_x} is lower compared to the base case. The exact reason for this is not discussed however a possibility could be that a lower cruise Mach number is assumed for flying at this lower altitude which effectively reduces the NO_x emission index.

[2] http://web.mit.edu/airlinedata/www/Res_IndusResources.html

By observing Figure 4.15 more closely, the fuel consumption and emissions of NO_x seem to increase in a non linear manner indicated by the lines turning steeper for altitude shifts from -2000 to -6000 ft and leveling off beyond -10000 ft. This behaviour is explained by Figures 4.5a and 4.5b. As observed in Section 4.3 the specific air range (SAR) deteriorates rather slow close to the optimum altitude around which there is a small altitude range which ensures a SAR close to the maximum attainable SAR. Since the base case altitude is close to the optimum altitude with respect to SAR, moving away from this point will result in a SAR which slowly starts to decrease. This explains the gradual increase in fuel consumption close to the optimum altitude. For altitude shifts larger than 6000 ft for the B77W and 14000 ft for the B788 the increase in fuel consumption and NO_x emissions starts to level off. This is due to the relaxation of the constant Mach number assumption below altitudes for which a constant Mach results in an airspeed above the maximum operating airspeed (V_{MO}). As a consequence, for altitudes lower than 24000 ft for the B788 and 26000 ft for the B77W the Mach number is reduced. This in turn leads to a smaller decrease in SAR and NO_x emission index as indicated by the kink in the SAR and EI_{NO_x} diagrams shown in Figures 4.5 and 4.6.

Figure 4.15 shows that by relocating cruise altitudes further down, the resulting penalty in fuel consumption continues to increase. For a cruise altitude shift of 18000 ft down, this penalty in fuel consumption is calculated to be 38% and 57% for the B77W and B788 respectively. Apart from the associated higher fuel costs, there are flights which will not be able to perform the flight since they can not carry the extra required amount of fuel. Within this research it was decided however to shift all trajectories down irrespective of whether they could perform the altitude shift considering the MTOW limit. This is because when a fraction of flights is kept at their original altitude this will give an unreal, distorted reflection of the increase in emissions corresponding to a shift in cruise altitude. The fraction of flights for which the altitude shift could not be performed however is analyzed and shown in Tables 4.7 and 4.8. From these tables it is observed that by displacing flights further down, the increasing fuel consumption results in an increasing portion of flights which can not perform their mission. For altitude scenarios up until -6000 ft this fraction of flights is found to remain within 1% which is considered acceptable. For larger altitude shifts however this percentage increases up to 7.2% of flights for the B788 and 4.2% of flights for the B77W which is considered significant.

4.7.5. Climate impact alternative scenarios

For evaluating the climate impact of the alternative scenarios, the same historic and future emission scenarios are used as for the basecase. Furthermore, similar to the base case all inventories are scaled up to the amount of kilometers of the TRADEOFF inventory. Additionally, the fuel consumption and emissions of NO_x are scaled by the same factor. This process is discussed in Section 4.7.1. The result of the temporal development of the temperature response of the alternative scenarios in comparison to the base case is presented in Figures 4.16a to 4.16f for the short term forcing components (Contrail cirrus, water vapor and ozone). The long term forcings (CH_4 and CO_2) and the total climate impact are presented in Figures 4.17 and 4.18.

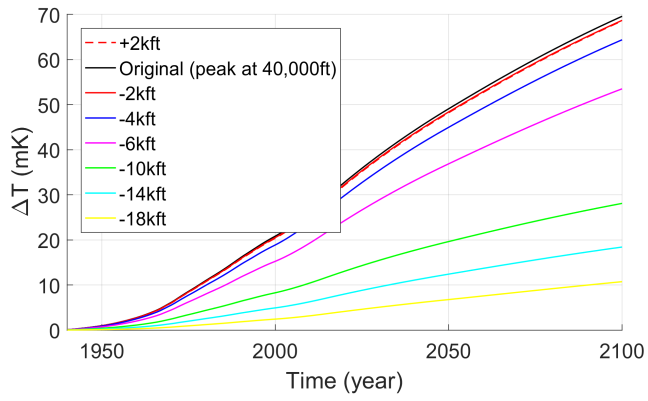

(a) Contrails (Cirrus) B788

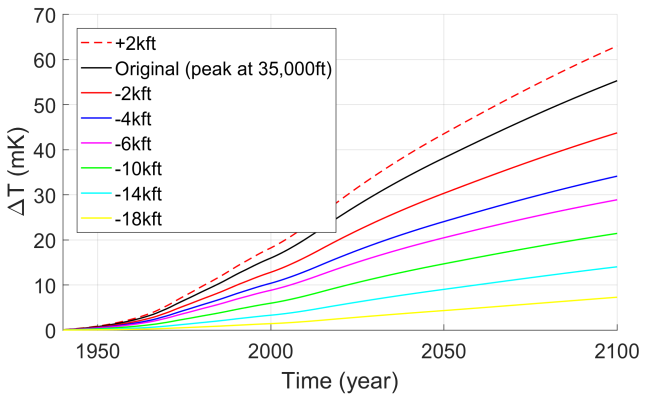

(b) Contrails (Cirrus) B77W

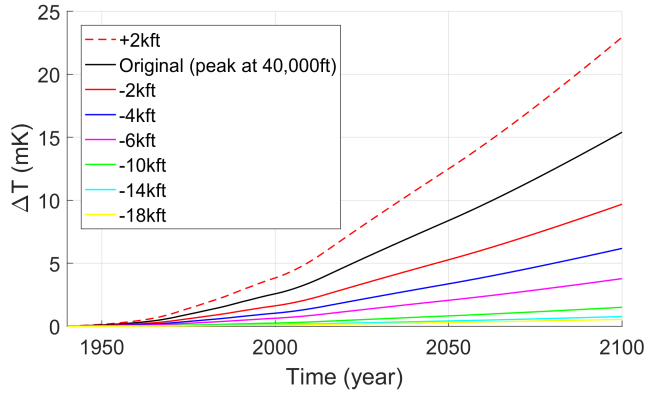

(c) Water vapor, (H_2O) B788

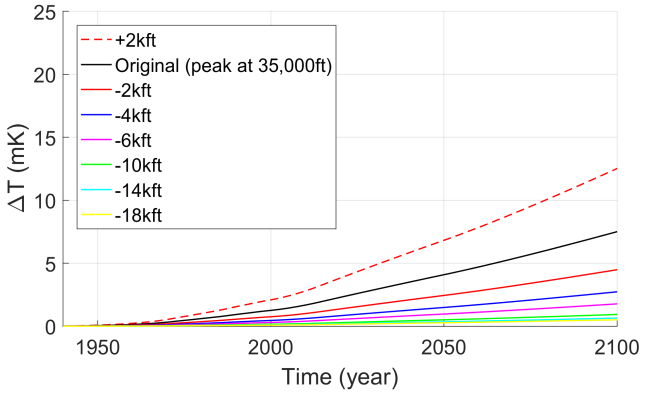

(d) Water vapor, (H_2O) B77W

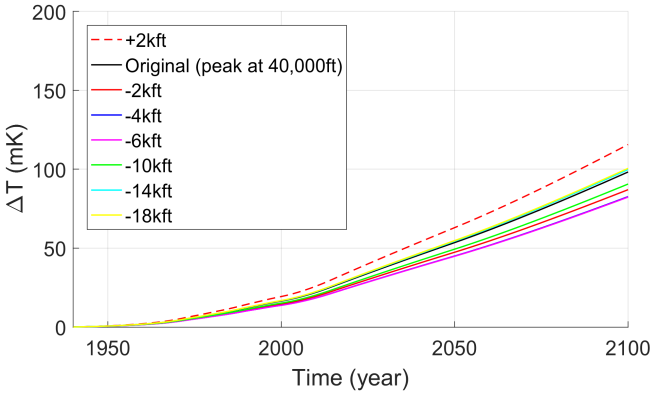

(e) Ozone, (O_3) B788

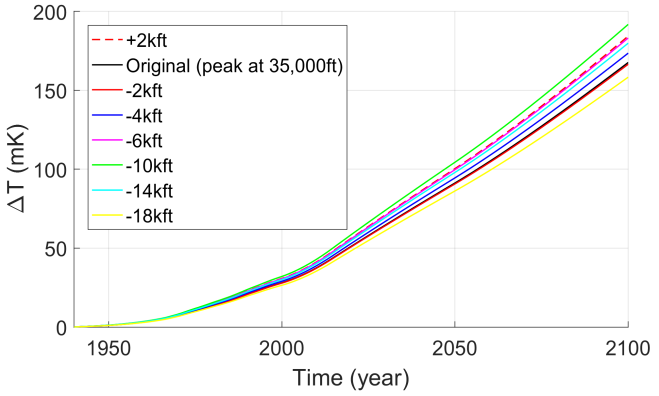

(f) Ozone, (O_3) B77W

Figure 4.16: Temperature response of contrail cirrus, H_2O and O_3 through a displacement of flight altitudes by 2000 ft up, 2000 ft down, 4000 ft down, 6000 ft down, 10000 ft down 14000 ft down and 18000 ft down relative to the base case.

Comparing the short term forcing components of the B788 to the B77W inventory, large differences are observed. First of all, considering the climate impact of contrail cirrus it is observed that for the B788 all alternative scenarios including the upward altitude shift result in a lower climate impact compared to the base case. For the B77W this is not the case where the +2000 ft scenario results in a higher climate impact. Furthermore it is observed that for both aircraft types, the contrail forcing is lowered continuously as the cruise altitude decreases. Interestingly it is observed that for the B788 in particular the shift between minus 6000 ft and minus 10,000 ft shows to have a large impact which corresponds to a shift in the fuel consumption peak from 34,000 to 30,000 ft. For the B77W this large impact is observed around the same altitude but now represented by the the base case around 34,000 ft and the altitude scenario of -4000 ft.

For the climate impact of water vapor the most prominent difference comparing both aircraft is the absolute magnitude of the forcing difference between the two aircraft types. As explained above this is due to the large altitude difference of the base case. By relocating the altitude of the B788 inventory 6000 ft down it is observed that the forcing is in the same order of magnitude of that of the B77W base case. Furthermore for both aircraft types it holds that as the altitude is shifted down, the forcing of water vapor decreases. This can be attributed to the reduced water vapor lifetime at lower emission altitudes.

Comparing the climate impact of ozone for both aircraft types it is observed that the range of calculated forcings is small, in particular for the B77W. The reason for this is as the altitude is shifted down the NO_x emissions are emitted in a less sensitive region resulting in a lower ozone production. This effect however is offset by the larger quantify of the NO_x emissions by flying at a lower altitude. As a result the climate optimal altitude in terms of ozone is a tradeoff between the sensitivity of the emission altitude and the quantity of the emission. For the B788 this results in an optimal altitude of -6000 ft whereas for the B77W the -18,000 ft shift results in the lowest ozone forcing although it is only marginally lower compared to the base case.

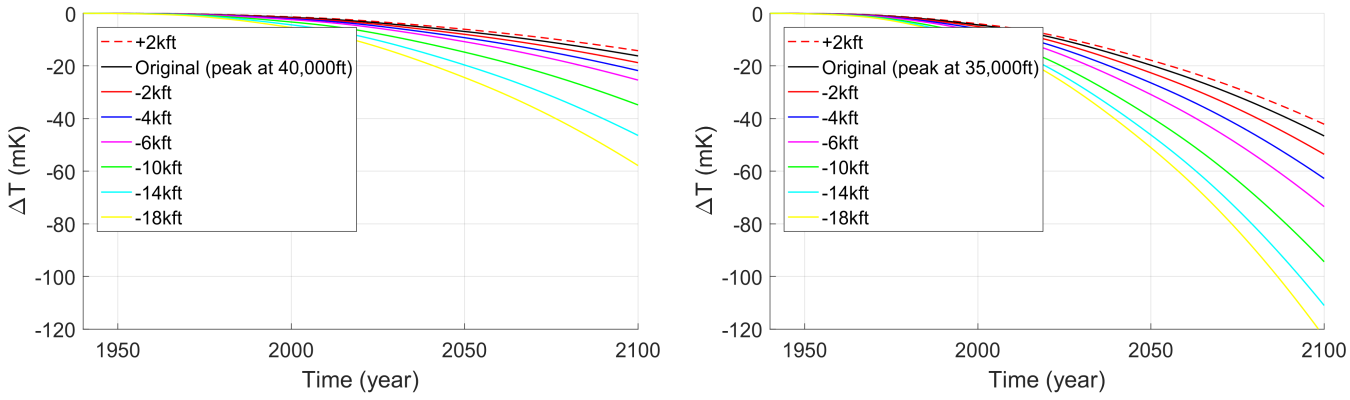

(a) Methane, (CH_4) B788

(b) Methane, (CH_4) B77W

Figure 4.17: Temperature response for CH_4 through a displacement of flight altitudes by 2000 ft up, 2000 ft down, 4000 ft down, 6000 ft down, 10000 ft down 14000 ft down and 18000 ft down relative to the base case.

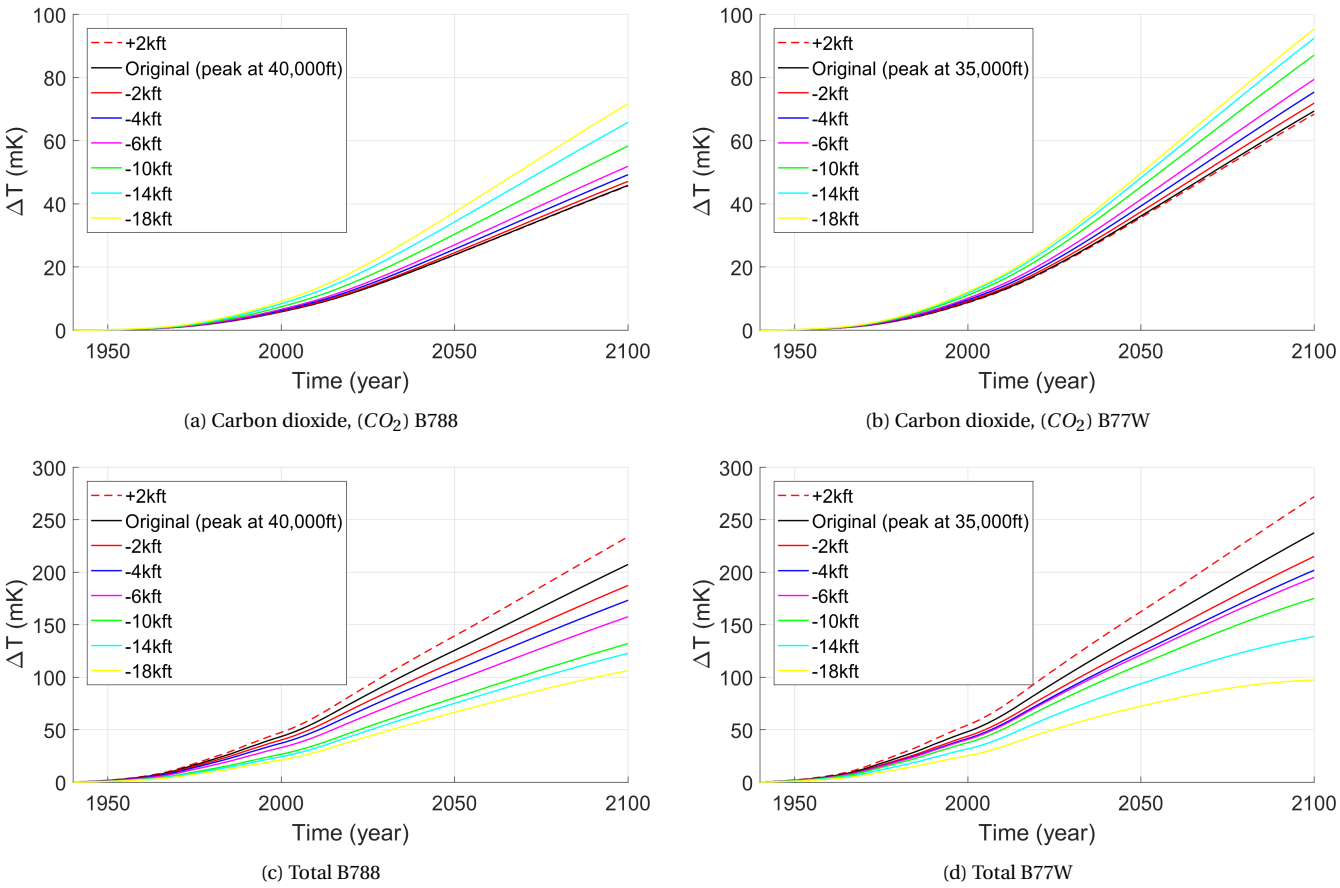

(a) Carbon dioxide, (CO_2) B788

(b) Carbon dioxide, (CO_2) B77W

(c) Total B788

(d) Total B77W

Figure 4.18: Temperature response for CO_2 and all forcings combined through a displacement of flight altitudes by 2000 ft up, 2000 ft down, 4000 ft down, 6000 ft down, 10000 ft down 14000 ft down and 18000 ft down compared to the base case

Analyzing the results of climate impact development of CO_2 as shown in Figure 4.18a and 4.18b it is observed that the forcing continuously increases as the altitude is lowered. This is due to the larger fuel consumption corresponding to these scenarios as shown in Figure 4.15. Furthermore, it is observed that the increase in forcing is larger for the B788 than for the B77W for altitude scenarios of -10,000 ft and lower. This can be attributed to larger fuel penalty of the B788 inventory for altitude shifts larger than 10,000 ft as shown in Figure 4.15.

For methane a similar result is found as for CO_2 however there is a difference in sign. The lower the emission altitude, the more NO_x is produced resulting in an overall higher OH concentration which results in a reduction of methane lifetime and therefore a larger negative forcing as shown in Figure 4.17.

By adding up the contribution of all discussed forcing components, the total radiative forcing is found as shown in Figures 4.18 c and 4.18 d. Both Figures indicate that by lowering the cruise altitude, the total climate impact is reduced. The two forcing components which have the largest influence in this climate impact reduction are forcings from contrail cirrus which are significantly reduced and the negative forcings of methane which are increased both leading to the lowest overall forcing for the lowest cruise altitude. The relative reduction in climate impact of all climate forcing components will be further analyzed in Section 4.7.6.

4.7.6. Analyzing cruise altitude sensitivity of individual forcing components

To analyze the altitude sensitivity of the individual forcing components in more detail, the relative difference in temperature change from each forcing component with respect to the base case is calculated for the year 2100. The result of this analysis is shown in Figures 4.19a to 4.19f where the relative difference with respect to the base case is calculated in terms of a percentage based on the results presented in Section 4.7.5. Additionally the altitude sensitivity of the TRADEOFF inventory is plotted as reference which was previously shown in Figure 3.31.

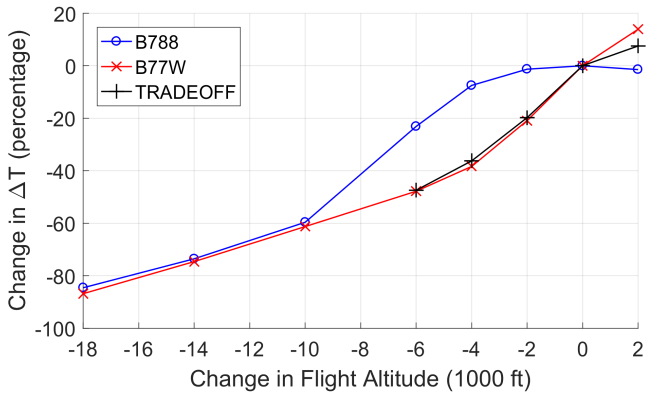

(a) Contrails (Cirrus)

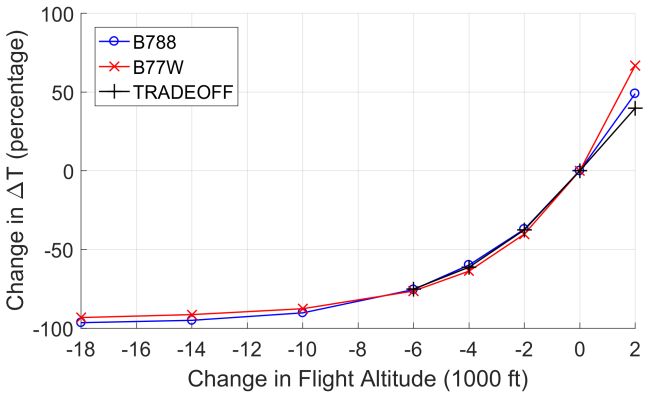

(b) Water vapor, (H_2O)

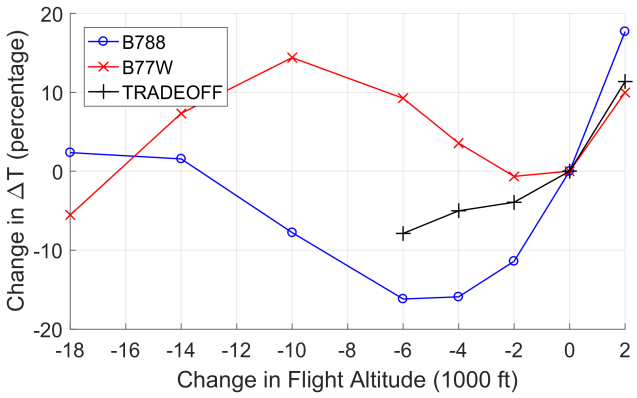

(c) Ozone, (O_3)

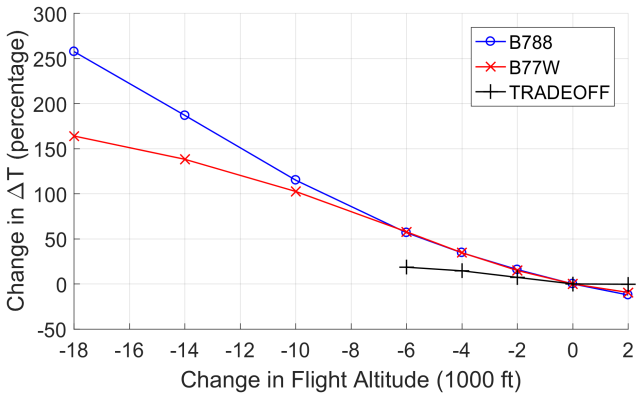

(d) Methane, (CH_4)

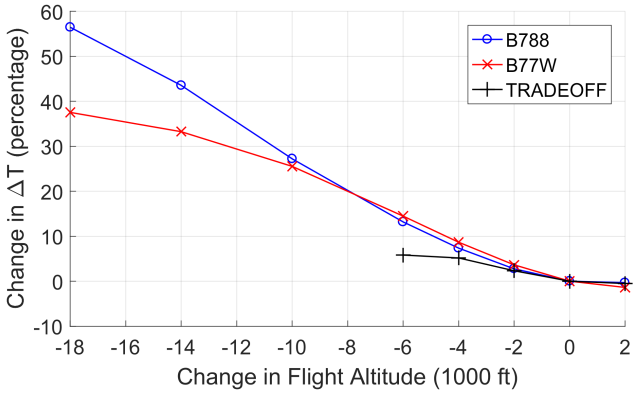

(e) Carbon dioxide (CO_2)

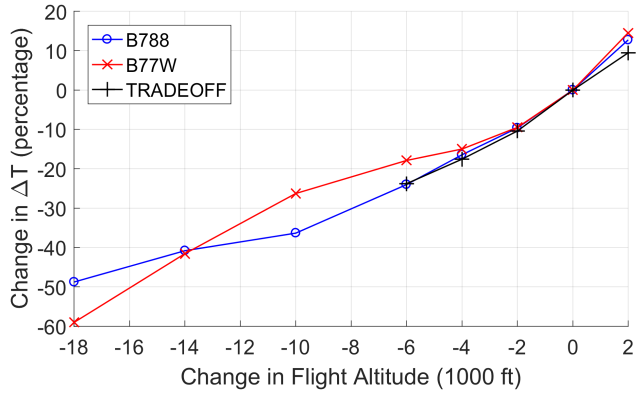

(f) Total

Figure 4.19: Temperature differences (in percentage) for all individual forcing components with respect to the base case through a displacement of flight altitudes by 2000 ft up, 2000 ft down, 4000 ft down, 6000 ft down, 10000 ft down, 14000 ft down and 18000 ft down calculated for 2100.

Analyzing Figures 4.19a to 4.19f a few observations are made. First of all, considering the contrail forcing it is observed that the B77W inventory shows the same altitudinal sensitivity as the TRADEOFF inventory where the contrail forcing decreases rapidly as the cruise altitude is lowered. Reducing cruise altitudes by 6000 ft reduces the climate impact of contrails by approximately 48% which is in agreement with the findings from Frömming [16]. This is due to the similar altitudinal profile of the B77W and TRADEOFF emission inventories with a peak in emissions located at 35,000 ft. In contrast, the B788 inventory shows a significantly slower contrail reduction with altitude. Interestingly, by lowering flight altitudes by 2000 ft there is no significant reduction in contrail forcing. This is explained by the high cruise altitude of this inventory which is around 40,000 ft. Apparently, decreasing the cruise altitude by 2000 ft does not shift the trajectories into a region with a lower potential contrail coverage. This phenomenon is similar to what was found by Fichter et al. (2005) [13] which showed that for long-haul intercontinental flights in the northern hemisphere which typically fly a high cruise altitude a 2000 ft reduction in flight altitude resulted in a small increase in contrail coverage [13]. To explain this effect in more detail, Figure 4.20 is presented which shows the climate impact of contrails as function of the absolute cruise altitude resulting from the altitude shifts.

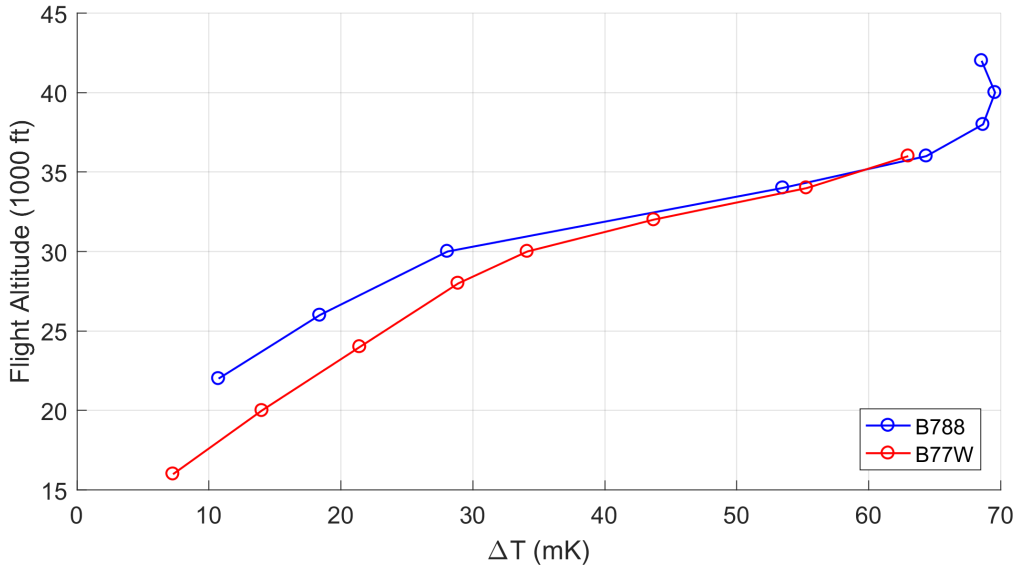

Figure 4.20: Absolute climate impact (in mK) of contrail cirrus on the x-axis as function of the cruise altitude on the y-axis. Here the Flight altitude is taken as the altitude around which the peak in flown kilometers is located as a result of the altitude shift. For the base case this is 40,000 ft for the B788 and 34,000 ft for the B77W.

From Figure 4.20 it is observed that for high cruise altitudes the change in climate impact as function of a given altitude shift is lower than for lower cruise altitudes. This explains the behaviour observed in Figure 4.19a. Furthermore for altitudes lower than 30,000 ft it is observed that the climate impact of the B77W inventory is larger compared to the B788. This can be attributed to two factors. First of all, it observed from Figure 4.4 that the B77W inventory has a higher portion of flown kilometers above the altitude peak compared to the B788. This effectively results in a higher climate impact according to the general trend shown in this figure. Secondly, according to the latitudinal distribution of the trajectories shown in Figure 4.3, it is found that for the B77W there is a significant portion of flights around a latitude of 60 degrees north. In this region the atmosphere is more sensitive for contrails at lower altitudes according to Figure 2.4. For this reason the contrail forcing for the B77W is higher at lower altitudes.

Despite the slower reduction in contrail forcing for the B788 as function of a shift in altitude, the contrail forcing is reduced by 23% when an altitude shift of 6000 ft down is considered. Furthermore by relocating cruise altitudes down by 18000 ft a reduction in climate impact is found of more than 80% for both aircraft types.

Analyzing the found altitude sensitivity of the ozone forcings, a different result is found for all three inventories. First of all the B788 inventory shows a decreasing climate impact of ozone for altitude shifts between -2000 and -6000 ft. This is because the the original flight altitude is very sensitive to the emissions of NO_x due to the slow washout processes. As a consequence, moving the emissions downward from the original altitude results in a reduction in ozone impact with a maximum reduction of 16% for an altitude shift of 6000 ft. When the cruise altitude is reduced further, this effect is offset by the increase in the quantity of NO_x emissions indicated by the rising curve. For the TRADEOFF inventory a decreasing trend is found as well however the reduction in ozone climate impact is lower in magnitude compared to the B788. This can be attributed to the reduced sensitivity of ozone at lower altitudes. For the B77W inventory there is hardly any beneficial effect found by lowering flight altitudes where for altitude shifts of -4000 ft to -14000 ft the climate impact of ozone is even increased. This is due to the increased quantity of NO_x in combination with the altitude becoming less sensitive to the location of the emissions effectively resulting in a larger ozone production. Relocating cruise altitudes by 18000 ft results in a 5% reduction in ozone climate impact.

For water vapor all three emission inventories show the same behaviour. this is due to the processes controlling water vapor perturbations and radiative forcing follow linear relations according to Fichter [12]. Similar to the TRADEOFF inventory, the climate impact of water vapor from both aircraft types can be reduced by 75% when the altitude is reduced by 6000 ft. Furthermore when the altitude is shifted 18000 ft down nearly all water vapor effects are mitigated.

For CO_2 and CH_4 the B788 and B77W inventories show similar results where the climate impact increases in magnitude for a lower flight altitude. This is due to the higher fuel consumption resulting in more CO_2 emissions and the higher NO_x emissions which in turn result in a reduced methane lifetime. A large difference is observed between the two aircraft types and the TRADEOFF inventory which shows a smaller increase of both the CO_2 and CH_4 forcings. This is explained by looking at Figure 4.15 which shows that the TRADEOFF inventory calculates significantly smaller increases in fuel consumption and NO_x emissions relative to the base case. This smaller penalty in emissions results in a lower increase in climate impact.

Finally, considering the total reduction in climate impact it is observed from Figure 4.19f that by reducing cruise altitudes by 6000 ft, the climate impact of the B788 is reduced by 25% which is in agreement with the results found for the TRADEOFF inventory. Furthermore this climate impact reduction is in agreement with the result found by Frömming [16]. The climate impact reduction for an altitude shift of -6000 ft for the B77W is -19% which is slightly lower. The main cause for this difference is the climate impact of ozone which is increased for the B77W when altitudes are reduced by 6000 ft. For an altitude shift of 18000 ft the total climate impact is reduced by 50% for the B788 and almost 60% for the B77W. This difference can be attributed to the difference in ozone forcing where the forcing for the B788 is slightly increased whereas for the B77W it is decreased.

4.7.7. Total climate impact reduction of individual forcing components

Now that Figures 4.19a to 4.19e have shown the change in climate impact of each individual forcing component as a result of a shift in cruise altitude, it is interesting to analyze the contribution of each forcing component to the total reduction in climate impact. This contribution will depend on the magnitude of the components climate impact of the base case as shown in Figures 4.12a and 4.12b and on the climate impact reduction as shown in Figure 4.19. Results of this analysis are presented in Figures 4.21a to 4.21f.

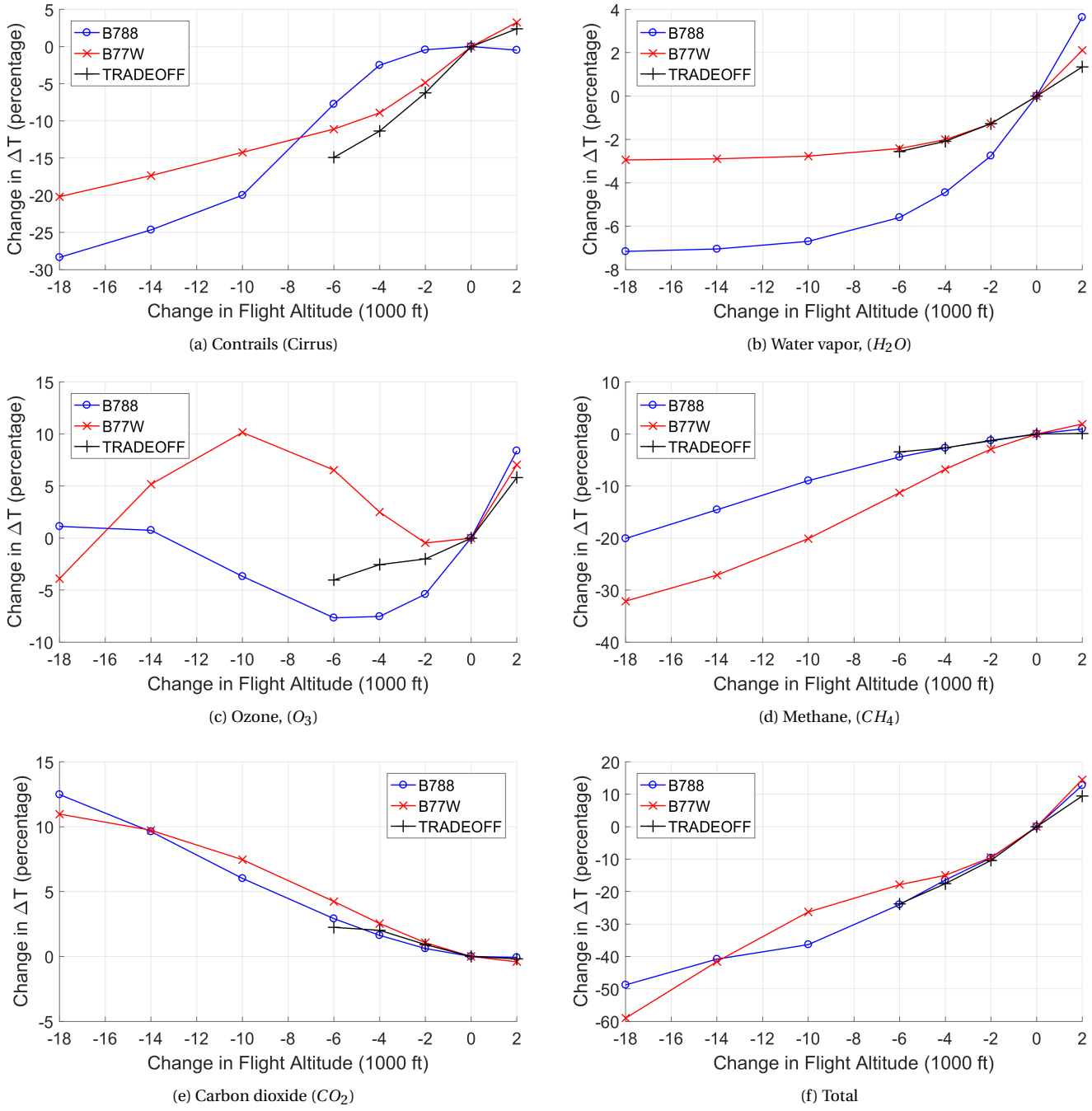

(a) Contrails (Cirrus)

(b) Water vapor, (H_2O)

(c) Ozone, (O_3)

(d) Methane, (CH_4)

(e) Carbon dioxide (CO_2)

(f) Total

Figure 4.21: Total climate impact reduction in percentage for all individual forcing components with respect to the base case through a displacement of flight altitudes by 2000 ft up, 2000 ft down, 4000 ft down, 6000 ft down, 10000 ft down, 14000 ft down and 18000 ft down calculated for 2100.

From Figure 4.21a it is observed that for an altitude shift of 6000 ft down, the reduction in climate impact from contrail cirrus is responsible for a reduction in the total climate impact of 8% and 12% for the B788 and B77W respectively. This is significant compared to the total reduction of respectively 25% and 19% shown in Figure 4.20f. Furthermore a relocation of cruise altitudes by 18000 ft down results in a total climate impact reduction due to a lower contrail coverage of 20% for the B77W and 28% for the B788. Here the contribution of both aircraft types is different although both types showed a climate impact reduction of 80% as shown in Figure 4.19 a. The reason for this is the higher contribution of contrails towards the total climate impact of the B788 as shown in Figure 4.12.

Although Figure 4.19b showed that the climate impact from water vapor can be reduced by 75% when relocating cruise altitudes 6000 ft down, Figure 4.21b shows that this only results in a 6% reduction of the total climate impact for the B788. The reason why the large reduction in climate impact from H_2O results in a modest reduction in the total climate impact is the result of the small contribution of water vapor towards the total climate impact as observed in Figure 4.12. The difference between the two aircraft types originates from the initial contribution of water vapor to the total climate impact which is larger for the B788. Reducing cruise altitudes further down does results in a larger contribution towards the climate impact reduction however since the forcing of water vapor is already reduced by 75% for an altitude shift of 6000 ft, the additional gain is limited.

Another large contributor to the total climate impact reduction for a 6000 ft lower cruise altitude is the lower ozone forcing for the B788. Figure 4.21c shows that the reduction in ozone forcing results in a total climate impact reduction of 8%. For the B77W on the other hand ozone is responsible for an increase in the total climate impact. Reducing cruise altitudes down by 18000 ft mitigates this beneficial effect for the B788.

The decrease in methane lifetime contributes significantly to the total climate impact reduction as well where for a shift in cruise altitude of 6000 ft the total climate impact is reduced by 4% and 11% for the B788 and B77W respectively. Reducing cruise altitudes further increases this percentage to 20% for the B788 and 32% for the B77W. This difference in climate impact reduction originates from the initial contribution of methane to the total climate impact which is larger for the B77W.

As a result of the downward shifts in cruise altitude the fuel consumption is increased which results in a penalty in climate impact. Figure 4.21e shows that for an altitude shift down of 6000 ft, CO_2 is responsible for an increase in total climate impact of respectively 3% and 4% for the B788 and B77W respectively. This percentage grows to 12% and 11% for an altitude shift down to 18000 ft. The penalty in fuel consumption and associated fuel costs is higher where for an altitude shift of 6000 ft down the fuel consumption increases by 13% and 14% for the B788 and B77W inventories respectively. For an altitude shift of 18000 ft the penalty in fuel consumption increases up to respectively 57% and 38% for the B788 and B77W.

In summary, the largest contributors to the total climate impact reduction for a 6000 ft shift in altitude are O_3, contrail cirrus and H_2O for the B788 whereas for the B77W these are contrail cirrus and CH_4. For an altitude shift of 18000 ft these are contrail cirrus and CH_4 for both aircraft types. By adding up the contribution of all forcing components Figure 4.21f shows the total climate impact reduction as function of the shift in altitude. For an altitude shift of 6000 ft down, the total climate impact is reduced by 24% and 18% for the B788 and B77W respectively. Shifting the cruise altitude down further by 18000 ft results in a larger climate impact reduction of respectively 49% and 59% for the B788 and B77W. However the corresponding penalties in fuel consumption and associated fuel costs increase to respectively 57% and 38% which are considered unacceptable.

4.7.8. Total climate impact reduction of emission species

Based on the results from Section 4.7.7, the total climate impact reduction of the three main emission species (CO_2, NO_x and H_2O) can be analyzed. This is done by grouping the contribution of CH_4 and O_3 which are both dependent on the emission of NO_x. Similarly the climate impact contributions of H_2O and contrail cirrus are grouped since they are both a result of the emissions of H_2O. As a result Figure 4.22 is presented showing the total change climate impact reduction as function of all three emission species.

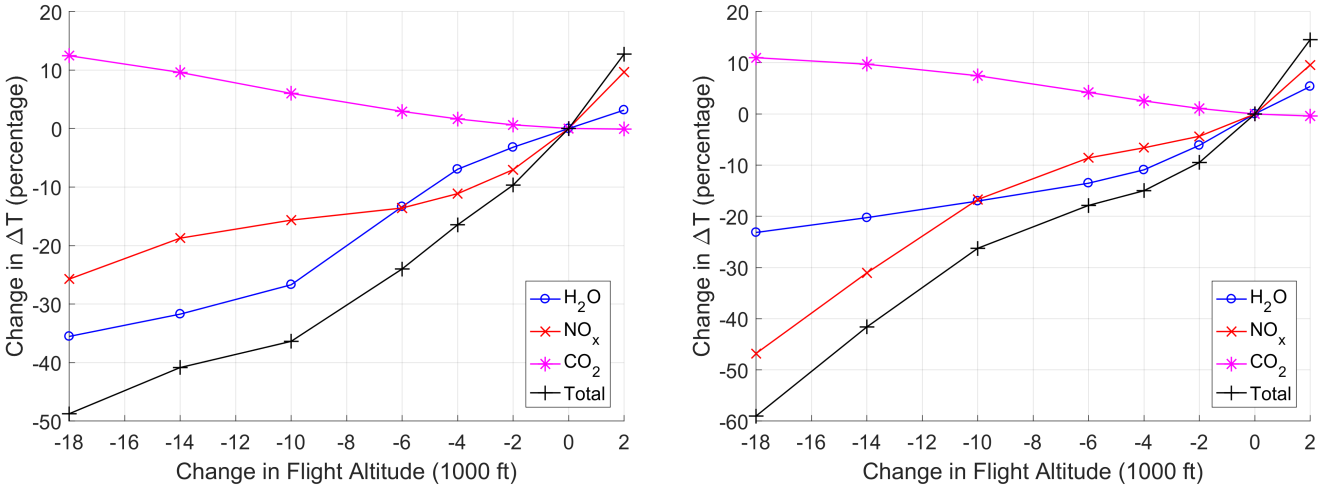

(a) B788

(b) B77W

Figure 4.22: Change in total climate impact due to a shift in cruise altitude as function of the emissions of CO_2, NO_x and H_2O

Figure 4.21 shows that for an altitude shift of 6000 ft down, both the emissions of NO_x and H_2O contribute equally to the resulting climate impact reduction for the B788. For the B77W the contribution of H_2O is slightly higher due to the increase in ozone forcing observed in Figure 4.21c. When cruise altitudes are shifted down by 18000 ft the largest climate impact reduction for the B788 is caused by the reduced climate impact of H_2O emissions whereas for the B77W this is due to the climate impact reduction of NO_x.

4.8. Uncertainty Analysis

In this section the uncertainties will be discussed arising from the assumptions which are considered to have the largest impact. These include the assumed cruise Mach number, payload weight and the emission growth scenario. The uncertainty analysis is performed for the B788 aircraft since Piano-X performance data for this aircraft is retrieved under a personal license making it better accessible. Performance data for the B77W on the other hand is only available from a TU Delft computer with a commercial Piano-X license and therefore is less suitable to perform an uncertainty analysis.

4.8.1. Cruise Mach number

From the performed Mach number analysis investigating the correlation between Mach number and cruise altitude it was found that aircraft fly a constant Mach number throughout their range of operational cruise altitudes. This does however lead to a penalty in fuel consumption since the Mach number for which the optimum SAR is obtained decreases as the flight altitude is lowered [14]. The reason for this is that by flying lower, the air density is higher which will lower the required velocity for the same amount of lift. When the velocity is kept constant however, the excess amount of lift will have to be compensated by reducing the angle of attack. This in turn will move it away from its optimal value and thereby increase the aircraft drag and fuel consumption.

To investigate the aircraft performance as function of Mach number in more detail, the SAR and EI_{NO_x} as function of altitude have been analyzed with Piano-X. This is done for four different Mach numbers, the original Mach number of 0.84 and three lower Mach numbers of 0.80, 0.76 and 0.72. Furthermore, the weight is kept constant for this analysis at a 33% fuel load corresponding to the median of the found fuel loads as shown in Figure 4.9a. Results of this analysis are shown in Figures 4.23a and 4.23b.

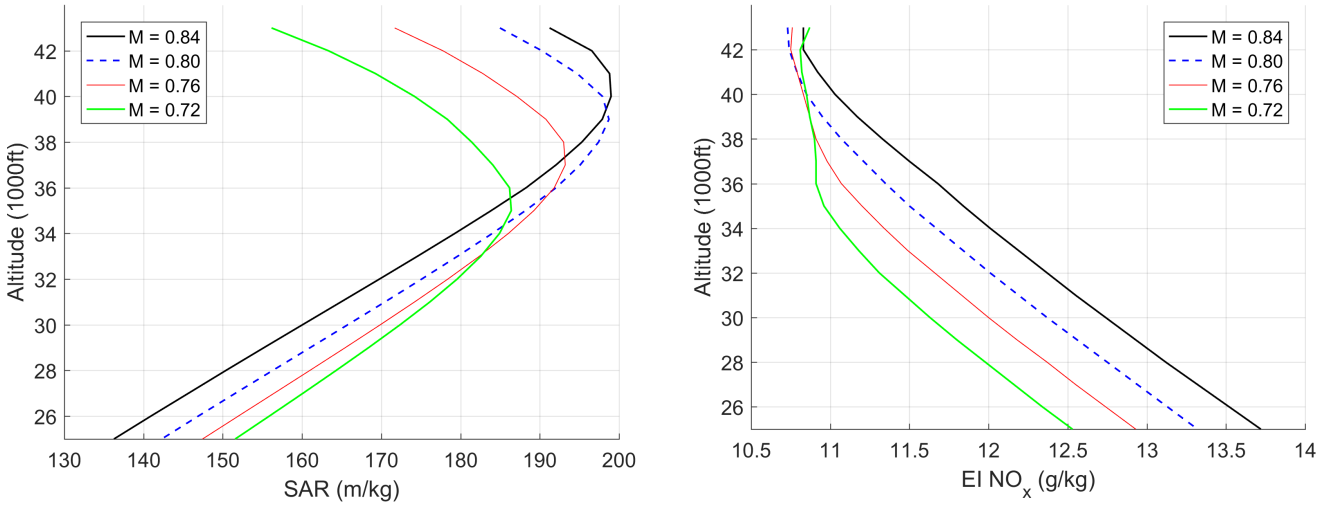

(a) SAR

(b) EI_{NOx}

Figure 4.23: SAR and EI_{NOx} as function of altitude for constant weight at 33% fuel load and varying Mach number for the B788

By analyzing the SAR as function of Mach number and altitude it is observed that at altitudes of 40,000 ft and higher a Mach number of 0.84 results in the highest SAR. This explains why the majority of trajectories were found to be flown at this Mach number. Furthermore it is observed that the Mach number resulting in the highest SAR decreases as the cruise altitude is lowered. This indicates that if the altitude is shifted down, fuel can be saved if the Mach number is lowered. This effect is quantified in Table 4.9 showing the SAR as function of altitude from the nominal cruise altitude of 40,000 ft down to 30,000 ft.

Cruise altitude (ft)	M = 0.84	M = optimal	Fuel penalty ratio
40,000	199.0	199 +(0%)	0
38,000	195.3 (+1.9%)	197.4 (+0.8%)	0.43
36,000	188.3 (+5.6%)	192.4 (+3.4%)	0.60
34,000	179.3 (+11.0%)	186.0 (+7.0%)	0.64
32,000	169.8 (+17.2%)	179.6 (+10.8%)	0.63
30,000	160.0 (+24.3%)	172.9 (+15.1%)	0.62

Table 4.9: Increase in fuel consumption as function of an altitude shift calculated for a constant Mach number and for an adjusted Mach number.

Table 5.9 shows the development of SAR as function of altitude for maintaining a Mach number of 0.84 compared to a scenario where the Mach number is adjusted to the most optimal value. Furthermore, numbers in parenthesis indicate the increase in fuel consumption compared to the original 40,000 ft altitude. From Table 4.9 it is observed that by maintaining the original Mach number, an altitude shift of 6,000 ft results in a fuel penalty of 11%. This result is in agreement with the found fuel penalty as function of an altitude shift of 6,000 ft shown in Figure 4.15. If on the other hand the Mach number is reduced to the in this case optimal Mach number of 0.76 the fuel increase is reduced to 7%. To quantify the overall savings for a range of altitude shifts, a fuel penalty ratio is defined which represents the reduction factor of the penalty in fuel. For example, when reducing the cruise altitude to 34,000 ft and reducing the Mach number to an optimal value of 0.76, the fuel penalty is only 64% of the penalty resulting from maintaining a Mach number of 0.84. This factor is found to be approximately constant.

For the emission index of NO_x it is observed that for the analyzed combinations of fuel load and Mach numbers, the lowest Mach number always results in the lowest emission index independent of cruise altitude. This indicates that by reducing the cruise Mach number to the most optimal Mach number for which the highest SAR can be attained, both the fuel consumption as well as the EI_{NO_x} are reduced, both resulting in a lower emission of NO_x. The effect of reducing the cruise Mach number on the EI_{NO_x} is quantified in Table 4.10. It shows that by flying a constant Mach number, the emission index increases rapidly whereas adjusting the Mach number to the one resulting in the highest SAR results in a EI_{NO_x} penalty which stays approximately constant at only 2%.

Cruise altitude	M = 0.84	M = optimal
40,000	11.03	11.03 +(0%)
38,000	11.33 (+2.7%)	11.07 (+0.4%)
36,000	11.68 (+5.9%)	11.2 (+1.5%)
34,000	12.01 (+8.9%)	11.34 (+2.8%)
32,000	12.37 (+12.1%)	11.31 (+2.5%)
30,000	12.74 (+15.5%)	11.27 (+2.2%)

Table 4.10: Increase in NO_x emission index as function of an altitude shift calculated for a constant Mach number and for an adjusted Mach number.

Based on these observations it is expected that for all alternative scenarios the penalty in fuel consumption can be reduced by 40% and the penalty in NO_x emission index can be maintained at 2% when the Mach number is adjusted down. Furthermore it is expected that similar results can be found for the B77W. By assuming these updated penalties in fuel consumption and the resulting penalty in NO_x emissions, Figure 4.24 is constructed. By implementing the penalty in EI_{NO_x} of 2% it is observed that the penalty in fuel consumption and NO_x emissions follow the same trend. Furthermore the overall magnitude is significantly reduced compared to the penalty shown in Figure 4.15 and is thereby closer to the penalties of the TRADEOFF scenario shown in Figure 4.15.

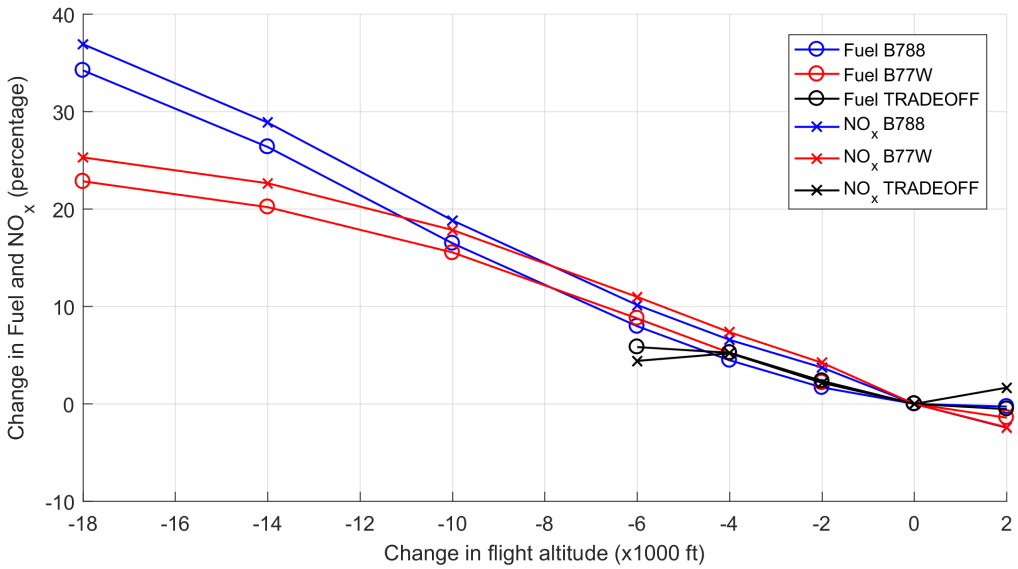

Figure 4.24: Change in fuel consumption and NO_x emissions as function of a relocated altitude profile and adjusted Mach number for the B788, B77W and TRADEOFF emission inventories

Considering the climate impact of the resulting adjusted emission inventories, the reduced penalty in fuel consumption and NO_x emissions can have a significant effect on the forcings of CO_2, O_3 and CH_4. The resulting climate impact of these forcing components and the updated total climate impact is shown in Figures 4.25a to 4.25d.

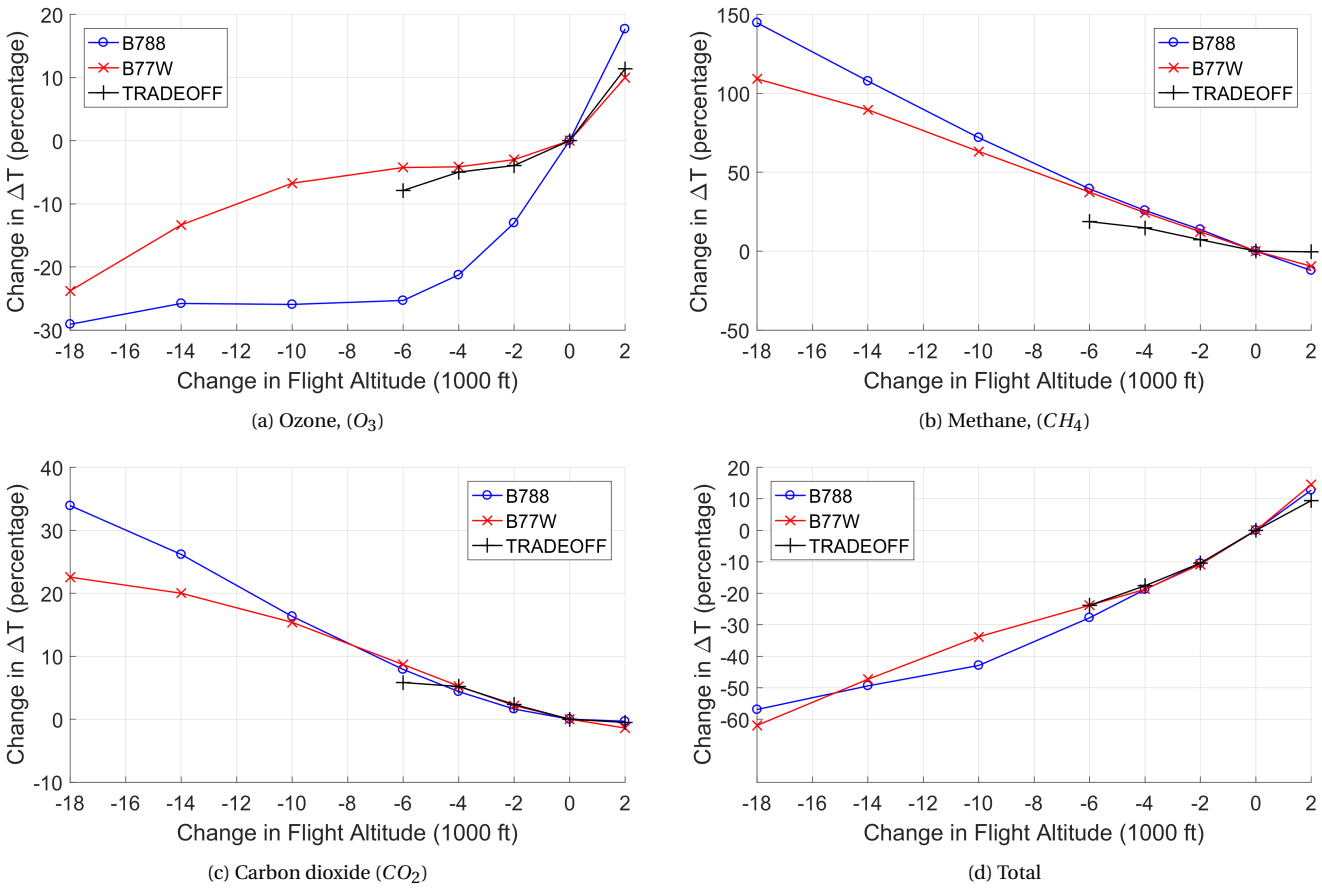

(a) Ozone, (O_3)

(b) Methane, (CH_4)

(c) Carbon dioxide (CO_2)

(d) Total

Figure 4.25: Temperature differences (in percentage) for the forcing components O_3, CH_4, CO_2 with respect to the base case through a displacement of flight altitudes by 2000 ft up, 2000 ft down, 4000 ft down, 6000 ft down, 10000 ft down, 14000 ft down and 18000 ft down calculated for 2100.

First of all, by reducing the penalty in fuel consumption the additional forcing of CO_2 due to a lower altitude will reduce. This is shown in Figure 4.25c where the increase in climate impact is found to be approximately 8% for an altitude shift of 6000 ft down compared to 14% found in Figure 4.19e. Furthermore the climate impact of both O_3 and CH_4 are reduced compared to the climate impact shown in Figures 4.19c and 4.19d due to the lower penalty in NO_x emissions. As a result the total climate impact reduction is larger as well. Figure 4.19f showed that the total climate impact reduction of both aircraft types for an altitude shift of 6000 ft was respectively 18% for the B77W and 25% for the B788. By adjusting the cruise Mach number the total climate impact reduction is found to increase to respectively 28% for the B788 and 24% for the B77W.

4.8.2. Aircraft payload weight

As discussed in Section 3.4.7 the estimation of the payload weight is based on assumptions for aircraft capacity, passenger load factor and passenger weight. Results showed that with the current assumptions all flights can perform their mission without exceeding the total fuel capacity or the MTOW. Furthermore the intersection of the obtained trendline showed that the maximum cruise distance could just be reached at MTOW. This indicates that if the payload is assumed higher, the MTOW limit will be breached. Furthermore, by assuming the payload weight lower, a larger distance can be flown at MTOW compared to the listed maximum range. Therefore, based on the trendline of the results, the average payload is considered to be correct.

There is one indication however that suggests that the payload could be assumed too low. According to Tables 4.7 and 4.8 both aircraft types can reduce their fuel consumption when increasing their altitude by 1000 and 2000 ft respectively. A reason for this could be that they did fly at their optimum altitude if their weight was higher than calculated. As a result of a higher TOW the optimum altitude is lower as observed in Figures 4.5a and 4.5b. This however is by assuming that the aircraft would have flown a fuel optimal trajectory which does not have to be the case.

Based on these observations is interesting to investigate the sensitivity of the cruise fuel consumption as a function of the assumed payload weight. For this reason, all B788 flights on 20 November are analyzed by assuming a payload from 0 to 40,000 kg in steps of 10,000 kg. 40,000 kg was chosen based on the maximum zero fuel weight which limits the maximum allowed payload to 42,000 kg. Additionally the calculated average payload weight of 25,000 kg is included in the analysis. As a result Table 4.11 shows the variation of total fuel consumption as function of the payload weight. Numbers in parenthesis indicate the difference with respect to the scenario where the payload is 25,000 kg as this is the average payload weight used in this work.

Payload (kg)	Fuel (10^6 kg)	NO_x emissions (10^3 kg)
0 (-100%)	10.08 (-7.7%)	110.1 (-9.8%)
10,000 (-60%)	10.29 (-5.8%)	113.1 (-7.4%)
20,000 (-20%)	10.68 (-2.2%)	118.7 (-2.8%)
25,000	10.92	122.1
30,000 (+20%)	11.19 (+2.5%)	126.0 (+3.2%)
40,000 (+60%)	11.84 (+8.4%)	135.6 (+11.1%)

Table 4.11: Variation of fuel consumption as function of payload weight

From Table 4.11 it is observed that as expected the fuel consumption and NO_x emissions increase as the payload is increased and decrease if the payload is decreased. The relative increase or decrease in emissions of NO_x is slightly larger due to the varying NO_x emission index which increases with TOW in combination with the varying fuel consumption. By varying the payload weight by 20% with respect to the average payload weight results in a change in fuel consumption ranging from -2.2% to +2.5% which is considered small. For larger variations in payload weight of 60% the change in fuel consumption ranges between -5.8% and +8.4% which is significant.

4.8.3. Future emission scenario

In this work the IPCC Fa1 emission growth scenario (Penner et al. 1999) is assumed which comprises an annual growth in emissions of 1.7% from 1990 to 2050. The emission growth is extended to 2100 by applying a medium growth rate of 1% per year similar to Frömming et al. (2012) [16]. Comparing this growth of 1.7% to the observed growth in emissions of 1.6% from 2004 to 2017 discussed in the introduction shows good agreement. Therefore it is assumed in this work that this growth will persist until 2050. After that however the the work from Frömming predicts a lower annual increase of 1% due to the increase in fuel efficiency.

It should be noted that during the period from 2004 to 2017 the RPK grew by an annual 5.9%. The reason why this translated in a lower increase in fuel consumption is due to two factors, the improvements in fuel efficiency and the increasing passenger load factor. According to ICAO statistics the passenger load factor increased from 75% to 82%. This load factor however can not increase beyond 100% and therefore this alleviating effect on the aircraft emissions will eventually stop. By assuming the RPK will continue to grow at the same rate this would lead to a larger than 1% annual increase in fuel consumption from 2050 onward.

Based on this reasoning, this work investigated the effect of a 1.7% annual increase in emissions from 1990 until 2100. Results of this analysis are presented in Figures 4.26a and 4.26b showing the radiative forcing and temperature response where the solid lines indicate the original scenario representing a growth scenario of 1% from 2050 to 2100. The dashed lines indicate the alternative scenario where a growth of 1.7% is simulated.

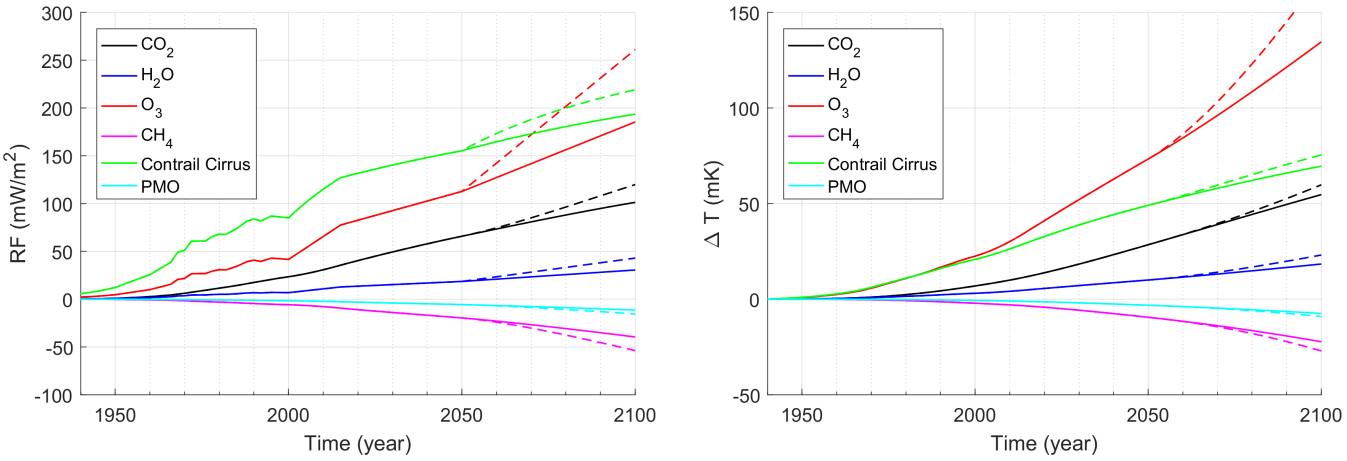

(a) Radiative forcing

(b) Temperature change

Figure 4.26: Radiative forcing and temperature response for all individual forcing components for two different future emission scenarios.

Observed from these figures is that by increasing the emission growth to an annual increase of 1.7% the climate impact of all forcing agents increases. Furthermore at the year 2050 a kink can be observed where the forcings start to increase faster despite the growth rate being constant. This behaviour can be explained by taking a closer look at the growth rates from 1990 to 2100. Although the average annual growth between 1990 and 2050 is 1.7%, a faster increase increase is observed between 2000 and 2015. To compensate for this larger growth rate, the growth between 2015 and 2050 is reduced to approximately 1% to obtain an overall growth of 1.7% between 1990 and 2050. The transition from 1% to 1.7% explains the kink in the radiative forcing response.

Furthermore it is observed that the magnitude of the increase in ozone forcing is significantly larger compared to the forcings of contrail cirrus and CO_2. This is a result of the saturation effect present for CO_2 and contrail cirrus which do not linearly scale with emissions and flown kilometers. This saturation effect is not present for the forcing of ozone.

Secondly for the results presented in this work, the assumed Fa1 scenario is applied to both the emissions of CO_2 and NO_x as well as the flown kilometers. The amount of flown kilometers however will increase faster relative to the emissions of CO_2 and NO_x due to the increase in fuel efficiency. Therefore it is interesting to investigate the effect of a higher increase in flown kilometers. By taking into account the annual increase in RPK of approximately 6% and combining this with an increase in loadfactor from 75% to 82% (which is an average increase of 1% per year) this will result in an increase in flown kilometers of approximately 5% each year which is a factor three higher compared to the current assumed growth rate. As a result of this increase in flown kilometers the radiative forcing of contrail cirrus will increase. This will increase reduction in climate impact that can be achieved by lowering flight altitudes.

5

Conclusion and Discussion

In this study an assessment is done on the effect of cruise altitude changes on the climate impact of two different aircraft types, the Boeing 787-800 (B787-800) and Boeing 777-300ER (B777-300ER). The basis for this research is an assembly of 2,738 historical trajectories retrieved from Flightradar24. Based on this trajectory data the fuel consumption and corresponding emissions during the cruise phase of all flights were determined by using Piano-X aircraft performance data. Furthermore the effect of wind was taken into account by incorporating weather data from the European Centre for Medium-Range Weather Forecasts. The resulting emission inventories were used as input for the climate response model AirClim to assess the climate impact of the assembled datasets. This climate impact assessment was performed for the original cruise altitude profile of both aircraft types found in the trajectory data (the basecase) as well as for alternative scenarios with a relocated cruise altitude of 2000 ft up 2000 ft down, 4000 ft down, 6000 ft down, 10,000 ft down, 14,000 ft down and 18,000 ft down.

By analysing the climate impact of the base case of the two aircraft types, it was found that the total climate impact of the B777-300ER is approximately 15% larger compared to the B787-800 as quantified per flown kilometer. This difference is mainly due to the larger climate impact of the forcings of CO_2 and O_3 as a result of the larger emission quantity of CO_2 and NO_x for the B777-300ER. Furthermore it was found that the contribution of the individual forcing components to the total climate impact is dependent on the aircraft type. The climate impact of the forcing components of O_3 and CO_2 are larger and CH_4 is reduced for the B777-300ER which is mainly due to the larger emission quantity per flown kilometer. The forcings of contrail cirrus and water vapor on the other hand were found to be larger for the Boeing B787-800 as a consequence of the higher emission altitude.

By shifting cruise altitudes down, the total climate impact is reduced for both aircraft types where the minimal climate impact is found for the lowest analyzed cruise altitude. The reduction in climate impact is mainly the result of the reduced short term forcings from contrail cirrus, ozone and the induced destruction of methane. The magnitude of the total climate impact reduction as well as the contribution of the individual forcing components to this total climate impact reduction however was found to be dependent on the aircraft type and the relocation distance. Relocating the cruise altitude up by 2000 ft resulted in an increase in climate impact for both aircraft types of respectively 13% and 14% for the B787-800 and B777-300ER.

Relocating cruise altitudes 6000 ft down resulted in a climate impact reduction of 24 % for the B787-800 and 18% for the B777-300ER. The reduction in total climate impact for the B787-800 is the result of the reduced forcings from contrail cirrus, ozone, water vapor and methane which all contribute an approximately equal share to the total climate impact reduction. For

the B777-300ER on the other hand, the climate impact reduction is almost entirely the result of the reduced forcings of methane and contrail cirrus whereas the climate impact of ozone is increased due to the larger emission quantity of NO_x. This increase in ozone forcing for a 6000 ft reduced cruise altitude is the main reason for the smaller reduction in climate impact for the B777-300ER. As a consequence of this reduced cruise altitude the fuel consumption and associated fuel costs are found to increase by 13% and 14% for the B787-800 and B777-300ER respectively. The obtained reduction in climate impact for the B787-800 shows good agreement to the results presented by Frömming where for the same altitude shift of 6000 ft down, a total climate impact reduction of 25% was found for the TRADEOFF emission inventory. The associated increase in fuel consumption however, is only 6% which is significantly smaller compared to the fuel penalty found in this work. The reason for the larger penalty in fuel consumption found in this work is the large average cruise distance of 5400 and 6200 kilometers for the B787-800 and B777-300ER respectively, which is a factor three larger than the estimated cruise distance for the TRADEOFF inventory.

By relocating cruise altitudes further down by 18000 ft the resulting climate impact reduction of both aircraft types is found to increase to 49% for the B787-800 and 59% for the B777-300ER. For both aircraft types the largest contribution to this climate impact reduction is the result of the reduced forcings of contrail cirrus and the reduced forcing of methane. As a result of this reduced cruise altitude, the penalty in fuel consumption and fuel costs were calculated to increase to respectively 57% and 38% for the B787-800 and B777-300ER.

Based on the performed analysis on the influence of the cruise Mach number, it was found that the increase in fuel consumption for a shift in cruise altitude can be reduced when the Mach number is adjusted down. As a consequence, the nett climate forcings of CO_2 and NO_x were found to reduce which resulted in a further reduction in climate impact. For the relocated altitude of 6000 ft down, a reduction in total climate impact was found of 28% and 24% for the B787-800 and B777-300ER respectively. The corresponding increase in fuel consumption was reduced to respectively 8% and 9%.

All in all it can be concluded that there exists a considerable potential for mitigating the climate impact for both aircraft types. Although a relocation of cruise altitudes by 18000 ft down resulted in the largest climate impact reduction, the associated increase in fuel costs makes this scenario less interesting for commercial aviation. Relocating altitudes down by 6000 ft on the other hand shows a large potential for climate impact reduction as well however for a significantly lower increase in associated fuel costs. If in addition to an altitude shift the cruise Mach number is adjusted down, a further reduction in climate impact is found for both aircraft types while limiting the increase in associated fuel costs. Therefore, considering both the reduction in climate impact and the corresponding increase in costs, it is concluded in this research that an altitude shift of 6000 ft in combination with an adjusted cruise Mach number is the best option for reducing the climate impact from aviation.

A

Cruise altitude analysis Opensky network

This Appendix shows the result of the performed cruise altitude analysis based on data acquired from the Opensky network.

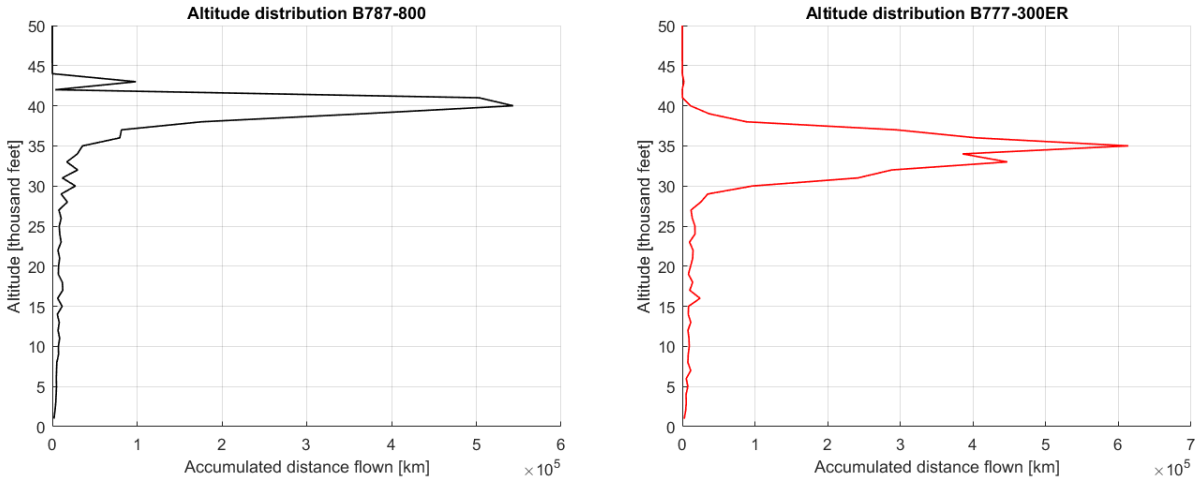

(a) B787-800

(b) B777-300ER

Figure A.1: Accumulated distance flown per altitude band in thousand feet for 500 flights operated with one specific aircraft type

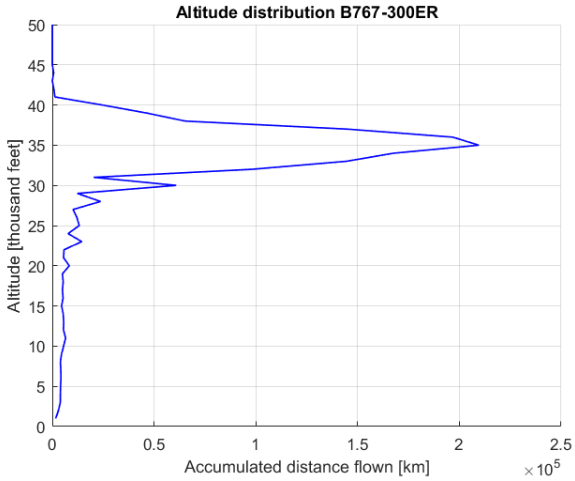

(c) B767-300ER

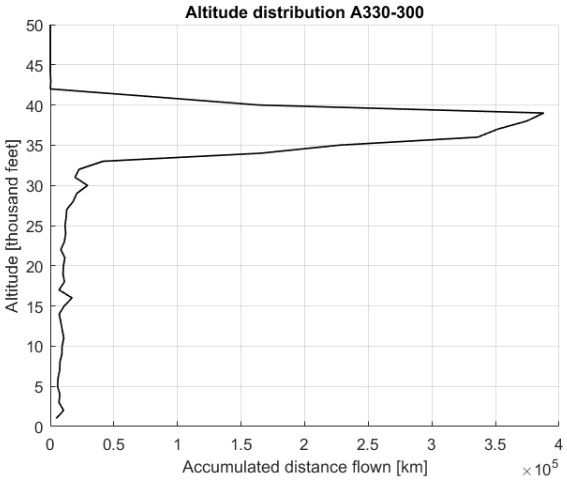

(d) A330-300

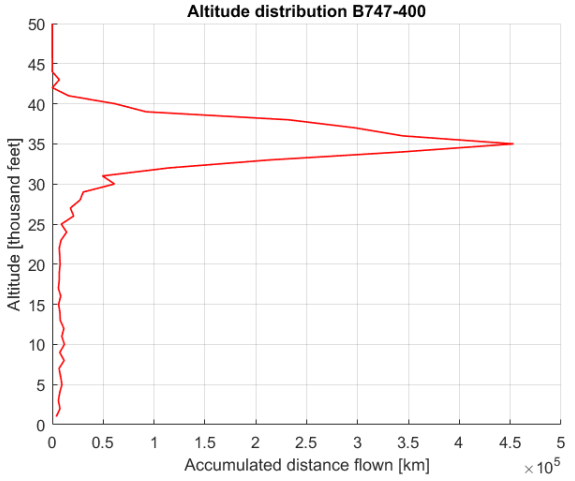

(e) B747-400

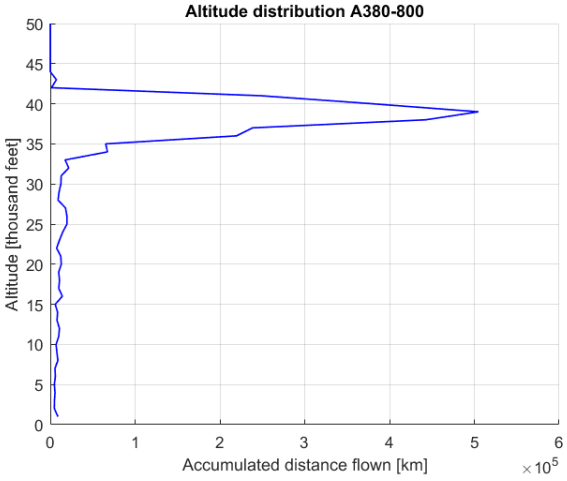

(f) A380-800

Figure A.1: Accumulated distance flown per altitude band in thousand feet for 500 flights operated with one specific aircraft type

B

Mach number analysis

B.1. Mach number distributions

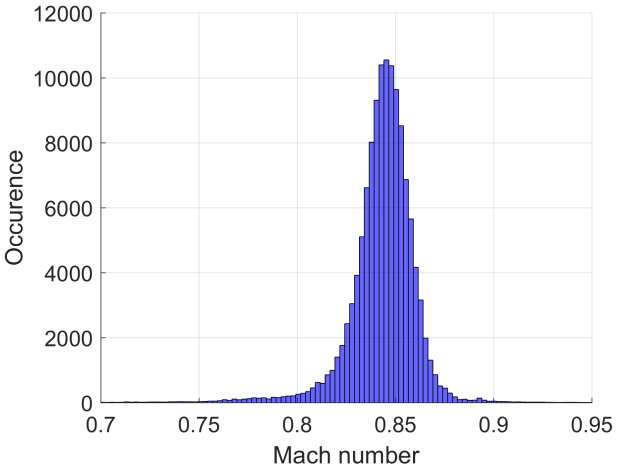

(a) B788 on November 20th. $\mu = 0.8443$, $\sigma = 0.0210$

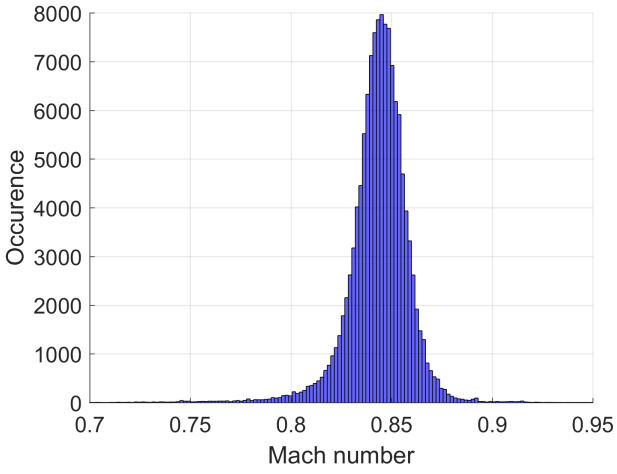

(b) B788 on March 30th. $\mu = 0.8442$, $\sigma = 0.0191$

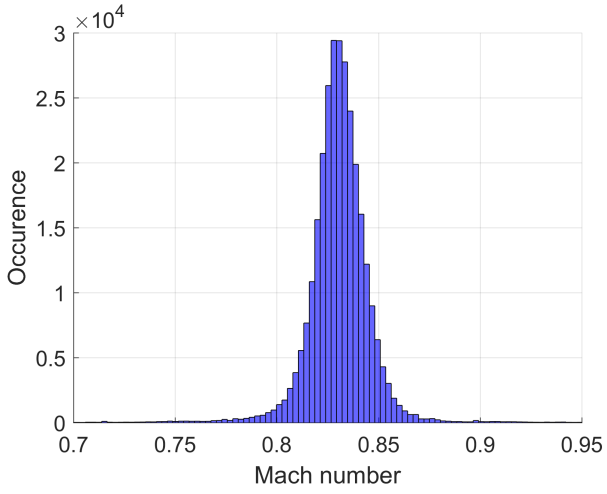

(c) B77W on November 20th. $\mu = 0.8308$, $\sigma = 0.0225$

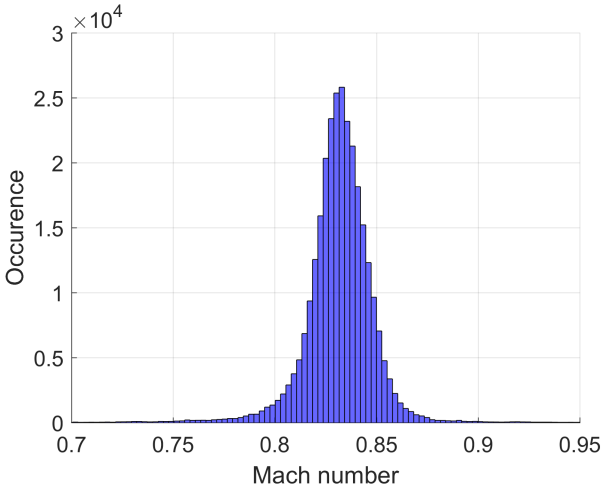

(d) B77W on March 30th. $\mu = 0.8323$, $\sigma = 0.0311$

Figure B.1: Histograms of all calculated instantaneous Mach numbers for the analysed B788 and B77W trajectories on two separate dates. Calculated mean Mach number (μ) and standard deviation (σ) are supplemented

B.2. Correlation between Mach number and flight altitude

This appendix shows the calculated Mach numbers for all analyzed cruise segments in relation to the flown cruise altitude for both aircraft types on two separate days in the form of a scatter plot. In addition a red line is shown indicating the calculated average Mach number as function of cruise altitude.

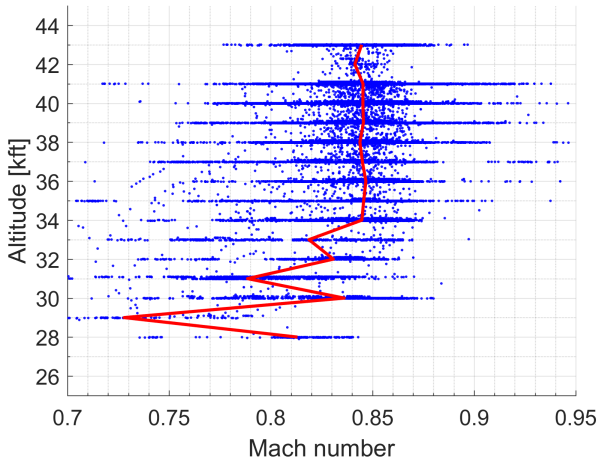

(a) B788 on November 20th

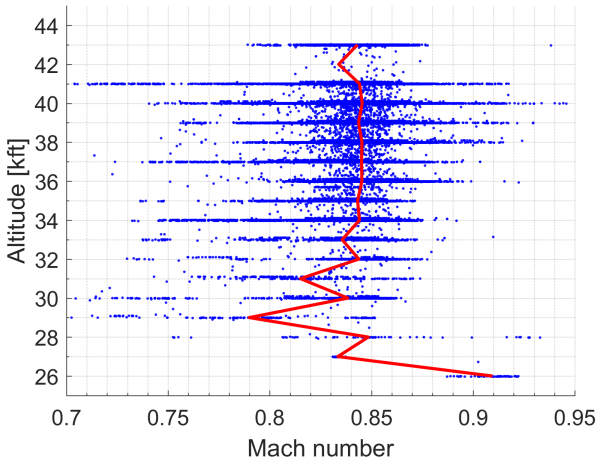

(b) B788 on March 30th

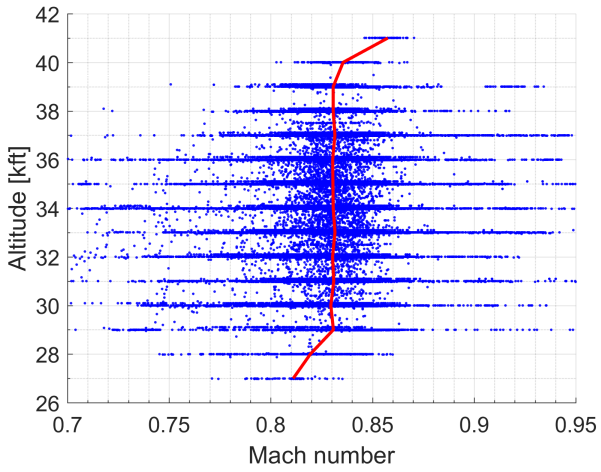

(c) B77W on November 20th

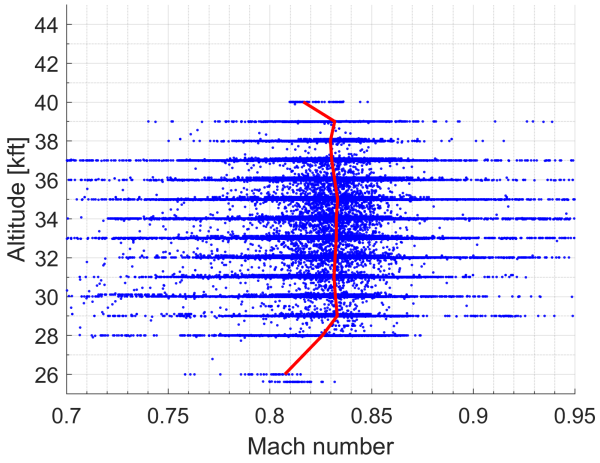

(d) B77W on March 30th

Figure B.2: Scatter plot showing the correlation between calculated Mach number and cruise altitude for the analysed B788 and B77W trajectories on two separate dates. The red line indicates the mean Mach number for each altitude level

C

Standard emission inventory characteristics

This section will provide additional information regarding the three used emission inventories AERO2k, Quantify and TRADEOFF which are used in Section 3.7.6.

C.1. Origin

The AERO2k inventory provides an aviation emission data set for the year 2002 for civil and military flights and is assembled by Eyers et al., 2004 [11].

The Quantify emission inventory is developed by the DLR-Institute of Atmospheric Physics and is based on global flight movement statistics from the Official Airline Guide (OAG). In addition non-scheduled air traffic from the AERO2k flight database was incorporated [23]. Furthermore in contrast to the AERO2k inventory the total fuel consumption for the Quantify inventory is scaled to the global sales data from the International Energy Agency (IEA).

For the TRADEOFF inventory aircraft movement data is converted to emissions by using the FAST (Future Aviation emissions Scenario Tool) model which was developed for the purpose of the TRADEOFF studies [19]. The movement data was taken identical to the one used in the ANCTAT/EC2 inventory (Gardner et al., 1998) and is based on movements for 1991/92. These movements were scaled to the year 2000. To determine the corresponding emissions sixteen aircraft-engine combinations were used representative of the global fleet [19]. The fuel flow profiles of these aircraft-engine combinations were modelled using the PIANO aircraft performance model and assuming a payload of 85% [19]. Cruise altitudes were prescribed based on actual flight data from EUROCONTROL using approximately 53,000 flights. Based on this data a correlation between cruise distance and cruise altitude was found which was used to model the cruise altitude of aircraft movements [13]. As a final step the emission inventories of fuel consumption, produced NO_x and distance flown were generated by using the FAST model on a 1x1 grid and a veritcal resolution of 2000 ft. [16][19]. Additional TRADEOFF scenarios were developed with a 2000 ft higher, 2000 ft lower, 4000 ft lower and 6000 ft lower cruise altitude according to the same method. This was done by taking the changes in aircraft performance for changed flight levels and corresponding changed fuel consumption into account [16]. Furthermore flight altitude changes were only implemented if the respective aircraft was able to perform the particular flight in terms of performance and fuel capacity [16]. This resulted in 1% of flights for which it was infeasible to shift them downwards whereas 10% of flights could not be relocated to a higher flight level. These flights were not shifted. The resulting characteristics of the relocated TRADEOFF emission inventories are shown in Table C.1

C.2. Characteristics

The characteristics of the used emission inventories are shown in Table C.1. Furthermore the latitudinal and altitudinal distrubitions of the used emissions are shown as density functions in Figures C.1 and C.2 which are similar to the distrubitions as presented in Grewe et al (2016) [23] and Dahlmann (2012) [7]

Inventory	reference year	Fuel (Tg)	NO_x (Tg_N)	Distance (10^9 km)	Vertical resolution (ft)
AERO2k	2002	176	0.68	33.2	1,000
Quantify	2000	214	0.85	30.5	2,000
TRADEOFF base	2000	152	0.60	25.4	2,000

Table C.1: Overview of standard emission inventory characteristics

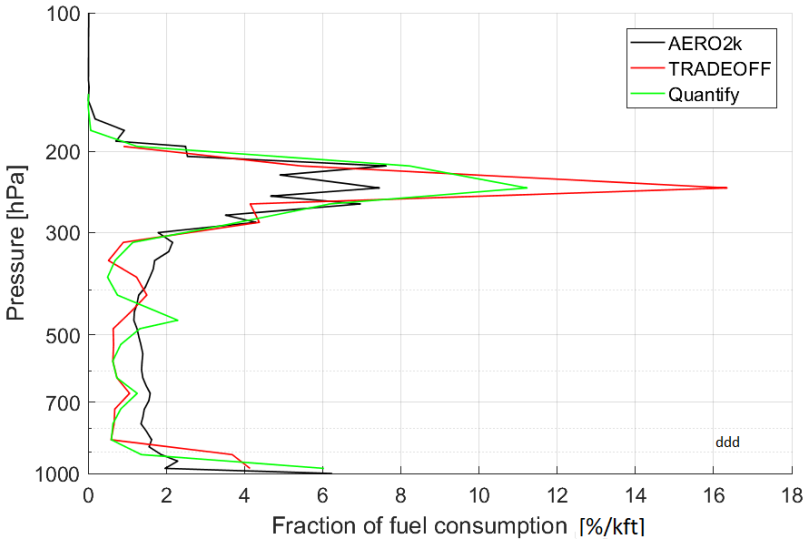

Figure C.1: Altitudinal distribution of emissions for the AERO2k, TRADEOFF and Quantify inventories given as density functions

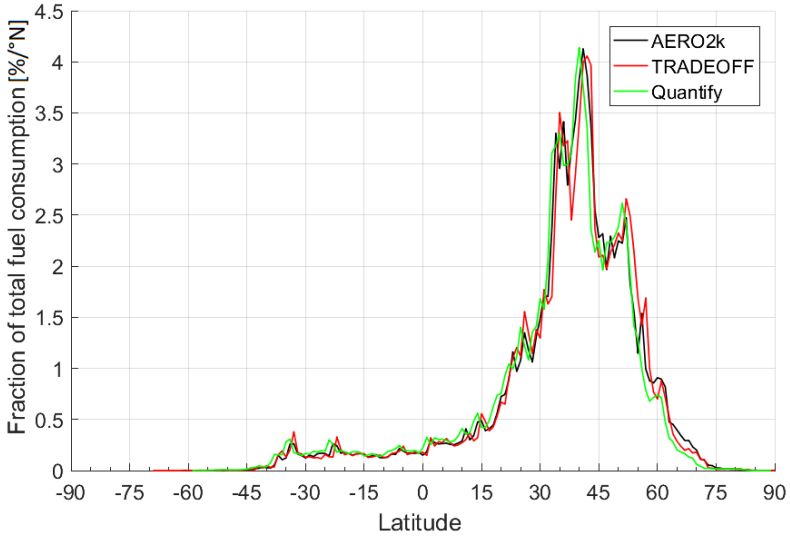

Figure C.2: Latitudinal distribution of emissions for the AERO2k, TRADEOFF and Quantify inventories given as density functions

D

Radiative forcing data

D.1. Verification data short term forcings TRADEOFF in year 2000

This work (AirClim)	Contrail Cirrus	H_2O	O_3
Base + 2000ft	50.3 (+6.5%)	2.5 (+40.0%)	24.9 (+11.4%)
Base case	47.2	1.8	22.4
Base case -2000ft	39.2 (-16.9%)	1.1 (-37.5%)	21.5 (-3.9%)
Base case -4000ft	32.5 (-31.1%)	0.7 (-61.4%)	21.3 (-5.0%)
Base case -6000ft	27.3 (-42.1%)	0.4 (-75.2%)	20.6 (-7.9%)

Table D.1: Radiative forcing data calculated with AirClim for the short term forcings in the year 2000 found in this work for the TRADEOFF base case and relocated scenarios. The difference with respect to the base case is shown in parenthesis and forms the basis for the data presented in Figure 3.31 a - c

Fichter (AirClim)	Linear Contrails	H_2O	O_3
Base + 2000ft	4.0 (+5.3%)	2.5 (+56.3%)	25.3 (+12.9%)
Base case	3.8	1.6	22.4
Base case -2000ft	3.5 (-7.9%)	1.1 (-31.3%)	21.7 (-3.1%)
Base case -4000ft	2.9 (-23.7%)	0.6 (-62.5%)	21.5 (-4.0%)
Base case -6000ft	2.3 (-39.5%)	0.5 (-68.8%)	20.9 (-6.7%)

Table D.2: Radiative forcing data for calculated with AirClim the short term forcings in the year 2000 presented by Fichter [12] for the TRADEOFF base case and relocated scenarios. The difference with respect to the base case is shown in parenthesis and forms the basis for the data presented in Figure 3.31 a - c and Figure 3.32

Fichter (E39/CA)	Linear Contrails	H_2O	O_3
Base + 2000ft	5 (+6.4%)	2.4 (+60.0%)	16.1 (+8.1%)
Base case	4.7	1.5	14.9
Base case -2000ft	4.2 (-10.6%)	0.9 (-40.0%)	14 (-6.0%)
Base case -4000ft	3.3 (-29.8%)	0.6 (-60.0%)	13.6 (-8.7%)
Base case -6000ft	2.4 (-48.9%)	0.4 (-73.3%)	12.9 (-13.4%)

Table D.3: Radiative forcing data calculated with E39/CA for the short term forcings in the year 2000 presented by Fichter [12] for the TRADEOFF base case and relocated scenarios. The difference with respect to the base case is shown in parenthesis and forms the basis for the data presented in Figure 3.32

D.2. Verification data all forcings TRADEOFF in year 2100

This work (AirClim)	Contrail Cirrus	H_2O	O_3	CH_4	CO_2
Base + 2000ft	140.5 (+7.9%)	11.2 (+39.9%)	111.3 (+11.4%)	-46.2 (-0.5%)	100.9 (-0.5%)
Base case	130.2	8.0	100.0	-46.4	101.5
Base case -2000ft	104.0 (-20.2%)	5.0 (-37.5%)	96.0 (-4.0%)	-49.8 (+7.3%)	103.8 (+2.3%)
Base case -4000ft	81.9 (-37.1%)	3.1 (-61.4%)	94.9 (-5.0%)	-53.2 (+14.7%)	106.7 (+5.2%)
Base case -6000ft	67.0 (-48.6%)	2.0 (-75.3%)	92.1 (-7.9%)	-55.1 (+ 18.7%)	107.5 (+5.9%)

Table D.4: Radiative forcing data for various forcings components in the year 2100 found in this work for the TRADEOFF base case and relocated scenarios. The difference with respect to the base case is shown in parenthesis and forms the basis for the data presented in Figure 3.31 d - e

Fichter (E39/CA)	Linear Contrails	H_2O	O_3	CH_4	CO_2
Base + 2000ft	23.1 (+7.9%)	9.9 (+45.6%)	73.6 (+9.2%)	-33.3 (-4.9%)	100.6 (-0.6%)
Base case	21.4	6.8	67.4	-35.0	101.2
Base case -2000ft	19.0 (-11.2%)	4.2 (-38.2%)	63.4 (-5.9%)	-38.4 (+9.7%)	103.6 (+2.4%)
Base case -4000ft	15.1 (-29.4%)	2.6 (-61.8%)	61.6 (-8.6%)	-41.9 (+19.7%)	106.0 (+4.7%)
Base case -6000ft	11.2 (-47.7%)	1.8 (-73.5%)	58.4 (-13.4%)	-43.6 (+ 24.6%)	106.6 (+5.3%)

Table D.5: Radiative forcing data calculated with AirClim (based on the base year 2000 calculated with E39/CA) for various forcings components in the year 2100 presented by Fichter [12] for the TRADEOFF base case and relocated scenarios. The difference with respect to the base case is shown in parenthesis and forms the basis for the data presented in Figure 3.31 d - e

Bibliography

[1] Airlinesfleet. URL. `https://airlinesfleet.com/`, accessed 14-9-2019.

[2] Appleman H. The formation of exhaust condensation trails by jet aircraft. *Bull. American Meteorol. Soc.*, 34:14–20, 1953.

[3] Baughcum S. and D. Sutkus and S. Henderson. Year 2015 aircraft emission scenario for scheduled air traffic. NASA CR-1998-207638, 1998.

[4] Brasseur G. and R. Cox and D. Hauglustaine and I. Isaksen and J. Lelieveld and D. Lister and R. Sausen and U. Schumann and A. Wahner and P. Wiesen. European scientific assessment of the atmospheric effect of aircraft emissions. *Atmos. Environ.*, 32:2329–2418, 1998.

[5] Burkhardt U. and B. Kärcher. Global radiative forcing from contrail cirrus. *Nature Clim. Change 1, 54-58*, 2011.

[6] Carbon Market Watch. The corsia: Icao's market based measure and implications for europe. Carbon Market Watch Policy Briefing, 2016.

[7] Dahlmann K. Eine methode zur effizienten bewertung von manahmen zur klimaoptimierung des luftverkehrs. Ph D. thesis. Fak. für Phys., Ludwigs-Maximilians-Universität München., 2012.

[8] Dahlmann K. and A. Koch and F. Linke and B. Lührs and V. Grewe and T. Otten and D. Seider and V. Gollnick and U. Schumann. Climate-compatible air transport system - climate impact mitigation potential for actual and future aircraft. *Aerospace 3, 38 doi:10.3390/aerospace3040038*, 2016.

[9] Dahlmann K. and V. Grewe and C. Frömming and U. Burkhardt. Can we reliably assess climate mitigation options for air traffic scenarios despite large uncertainties in atmospheric processes. *Trans. Res. Part D, 46, 40-55 doi:10.1016/j.trd.2016.03.006*, 2016.

[10] DVB Bank SE's Aviation Research department. An overview of commercial aircraft 2018-2019. 2017.

[11] Eyers C. and D. Addleton and K. Atkinson and M. Broomhead and R. Christou and T. Elliff and R. Falk and I. Gee and D. Lee and C. Marizy and S. Michot and J. Middel and P. Newton and P. Norman and M. Plohr and D. Raper and N. Stanciou. Aero2k global aviation emissions inventories for 2002 and 2025. *Technical Report 04/01114 QinetiQ*, 2004.

[12] Fichter C. Climate impact of air traffic emissions in dependency of the emission location. Ph.D. thesis Manchester metropolitan University, 2009.

[13] Fichter C. and S. Marquart and R. Sausen and D.S. Lee. The impact of cruise altitude on contrails and related radiative forcing. Meteorologische Zeitschrift, Vol. 14, No. 4, 563-572, 2005.

[14] Filippone A. On the benefits of lower Mach number aircraft cruise. The Aeronautical Journal, 2007.

[15] Friedl R. and S. Baughcum and B. Anderson and J. Hallett and K. Liou and P. Rasch and D. Rind and K. Sassen and H. Singh and I. Williams and D. Wuebbles. Atmospheric effects of subsonic aircraft: Interim assessment of the advanced subsonic assessment program. *NASA Reference Publication*, Publication 1400, 1997.

[16] Frömming C. and M. Ponater and K. Dahlmann and V. Grewe and D.S. Lee and R. Sausen. Aviation induced radiative forcing and surface temperature change in dependency of the emission altitude. JJ. Geophys. Res., 117, D19104, doi:10.1029/2012JD018204, 2012.

[17] Fuglestvedt J. and T. Berntsen and G. Myhre and K. Rypdal and R. Bieltvedt Skeie. Climate forcing from the transport sectors. Proceedings of the National Academy of Sciences, 2008.

[18] Fuglestvedt J. and T. Berntsen and I. Isaksen and H. Mao and X. Liang and W. Wang. Climate effects of NO_x emissions through changes in tropospheric O_3 and CH_4 a global 3-D model study. *CICERO*, 1997.

[19] Gauss M. and I.S.A. Isaksen and D.S. Lee and O.A. Søvde. Impact of aircraft nox emissions on the atmosphere - tradeoffs to reduce the impact. Atmospheric Chemistry and Physics, 2006.

[20] Gierens K. and P. Spichtinger. On the size distribution of ice-supersaturated regions in the upper troposphere and lowermost stratosphere. *Annales Geophysicae*, 18:499–504, 2000.

[21] Grewe V. Aircraft emissions and climate effects-1. *Lecture slides*, TU Delft, 21 Feb 2018.

[22] Grewe V. and A. Stenke. Airclim: an efficient tool for climate evaluation of aircraft technology. Atmospheric Chemistry and Physics, 2008.

[23] Grewe V. and L. Bock and U. Burkhardt and K. Dahlmann and K. Gierens and L. Hüttenhofer and S. Unterstrasser and A. Rao and A. Bhat and F. Yin and T. Reichel and O. Paschereit and Y. Levy. Assessing the climate impact of the ahead multi-fuel blended wing body. *Meteorologische Zeitschrift, Vol. 26, No. 6*, pages 711–725, 2016.

[24] Grewe V. and M. Damaris and C. Fichter and R. Sausen. Impact of aircraft nox emissions. part 1: Interactively coupled climate-chemistry simulations and sensitivities to climate-chemistry feedback, lightning and model resolution. *Meteorologische Zeitschrift, Vol. 11, No. 3*, 11 No 3:177–186, 2002.

[25] Grewe V. and M. Damaris and R. Hein and I. Koehler and R. Sausen. Impact of future subsonic aircraft NO_x emissions on the atmospheric composition. *Geophys. Res. Lett.*, 26: 47–50, 1999.

[26] Grewe V. and M. Plohr and G. Cerino and M. Di Muzio and Y. Deremaux and M. Galerneau and P. de Saint Martin and T. Chaika and A. Hasselrot and U. Tengzelius and V.D. Korovkin. Estimates of the climate impact of future small-scale supersonic transport aircraft- results from the hisac eu-project. The Aeronautical journal Volume 114 No 1153, 2007.

[27] Grimme W. and M. Jung. Towards more sustainability? - the development of aviation emissions from germany between 1995 and 2016. German Aerospace Center (DLR), 2016.

[28] Hansen J. and M. Sato and R. Ruedy. Radiative forcing and climate response. *J. Geophys. Res., 102(D6), 6831–6864*, 1997.

[29] Hasselmann K. and S. Hasselmann and R. Giering and V. Ocana and H. Storch. Sensitivity study of optimal co2 emission paths using a simplified structural integrated assessment model (siam). *Climate Change 37, 345-386*, 1997.

[30] IATA. Fact sheet climate change. `https://www.iata.org/pressroom/facts_figures/fact_sheets/Documents/fact-sheet-climate-change.pdf`, visited on 23-1-2019.

[31] ICAO. Annex 6 part I section 4.3.6 fuel requirements. Ninth edition, 2010.

[32] ICAO. EDTO course - module 6 flight operations considerations page 33. Workshop, 2016.

[33] ICAO. Aircraft engine emissions databank. EASA, assessed 14-11 2019. URL `https://www.easa.europa.eu/node/15672`.

[34] ICAO. Icao long-term traffic forecasts. `https://www.icao.int/Meetings/aviationdataseminar/Documents/ICAO-Long-Term-Traffic-Forecasts-July-2016.pdf`, visited on 28-1-2019.

[35] ICAO Tenth session of the statistics division. Available capacity and average passenger mass. *STA/10-WP/5*, 2009.

[36] International Civial Aviation Organization (ICAO). Aviation's contribution to climate change. *HLM-ENV/09-IP/04*, 2009.

[37] International Civial Aviation Organization (ICAO). Annual report air transport statistics. 2017.

[38] International Energy Agency (IEA). Oil information 2006, table 9, 749 pp. *Energy agency*, 2007.

[39] IPCC. Radiative forcing of climate change. `https://www.ipcc.ch/site/assets/uploads/2018/03/TAR-06.pdf`, visited on 3-4-2019.

[40] IPCC 2001 Houghton, J.T. and Y. Ding and D.J. Griggs and M. Noguer and P. van der Linden and X. Dai and K. Maskell and C.A. Johnson. Climate change 2001: The scientific basis. contribution of working group I to the third assessment report of the intergovernmental panel on climate change, 2001.

[41] IPCC 2014. Climate change 2014: Synthesis report. contribution of working groups i, ii and iii to the fifth assessment report of the intergovernmental panel on climate change [core writing team, r.k. pachauri and l.a. meyer (eds.)]. Cambridge University Press, 2014.

[42] Janes. Janes all the world aircraft. 1.

[43] Jensen L. and H. Tran and R. Hansman. Cruise fuel reduction potential from altitude and speed optimization in global airline operations. *USA/Europe Air Traffic Management Research and Development Seminar (ATM2015) paper*, 2015.

[44] Johnston H. Reduction of stratospheric ozone by nitrogen oxide catalysts from supersonic transport exhaust. *Science*, 173:517–522, 1971.

[45] Kharina A. and D. Rutherford. Fuel efficiency trends for new commercial jet aircraft: 1960 to 2014. *Whitepaper The International Council On Clean Transportation*, 2015.

[46] Kärcher B. Formation and radiative forcing of contrail cirrus. *Nature*, 2018.

[47] Lary D. Catalytic destruction of stratospheric ozone. *J. Geophys. Res.*, 102:515–526, 1997.

[48] Lee D. and D. Fahey and P. Forster and P. Newton and R. Wit and L. Lim and B. Owen and and R. Sausen. Aviation and global climate change in the 21st century. Atmospheric Environment, 43(22-23):3520–3537, 2009. ISSN 1352-2310. doi: 10.1016/j.atmosenv.2009.04.024., 2009. URL `http://dx.doi.org/10.1016/j.atmosenv.2009.04.024`.

[49] Lee D.S. and G. Pitari and V.Grewe and K. Gierens and J.E. Penner and A. Petzold and M.J. Prather and U. Schumann and A.Bais and T. Berntsen and D. Iachetti and L.L. Lim and R. Sausen. Transport impacts on atmosphere and climate: Aviation. Atmospheric Environment 44 (2010) 4678-4734, 2010.

[50] Lissys Ltd. Piano-x. `http://www.lissys.demon.co.uk/PianoX.html`, 2019.

[51] Lovegren J.A. and R.J. Hansman. Quantification of fuel burn reduction in cruise via speed and altitude optimization strategies, 2011.

[52] Mannstein H. and K. Gierens and P. Spichtinger. How to avoid contrail cirrus. DLR Institut für Physik der Atmosphäre, 2007.

[53] Meerkötter R. and U. Schumann and D. Doelling and P. Minnis and T. Nakajima and Y. Tsushima. Radiative forcing by contrails. *Ann Geophys*, 17:1080–1094, 1999.

[54] Ministry of Defence. Turbine fuel, kerosine type, jet a-1. *Defence Equipment and Support DStan*, 7:(Amd 3), 2015.

[55] Minnis P. and D. Young and D. Garber and L. Nguyen and W. Smith and R. Palikonda. Transformation of contrails into cirrus during succces. *Geophys. Res. Lett.*, 25:1157–1160, 1998.

[56] Myhre G. and E. Highwood and K. Shine and F. Stordal. New estimates of radiative forcing due to well mixed greenhouse gases. *Geophys. research letters, Vol.25, No 14*, pages 2715–2718, 1998.

[57] Penner J. and D. Lister and D. Griggs and D. Dokken and M. McFarland. Aviation and the global atmosphere: A special report of IPCC working groups I and III. Cambridge Univ. Press, Cambridge, U.K., 1999.

[58] Poll D.I.A. On the relationship between non-optimum operations and fuel requirement for large civil transport aircraft, with reference to environmental impact and contrail avoidance strategy. *The Aeronautical Journal*, 2018.

[59] Ponater M. and S. Pechtl and R. Sausen and U. Schumann and G. Hüttig. Potential of the cryoplane technology to reduce aircraft climate impact: a state-of-the-art assessment. Atmos. Environ., 2006.

[60] Robertson W. and R. Root and D. Adams. Boeing fuel conservation strategies. *Boeing commercial aero magazine Quarter 2 2010*, 2, 2010.

[61] Ruijgrok G. *Elements of airplane performance*, volume TU Delft. 2009.

[62] Sausen R. and I. Isaksen and V. Grewe and D. Hauglustaine and D.S. Lee and G. Myhre and M. Köhler and G. Pitari and U. Schumann and F. Stordal and C. Zerefos. Aviation radiative forcing in 2000: An update on ipcc (1999). Meteorologische Zeitschrift, Vol. 14, No. 4, 555-561, 2005.

[63] Sausen R. and U. Schumann. Estimates of the climate response to aircraft co2 and nox emissions scenarios. Clim. Change 44, 27-58, 2000.

[64] Schumann U. On conditions for contrail formation from aircraft exhausts. *Meteorol. Z.*, 5 No 1:4–23, 1996.

[65] Schumann U. The impact of nitrogen oxides emissions from aircraft upon the atmosphere at flight altitudes - results from the AERONOX project. *Atmospheric Environment*, 31 No 12:1723–1733, 1997.

[66] Schumann U. and K. Graf and H. Mannstein. Potential to reduce the climate impact of aviation by flight level changes. Article, 2011.

[67] Seatguru. URL. `https://www.seatguru.com/browseairlines/browseairlines.php`, accessed 14-9-2019.

[68] Snijders T. and J. Melkert. Effect of cruise altitude and alternative aviation fuels on radiative forcing. American Institute of Aeronautics and Astronautics, 2011.

[69] Stordal F. and M. Gauss and G. Myhre and E. Mancini and D. Hauglustaine and M. Köhler and T. Berntsen and E.J.G. Stordal and D. lachetti and G. Pitari and I.S.A. Isaksen. Tradeoffs in climate effects through aircraft routing: forcing due to radiatively active gases. Atmospheric Chemistry and Physics Discussions, 6, 10733-10771, 2006, 2006.

[70] Vedantham A. Aviation and the global atmosphere: A special report of IPCC working groups I and III. Cambridge Univ. Press, Cambridge, U.K., 1999.

[71] Wang W. and N. Sze. Coupled effects of atmospheric n_2o and o_3 on the earth's climate. *Nature*, 286:589–590, 1980.